Mixed convection

A CFD study in a side heated cavity filled with coarse grained porous media.

J.E.D. de Geus

Technische Universiteit Delft

TU Delft

Mixed convection

A CFD study in a side heated cavity filled with coarse grained porous media.

by

J.E.D. de Geus

to obtain the degree of Master of Science in Chemical Engineering
at the Delft University of Technology,
to be defended publicly on Friday September 7, 2018 at 9:30 AM.

Student number:	4158717	
Project duration:	November 15, 2017 – September 7, 2018	
Thesis committee:	Dr. S. Kenjereš Dipl.-Ing.,	TU Delft, supervisor
	M. Chakkangal MSc,	TU Delft, daily supervisor
	Prof. dr. ir. C. R. Kleijn,	TU Delft
	Dr. P. E. Boukany,	TU Delft

TU Delft

Abstract

The interest of this project stems from its application in the blast furnace hearth in the steel and iron making industries. In the reactor iron ore is converted by an oxidation reaction into liquid metal. Hot air is blown into the vessel by which temperatures of 1300°C are reached. Pieces of ore and impurities from the input form a porous medium in the heart of the reactor. It is desired to have more insight in the process conditions for economic and energy saving purposes.

This iron-making process is intensely exothermic, so in order to control the process the reactor wall has to be cooled. Due to the temperature difference between the hot core and cooled sides, a natural convection flow arises.

The liquid metal is tapped off at the reactor wall, resulting in a forced convective flow inside the centre of the reactor called the hearth. The two flows together form a mixed convection regime. This is characterized by asymmetries and complex temperature distributions. Hotspots are observed close to the walls leading to a reduction in lifetime of the reactor, process productivity and product quality.

The influence of this coarse grained porous media on the flow and heat temperature field is elaborated in this thesis project. The flow being opaque and the high temperatures make it difficult to carry out experimental studies. This is why computational fluid flow modeling is used to get more insight in the process. A side heated lid-driven cavity is simulated with a Direct Numerical Simulation (DNS) in the open source code OpenFOAM. The simulations are carried out for coarse grained porous media (porosity ε=0.38) of spherical hydrogel beads in a Body-Centered Tetragonal (BCT) structured packing for assisting and opposing mixed convection. The thermal conductivity of the beads is equal to the working fluid (water). The research was conducted for the range of Rayleigh number (Ra) of $10^5 \leq Ra \leq 10^7$.

The present results show a reduced heat transfer for the cavity filled with porous media compared to the water filled cavity for the low Ra regime ($Ra=10^5$), which diminishes with an increase in Ra. In the case of natural convection and low Ra the Nusselt number (Nu) is about five times higher for the water filled cavity compared to the cavity filled with coarse grained porous media. For high Ra ($Ra=10^8$) the heat transfer rates for both cavities are in the same order or magnitude.

Higher heat transfer values are reported for assisting mixed convection compared to opposing mixed convection. For high Ra ($Ra=10^7$) the heat transfer rate for the assisting situation is almost nine times higher than for the opposing case. A minimum of Nu is found when the shear force created by the wall movement is proportional to the buoyancy force. The two forces dampen each other out and heat is mostly transferred by conduction. Furthermore, the higher heat transfer values are found with a higher forced component (wall velocity).

Lastly, a modification was proposed for the dimensionless Richardson (Ri) number, that expresses the ratio of the buoyancy term to the flow shear term. Ri was multiplied with square root of Darcy (Da) to take into account the influence of the coarse grained porous media. With the help of this expression, the assisting and opposing mixed convection regime was determined for the range of $0.001 < Ri_m \leq 100$. To validate this expression for Ri_m (Richardson medium), more data has to be analyzed from situations with higher Ra or from mixed convection by a ventilated cavity for example.

The two conclusions that can be drawn from this thesis for the design and operating conditions at the blast furnace are:

1. an opposing mixed convection situation can lead to a lower and a minimum in Nu.
2. a lower forced convection flow will lead to lower heat transfer values.

So, it is important to look further into the direction and magnitude of the forced flow. The next logical step for this model will be to simulated mixed convection with a forced convection flow created by an in- and outlet in the cavity. This geometry will show closer similarities with the reactor.

Preface

This thesis has been written as final part of my master degree in Chemical Engineering at Delft University of Technology. For the past eight months I have been working on this thesis at the Transport Phenomena group.

There are a few people I would like to thank for their help and support during this thesis project. First of all, I would like to express my gratitude and appreciation for my daily supervisor Manu Chakkingal. Your continued guidance and feedback helped me a lot. Thank you for making time for me, even during the times you were back in India.

My special thanks to prof. dr. ir. C.R. Kleijn, dr. ir. M.J. Tummers and dr. S. Kenjeres Dipl.-ing for the biweekly meetings with lots of fruitful discussions. Besides, I would like to thank for the opportunity to join and present at the progress meetings at Tata Steel. Thank you Iman Ataei Dadavi for your critical view on my results. Additionally, I enjoyed working and discussing with you Nima Rounaghi. Thank you for sharing your experimental results with me.

Thank you Dr. P. Boukany for being part of my thesis committee. I would also like to thank the rest of the people at the TP group. You were all very kind and I liked working at the student computer corner. I have good memories of the TP excursion to Cosun and Suikerunie, the diner, the drinks afterwards in the De Ruif and the bbq at Knus.

Ultimately, I want to express my gratefulness to my friends and family. Many thanks to Agnes, Cathleen, Sharon, Marise and Aart for your feedback. Marise: thank you for the tasty lunches! I appreciated our many coffee breaks and lunches with you Bob. Lastly, I would like to express my deep gratitude to Monique, Sterre and ofcourse to Kasper for your support!

Julia de Geus
Delft, August 2018

Contents

List of Tables

List of Figures

Nomenclature

Acronyms

BCT	Body Centered Tetrahedrogonal
BL	Boundary Layer
CFD	Computational Fluid Dynamics
DNS	Direct Numerical Simulation
FC	Forced Convection
LES	Large Eddie Simulations
LSC	Large Scale Circulation
MC	Mixed Convection
NC	Natural Convection
NS	Navier Stokes
OpenFOAM	Open source Field Operation and Manipulation
PISO	Pressure Implicit with Splitting of Operator
RANS	Reynolds Averaging Navier Stokes
REV	Representative Elementary Volume

Dimensionless Numbers

Da	Darcy Number
Nu	Nusselt Number
Pr	Prandtl Number
Ra	Rayleigh Number
Re	Reynolds Number
Ri	Richardson Number

Greek Symbols

α	Thermal diffusivity, $k/\rho C_p$	m^2/s
β	Thermal expansion coefficient	K^{-1}
β_0	Thermal expansion coefficient at reference state	K^{-1}
Δt	Time step	-
δ_i	Boundary layer thickness of quantity i	m
ϵ_u	Kinetic energy dissipation rate	m^2/s^3
η_i	Length scale of quantity i	m

λ	Conductivity ratio, λ_f/λ_s	-
μ	Dynamic viscosity	kg/ms
ν	Kinematic viscosity, μ/ρ	m^2/s
ϕ''_q	Heat flux	W
ρ_0	Density at reference state	kg/m^3
ρ_i	Density of phase i	kg/m^3
τ	Temporal time scale	s
ε	Porosity	-

Roman Symbols

A	Aspect ratio	-
A_{box}	Surface where heat transfer takes place	m^2
C_f	Forchheimer Coefficient	-
C_p	Specific heat	m^2/s^2K
d_p	Sphere diameter	m
g	Acceleration due to gravity (acts along the Z-axis)	m/s^2
h	Heat transfer coefficient	W/m^2K
h^{global}	Global mesh size	m
K	Permeability	m^2
k_i	Thermal conductivity of phase i	W/Km
L	Height of the cavity	m
N	Minimal number of nodes	-
p	Pressure	Pa
T^*	Normalized temperature	-
T_0	Temperature at reference state	K
T_i	Temperature of phase i	K
u_i	Velocity in direction i	m/s
X,Y,Z	Represents the rectangular coordinate system	-

Subscripts

B	Batchelor
c	Cold
crit	Critical
eff	Effective
f	Fluid
FC	Forced Convection

h	Hot
K	Permeability
Kolm	Kolmogorov
LSC	Large Scale Circulation
m	Porous medium
mag	Magnitude
MC	Mixed convection
NC	Natural convection
p	Particle
por	Porosity
s	Solid
T	Themperal
Th	Thermal
Th.BL	Thermal boundary layer
u	Velocity
v.BL	Velocity boundary layer

1 Introduction

The interest for this project stems from its application in the blast furnace hearth in the steel and iron making industries. The goal of this research is to get more insight into the heat and flow distribution in a side-heated cavity filled with porous media. It is desired to have more insight in the process conditions for economic and energy saving purposes. This is encountered in many technical applications like fluid flow in geothermal reservoirs, separation processes in chemical industries, crude oil production, etc. Section 1.1 tells more about convective heat transfer. Section 1.2 elaborates more about the origin of the question from Tata Steel. Section 1.3 gives the aim of the thesis with the subsequently research questions.

1.1. Convective heat transfer

Convection is the heat transfer due to bulk movement of molecules in a domain. Natural convection occurs due to buoyancy forces as a result of density gradients induced by an imposed temperature difference. Forced convection is a mechanism in which fluid motion is generated by an external source (like a pump, fan, suction device, etc.). Together, they can form mixed convection. This is the situation when forced and natural convection act together to transfer heat. How much of each component is contributing to the total heat transfer depends mainly on the temperature, geometry and flow. Due to this wide range of variables, a lot of papers have been published on experiments and computational studies involving various type of fluids and geometries.

Improvement and understanding of heat transfer in thermal devices such as heat exchangers and electronic equipment became an important factor in industry. Combined forced and natural convection can also be seen in other industrial applications like solar boilers, drying processes, filtration systems, thermal insulation and groundwater and oil flows [6].

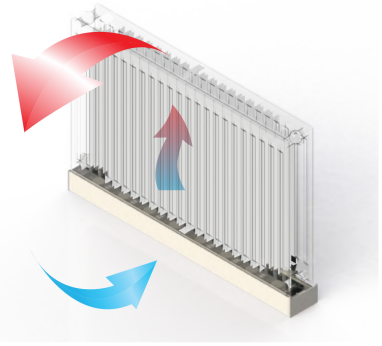

Figure 1.1: Example of an fan helping to improve the heat transfer from a radiator into the room. This product from ClimateBoosters ensures the heat from the radiator to be more uniformly divided in the room [2].

Furthermore, heat transfer in porous media is a wide studied object due to the increase of importance in industrial applications. In daily life, material containing pores or voids can be seen in for example beach sand, wood or the human lungs. For industrial applications, one can look at power stations, cooling equipment, combustion stations or high performance heat exchangers. The mixing of high and low energy fluids has a significant influence on the performance of the above-mentioned devices. The heat transfer can be enhanced between the two flows by working with a system containing porous media. A system with voids has two important characteristics: first, the dissipation area is greater than the conventional configurations that enhance heat transfer. Secondly, the irregularities of the individual beads mix the fluid more effectively [7].

The high variety of parameters that have an influence on the heat and flow profile makes it difficult to obtain a comprehensive correlation, and when it is, it is usually only accurate for a very bounded situation.

Mixed convection can be described in three general ways:

1. The first way is when natural convection aids forced convection. This can be seen when the buoyant motion is in the same direction as the forced flow, and thus enhancing the heat transfer. This can be seen when a fan is placed under a radiator as schematically depicted in figure 1.1. Since hot air rises naturally, the air being forced to move upward, adds to the total heat transfer.
2. The second way is when natural convection is moving in the opposite way of forced convection. In this case, the fan is placed upward over the radiator. In this way, the air rising upwards in natural motion is facing a forced flow going downwards. This does not enhance the heat transfer.
3. The third way is called transverse flow. This is the situation when the buoyant motion acts perpendicular to the forced motion. The mixing of fluids is enhanced and thus the heat transfer will increase. This situation can be seen when the fan blows in a horizontally way, over the radiator.

The above-mentioned points are clear for a simple situation, but there are some additional depending parameters in the case of a cavity filled with porous media. The solid spheres have an influence on the flow and heat characteristics, making it more complicated to understand the underlying physics. The chaotic behaviour of the fluid can be described with the Navier Stokes equations. The non-lineair behaviour of the fluid flow and temperature distribution is making the problem difficult to solve.

1.2. Background

The question and the problem stated for this project came from the blast furnace at the second largest steel producing company in Europe, Tata Steel. The company was recently merged with the Germain steel producer ThyssenKrupp under the new name thyssenkrupp Tata Steel (TKTT) [8]. In this thesis the name Tata Steel will be used since this was the name of the company at the start of this project. Million of tonnes of steel are produced on a yearly basis to meet the demand of high-quality steel. This makes that Tata Steel strives for reliable and robust process equipment.

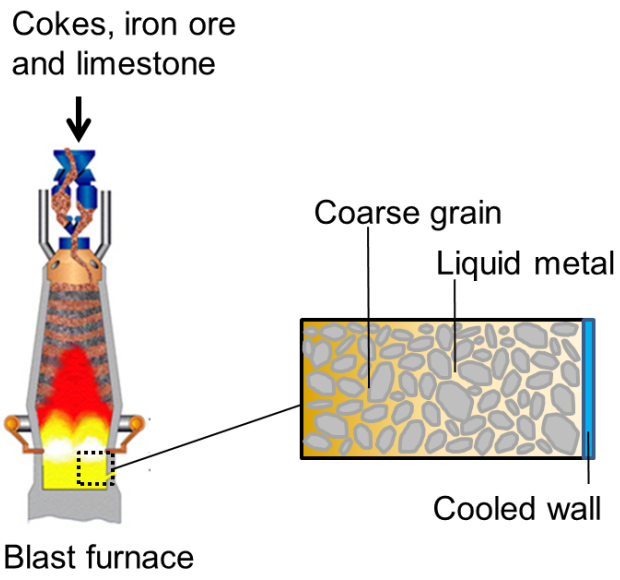

Figure 1.2: Schematic situation of the blast furnace at Tata steel.

The iron-making process

The production of steel mainly has to do with lowering the amount of carbon content in iron. The removal of carbon is done by an oxidation reaction. Impurities in the raw iron (nitrogen, silicon, and phosphor) are removed during the oxidation, and sulfur is removed by other chemical reactions. Other elements, such as nickel, manganese, and vanadium, are added to the steel to produce different levels of quality. The oxidation reaction is done in the blast furnace.

In this blast furnace (see figure 1.2) iron ore, cokes and limestone are charged from the top of the furnace and these materials are subjected to a series of complex chemical reactions. Hot air is blown into the furnace

via nozzles, where it reacts with the descending cokes. This blast air is an essential part of the process, by which a temperature of 1300 °C is reached.

The raw materials introduced at the top of the furnace take around six to eight hours to descend to the bottom, where their conversion into liquid iron and slag (impurities) is completed. This hot liquid metal and slag is then tapped off at regular intervals from the furnace.

In addition to liquid iron and slag, large quantities of hot gases (CO and CO_2) are produced. When the gases have exited the furnace, they are cleaned and cooled to allow them to be used for combustion purposes.

An essential feature of this iron-making process is that it is intensely exothermic. Therefore, cooling the furnace shell and lining is an essential requirement [9].

Hearth of the furnace

The hearth of the furnace is another important aspect of the reactor. Here, the hot liquid metal, along with the slag is collected. Then, it is tapped off and transferred for further processing. In these next processes, the liquid iron will be converted into high-quality steel for a wide range of customer sectors, including construction, automotive, lifting or the packing industry [10].

This hearth of the reactor is heavily lined internally with refractory material. Besides, there are also numerous cooling elements intended to allow a constant flow of circulating water. These cooling elements are placed to convey away the thermal energy and hence prolong the lifetime of the lining and enhance the quality of the product. The capacity of coolers is larger in the lower area of the reactor since more heat is generated at that location.

Figure 1.2 shows the schematic situation, where the hearth shows a coarse-grained porous media (with a typical diameter of 10-40 mm) of (unconverted) coke particles. The hearth of the furnace has a diameter of ~5 meters.

Life time

The temperature difference between the hot liquid metal and the cool walls induces a natural convection flow. The tapping off process results in a forced flow inside the hearth. Together, these two flows result in a mixed convection system, characterized by asymmetries and complex temperature distributions.

With extreme operating conditions (high temperature and high flowrates) and non-uniformity of the iron, local hot spots are observed causing damages to the reactor wall of the hearth.

In order to maintain safe operating conditions, high productivity and lifetime, a devastation of the reactor wall is highly unwanted. The large reactor dimensions and high temperatures make a repair at the wall a time consuming and costly operation. Besides, an eventual shut down and start up of the reactor (outside of the legal stop) will mean a less production and so less revenue.

Tata Steel wants to understand more about the appearance of the hot spots in order to save money. With the flow being opaque and the high operating temperatures, it is hard to perform experimental studies. That is why is looked into Computational Fluid Dynamics (CFD) to study this complex situation.

1.3. Aim of the thesis

The aim of the thesis is to study the mixed, forced and natural convection in a side heated cavity filled with hydrogel beads. This was split into several research questions that are described below.

Research questions

In this thesis a Direct Numerical Simulation (DNS) is performed on a side-heated cavity filled with solid spheres. This means that no turbulence model is used, and the whole range of spatial (3D) and time scales are solved. Forced convection is implemented by moving the side walls. In order to get a mixed convection system, the velocity of the walls has to be in the same order as in natural convection.

To frame it more specifically, the following research questions are addressed:

1. How does natural convective heat transfer in a side heated water filled cavity with coarse grained porous media differ from heat transfer in an (empty) water filled cavity?

2. How is the mixed convective flow in a porous media filled side heated lid-driven cavity influenced by the direction of the forced component of the flow?

3. How can mixed convection in a porous medium be expressed in a non-dimensional number?

In order to answer these questions a code is developed in OpenFOAM. The computational model for natural convection in an empty box is first verified with experimental data from master student Nima Rounaghi. Afterwards, the first question will be studied for an (empty) water filled cavity and a cavity filled with coarse grained porous media for the Rayleigh number range $10^5 \leq Ra \leq 10^7$. The focus on the second question will be for $Ra=10^7$. Lastly, the third question will be answered for $10^5 \leq Ra \leq 10^7$ for assisting and opposing mixed convection.

1.4. Outline

The present study is aimed to obtain more information about the heat and flow characteristics within a cavity with a porous media. First, in chapter 2 a literature study can be found about other performed research. Then, chapter 3 gives more information about the governing equations and the numerical methods used for this CFD study. The following four chapters elaborate the results on natural, forced, assisting mixed and opposing mixed convection respectively. All results are concluded in chapter 8 and recommendations for further reseach are made in chapter 9.

2

Theory

This chapter provides theoretical information about various aspects of the thesis and formulas which will be used for modeling and calculation purposes. In addition, the quantities that have an important role in the behaviour of fluid and the transfer of heat will be expressed in terms of dimensionless numbers and explained in this chapter. Firstly, the system and its corresponding assumptions are discussed in section 2.1. In the second and third section, the concepts of natural and mixed convection in an empty cavity are explained. Lastly, more information is given about porous media and the influence of the porosity on convection.

2.1. Introduction

In this study, flow and heat transfer characteristics are investigated in coarse-grained porous media. In order to do so, it is important to understand the underlying physics for natural and forced convection in a cavity. Numerous experimental and numerical studies have been published about natural and mixed convection in a 3D or 2D cavity. These will be discussed in this chapter.

The aim of the thesis is to get more insight into the heat and flow patterns of the cavity filled with porous media. A large number of numerical and experimental studies have put their efforts to imitate the convection streams in porous media.

Lauriat et al [11] concluded in their research about natural convection in a vertical porous cavity, that this porous medium can transport more heat than a pure fluid if the matrix is high permeable and the thermal conductivity of the solid particles is higher than that of the fluid.

The experiments with rectangular cavities and side heated walls performed by Seki et al [12], showed that it is clear that the Prandtl number (Pr) and aspect ratio $\frac{L}{W}$ had a significant effect on the heat transfer through the vertical porous layer.

In a recent experimental study carried out by Kurtbas and Celik [13], an assisting mixed convection situation was investigated in a box with an aluminum metal foam. There was found that the average Nusselt number increases with an increase in porosity.

A problem that has attracted significant attention is that of natural convection in horizontal porous layers heated from the bottom, also several variations of this problem have been studied in detail [14]. However, little is known in the literature about the natural and mixed convection in a side-heated box 3D with a Body Centered Tetragonal (BCT) packing of solid spheres.

Convective heat transfer can be characterized by three non-dimensional control parameters: Rayleigh number (Ra), Pr and aspect ratio (A=depth/height). Ra is associated with a buoyancy-driven flow, which governs the stability of the horizontal fluid layer subjected to a destabilizing temperature gradient. In heat transfer problems, Pr controls the relative thickness of the momentum and thermal boundary layer. When Pr is small, heat diffuses quickly compared to the velocity. Liquid metals (like the liquid iron in the blast furnace) are characterized by their small Pr number, this means that the thermal boundary is much bigger than the velocity boundary layer. See appendix A for more detailed information.

The influence on the flow and heat transfer can be measured with two response parameters: the Reynolds number (Re) and Nusselt number (Nu) respectively. Where Re is defined as the ratio of inertial forces to viscous forces in the fluid. Nu gives an estimate of the ratio of total heat transfer to conductive heat transfer. A

conduction dominated regime is found for a Nu~$O(1)$, and a larger Nu corresponds to more active convection.

Assumptions and simplifications

As mentioned in chapter 1, complex asymmetrical flow arises in the hearth of the furnace due to the porous matrix of unburned iron and impurities. This project is a part of making the step towards a computational model that is verified with experiments and can mimic the chemical and physical processes inside the furnace. Since this is a complex, challenging and long-term project, steps are made by PhD, master and bachelor studies. In this study, a side-heated cavity with coarse-grained porous media is investigated. This is already a complex situation, and therefore simplifications and assumptions are made to make the situation more manageable.

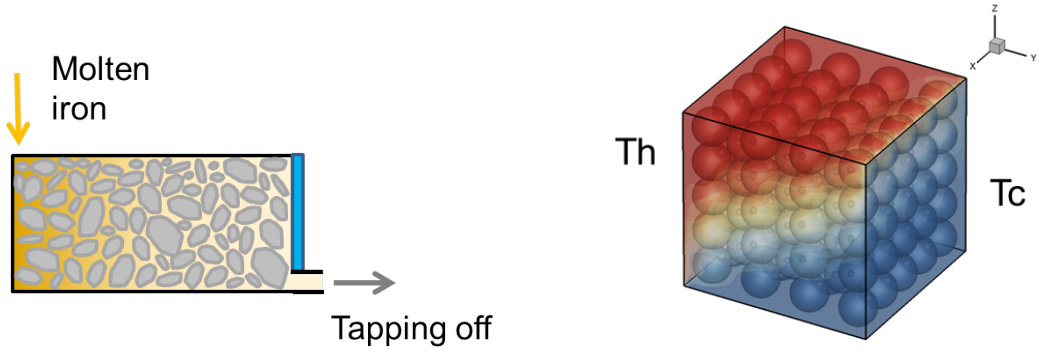

(a) Schematic view of the hearth of the furnace. A natural convection stream arises from the hot core and cold walls. Forced convection originates from the tapping off process.

(b) Configuration to investigate the heat and flow characteristics. The domain is side heated and as an aspect ratio of A=1. The working fluid is water (Pr=5.40). The spheres are in a BCT configuration and are made of hydrogel.

Figure 2.1: Figures representing natural and mixed convection in the hearth of the furnace and in the simulated situation.

Figure 2.1a schematically shows the hearth of the furnace where a natural convection stream arises due to the hot core and cooled wall, and a forced convection stream originates from the tapping off process. From here, the situation depicted in figure 2.1b is adopted to research the effect of pore-level flow and temperature field on macroscopic fields. The following assumptions are made:

- The local temperature difference in the hearth is small and therefore makes the heat transfer through radiation negligible compared to convective heat transfer.
- A small temperature difference implies that material properties can be taken as temperature independent e.g. constant.
- The irregular porosity inside the hearth is simplified by making evenly distributed configurations of spheres of the same size.

Furthermore, the side heated domain has an aspect ratio of A=1, BCT packing of spheres made from hydrogel and water (Pr=5.4) as working fluid is chosen as the scope of this project. Forced convection will be implied by giving certain walls a velocity. The parameters are chosen in such a way that experimental validation is possible, this is for example important for the packing configuration. A Simple Cubic Packing is harder to perform than a Body Centred. In addition, the walls will have moderate temperatures in order to avoid the phase or density change (water around 4°C) regime.

PhD student Manu Chakkingal is performing research to find more about the characteristics of different working fluids (with different Pr numbers), various configurations of spheres and the influence of sphere material. This is done for cavities with side heated and bottom heated walls (Rayleigh-Bénard convection). If this model is validated, it can become a part of the larger model.

2.2. Natural convection

In order to explore the heat and flow characteristics, it is important to know how natural convection works in an empty cavity. Natural convection is observed in fluids when a driving force is generated by the den-

sity variation due to a temperature gradient. Flow with a horizontal temperature gradient is characterized to be unstable at any Ra>0. The presence of a denser (lighter) fluid in the horizontal environment of a hotter (colder) element results in its immediate upward (downward) movement [15]. This results in a wall dominated flow and is schematically depicted in figure 2.2.

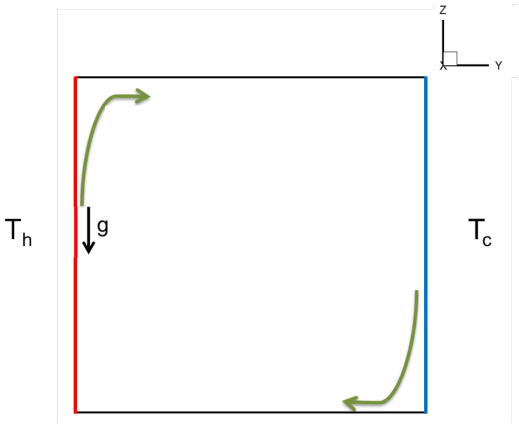

Figure 2.2: Schematic representation of natural convection with a horizontal temperature gradient.

Boundaries

The main motive force in a confined box noticeably manifests itself only in a thin near-wall zone. This zone is called the boundary layer, and in this layer the effects of viscosity are significant. Also, transport of heat from the heated to the cooled wall is carried out by the flow in the boundary layers. This region of a temperature field with the thickness δ_T is called the thermal boundary layer.

The variation of heat transfer (Nu) under the influence of Ra and Pr can be described by the theoretical model proposed by Grossmann and Lohse [16]. They decomposed the kinetic energy dissipation rate into boundary layer and bulk conditions; and the thermal dissipation rate into plume and background contributions. This theoretical model was originally founded for bottom heated Rayleigh-Bénard convection, but it was further vetted for vertical natural convection. They have proposed scaling parameters for Nu for the two regimes [17].

2.3. Mixed convection

In the hearth of the furnace, a mixed convection situation is observed. Mixed convection is the heat transfer mechanism in which the combined effects of forced and natural convection are of comparable magnitude. The contribution from each of them to the total heat transfer is determined by the temperature difference, properties of the fluid, geometry etc. Mixed convection is complex due to interaction of the buoyancy force with the shear force. The forced flow may aid or oppose the buoyancy forces, causing an increase or decrease in the heat transfer rate respectively. The ratio of natural to forced convection is expressed with the Richardson number. Mixed convection is observed when 1<Ri<10. A full derivation about Ri can be found in appendix A.

In literature, two major arrangements of mixed convection are reported: mixed convection due to a ventilated or a lid-driven cavity.

Ventilated cavity

Sing et al [18] did a numerical investigation of a 2D rectangular cavity with side heated walls in order to find the optimum placement of inlet and outlet for the best cooling effectiveness. The effect of the outlet position in a two-dimensional vented cavity with an inner heated square was found to have an influence on the average Nusselt number [19]. The need for a 3D numerical model was suggested in order to capture the temperature fields and heat transfer rate with increase in Ri for a rectangular air inlet and a rectangular channel outlet at the exit of the cavity [20].

In short, a lot of parameters on the inlet and outlet conditions (like position, size, flow rate etc) in a ventilated cavity seem to have an influence on the total heat transfer. For simplicity, a lid-driven cavity is decided to be the scope of the project.

Lid-driven cavity

In a lid-driven arrangement walls of the cavity have a velocity that creates a forced flow. The walls can move in the same or opposite direction as the natural flow; this means that the forced flow is aiding or opposing the buoyancy force respectively. This is schematically depicted in figure 2.3.

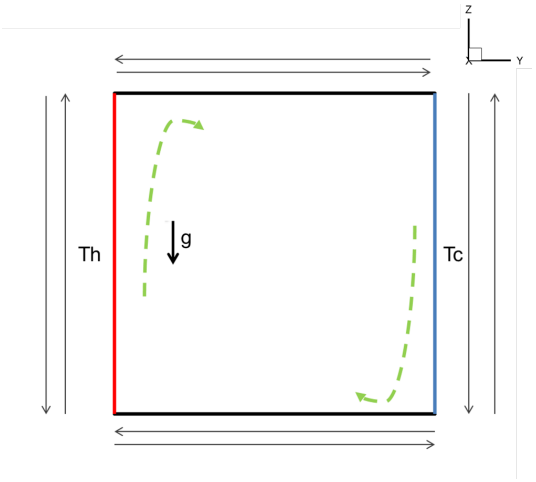

Figure 2.3: Schematic representation of mixed convection situation by movement of the lids. The green dotted line represents the flow due to natural convection. The movement of the walls will create a forced flow that can aid or oppose the buoyancy flow.

In the case where buoyancy and shear forces are opposing each other, a shear cell develops adjacent to the moving boundary, while a buoyancy cell fills the rest of the cavity. The size of each cell depends on the Ri number [21]. This causes the heat transfer rate to decrease compared to only a natural convection flow. With an increase of opposing shear force, the heat transfer rate decreases until a minimum is reached at Ri=1. Further increase in the opposing forced component results in the increase of heat transfer rate due to the formation of a shear dominant regime.

A numerical study investigated the influence of aiding and opposing shear force on the buoyancy force for Ri numbers in the range of 0.01-100 at Re=100. The different heat transport ranges for forced, mixed and natural convection were defined. It was found that the mixed convection range of Ri for the opposing-buoyancy case was seen to be wider than that of the aiding-buoyancy case [22].

It was also found by Oztop and Dagtekin [23] that both the Ri number and the direction of the moving walls affect the fluid flow and heat transfer in the cavity. Moreover, for Ri<1 the influence of the moving walls on the heat transfer is the same when the walls move in opposite direction. There was reported that the heat transfer is somewhat better for Ri>1 due to the formation of secondary cells on the walls and a counter-rotating cell at the center.

The direction of the top wall(s) moving also plays a significant role in the flow and heat transfer [24]. Amberthkar et al [25] simulated the heat transfer in a four-sided rectangular domain. The lower wall is moving to the left, the upper wall to the right, while the right wall is moving upwards and the left wall is moving downwards. They found that as Re increases, the horizontal temperature gradient near the vertical wall decreases. Therefore the overall heat transfer decreases.

2.4. Porous media

The last two sections reported the phenomena of convection in an empty cavity. As stated before, the interest of the project is finding the influence on the convection streams in coarse-grained porous media. The definition 'porous media' means a material containing pores/voids. In a natural porous medium, the pore distribution (size and shape) is highly irregular [4]. Examples of natural porous media are wood, beach sand or the human lungs.

In coarse-grained media, the porous length scale is comparable to the flow and thermal length scale. Therefore, the pore-scale flow and temperature field effects are of great relevance in understanding the pore-scale phenomena.

Darcy's law

The study of heat transfer in porous media has been mostly based on Darcy's model for porous media [26–28]. Here, the porosity is accounted for in a volume-averaged sense (for example with a Representative Elementary Volume-REV), assuming that the porous length scales are small compared to the thermal and flow length scales. Besides, this model is based on the assumption that inertia is negligible compared to viscous effects.

Darcy's law neglects the effects of a solid boundary or the inertial forces on the fluid flow and heat transfer through a porous media. Other attempts have been made by Brinkman and Forcheimer to take the viscous and drag terms into account. An overview of the equations and their validities is provided in appendix B. The focus of the present study is on coarse-grained porous media, i.e. porous media in which length scales (here: diameter of the spheres) are not small compared to the flow- and thermal length scales in the fluid. This makes that the Darcy model is no longer valid.

Thermal conductivity

The spheres are made from a different material than the working fluid, and thus having a different thermal conductivity. This can affects the total heat transfer in the domain, depending on the properties.

House et al [29] simulated an enclosure with a centered squared body where the size and thermal conductivity were varied. The variation of the thermal conductivity of the solid was found to have a big influence on the Nusselt number. If k_s is low and the body size small, a thermally conductive body can enhance the heat transfer rate. And with the same body size, a high thermal conductivity will reduce the total rate.

To learn more about the characteristics of the packed-bed reactor, the problem of natural convection in a horizontal porous layer was concerned. It was found that a porous medium can transfer a significantly larger amount of heat compared to the fluid alone. For this condition to hold, the matrix should be highly permeable and the thermal conductivity of the solid should be higher than for the fluid: $k_s > k_f$ [30].

Kathare et al [31] found similar results for the situation with metal foams. A metal foam is a porous medium with a high porosity and a structure characterized by thin fibers, or ligaments, of metal joining several others in a random manner throughout the medium. This results in an enhanced heat transfer due to increased mixing, interstitial heat transfer and a benefit of high stagnant conductivity.

Obstacles

Obstacles in a heated cavity will have an influence on the momentum and thermal boundary layer of the solid boundaries of the cavity and thus on the total flow and heat transfer. Besides, a boundary layer will develop on the solid spheres itself. It was observed that with more obstacles (square and circular rods were taken), Nu increases [32]. This is caused by the flow that migrates away from the wall and moves more towards the center of the cavity. This is caused by an increase in flow resistance closer to the wall. Besides, the difference between the thermal conductivity of the solid spheres and working fluid also has an impact on the heat transfer.

Das et al [33] found in their DNS study of flow and heat transfer through slender fixed-bed reactor with spherical particles that an increase in solid conductivity creates an increase in the overall heat transfer rate. This increase is relatively small, and for very high solid to fluid conductivity ratios the dependency flattens off. Simular observations were reported in an experimental study by Yagi and Wakao [34].

Moreover, it was stated that in the case of the constant wall temperature the amount of heat transferred to the spheres depends on the combined effect of particle conductivity and the contact area between the particle and wall. As the particle-wall contact area is very small, the amount of heat coming directly through the solid conduction is small and as a result the effect of solid conductivity is also small [33].

In an experiment with a porous medium with solid spheres, the heat transfer behavior was investigated in Keene [35].The tests showed that a thermal boundary layer develops around the spheres. A relation was found between the Rayleigh number and this thermal boundary layer thickness. At high Ra and small δ_{Th}/D, the situation closely matches with the one of a fluid layer. At a sufficiently thin boundary layer around the sphere, the influence of the solid is minimized so that the heat transport can be predicted by relations and equations of a homogeneous fluid layer.

2D numerical simulations of a side-heated cavity with porous media show the existence of an asymptotic regime where the heat transfer is independent of the permeability of the porous matrix. In this regime, convective heat transfer is the more dominant heat transfer mechanism compared to the conduction to the solid spheres. The heat transfer only depends on the fluid Ra number, solid-to-fluid conductivity ratio, and viscosity ratio. Furthermore, based on their results they concluded that a porous medium can transport more heat than a pure fluid if the porous matrix is highly permeable and the thermal conductivity of the solid particles is higher than that of the fluid [11].

Mixed convection

Mixed convection in a porous medium will also be obtained by moving walls.

Mixed convection boundary layer flow in a porous medium along a vertical wall was modeled by Ranganathan and Viskanta [36] with a 2D numerical simulation. They demonstrated the influence of the non-dimensional parameters Pr, $\frac{\mathrm{Gr}}{\mathrm{Re}}$ and Re on the velocity and temperature profiles at the boundary. They also found that porosity variations near the wall have a negligible effect on the results and that boundary friction and inertia are quite significant and cannot be ignored in the analysis.

The steady mixed convection flow in a porous 2D square cavity with an isothermal vertical wall and three adiabatic walls was investigated in a numerical study using the Darcy model. A forced flow was imposed to the system by providing an in- and outlet. It is shown that the global heat transfer into the enclosure is sensitive to changes in the aspect ratio [37].

To find the mixed convection regime in a box with porous media, the Darcy number (Da) have to be taken into account in the expression for Ri number. Da represents the relative effect of permeability of the medium versus its cross-sectional area. The proposed equation was founded by Keene [35]:

$$Da = \frac{K}{L^2}, \qquad K = \frac{\varepsilon^3 D^2}{150(1-\varepsilon)^2} \tag{2.1}$$

Where K is the permeability of the medium (m^2), L the characteristic lenght of the box (m), ε is the porosity or void fraction of the material and D the diameter of the particle. The following dimensionless numbers are proposed based on the medium *m* based on the article from Katare et al [31].

The Re number based on the permeability:

$$Re_K = Re_f\sqrt{Da} = \frac{\rho_f u\sqrt{K}}{\mu_f}, \tag{2.2}$$

where subscript f refers to the fluid phase and K to the permeability of the medium.

The Ra number based on the fluid properties:

$$Ra_m = Ra_f Da\lambda, \tag{2.3}$$

where λ=$\frac{k_f}{k_s}$, the conductivity ratio of fluid to solid. In this work the conductivities of the solid region (hydrogel) and the fluid part (water) are in the same order of magnitude, making λ=1.

Furthermore, Pr is based on two articles. First, the effective Pr number was based on [38]:

$$Pr_{eff} = Pr_{por} Da, \tag{2.4}$$

where the subscript *por* stands for porosity.

Kathare et al [31] gives a definition for Pr_p:

$$Pr_{por} = Pr_m \frac{Da^{-1/2}}{C_f} \tag{2.5}$$

Where C_f is the Forcheimer coefficient, this parameter can be found empirical.

Together, this forms the expression for $\mathrm{Pr_m}$:

$$Pr_m = \frac{\mu C_p}{k_m} = Pr_{eff} Da^{-1/2} C_f \tag{2.6}$$

The relationship for Ri based on the medium, $\mathrm{Ri_m}$, is formed on the dimensionless numbers based on the medium and permeability:

$$Ri_m = \frac{Ra_m}{Pr_m Re_K^2} = \frac{Ra_f\sqrt{Da}}{Pr_{eff} Re_f^2} \tag{2.7}$$

Equation E.7 is valid for values between ε=0-1, but not the values ε=0 or ε=1 itself.

Here, the length scales in the Ra and Re number are based on the size of the box. As mentioned, Aydm et al [22] found a wider mixed convection regime for opposing-buoyancy then for aiding-buoyancy. This same behaviour has not been found yet for the case with coarse-grained porous media to the best knowledge of the author.

2.5. Turbulence modelling

The objective of the model is to predict the quantities of interest for the given problem. For turbulent flows the wide range of length scales and complexity of the involving phenomena make most modeling approaches computational very expensive. Since the flow in probably all engineering applications has some turbulent characteristics, it is important to have better understanding of how to model this. Turbulent flows share three basic characteristics: they are irregular, time dependent and three-dimensional. Furthermore, it is characterized by chaotic changes in pressure and flow velocity. Mathematically, it is difficult to tackle the chaotic changes of motion in flows with even a simple geometry and boundary conditions.

Generally, laminar flow is stable when the Re number is below the critical value: $\mathrm{Re}_{\mathrm{crit}}$. This critical number depends on, among other things, the geometry. But this number is only approximate due to two reasons. First, the transition from laminar to turbulent flow is a gradual process. If Re is above the critical value, laminar and turbulent flow alternate in time and place. Besides, the magnitude of the flow disturbances are based on the large disturbances while the small disturbances can increase $\mathrm{Re}_{\mathrm{crit}}$ by orders of magnitude.

The fluctuating part of the velocity field can be imagined as a population of eddies with a range of sizes and lifetimes. Information about the turbulent flow can be obtained by examining the velocity, length scale and time scales associated with the largest and smallest eddies. A basic concept in the theory of turbulence is that energy is transferred in a cascade from larger to successively smaller eddies. The resolution required to resolve all scales involved in turbulence is beyond what is computational possible. That is why models are developed that take into account the unresolved terms. Therefore, there is a trade-off between computational cost and accuracy of the solution. Three approaches for modelling turbulence are depicted in figure 2.4 and are further explained below the figure.

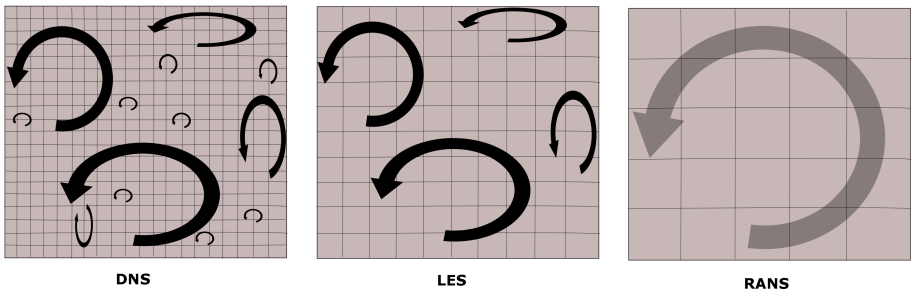

Figure 2.4: Three approaches for modelling turbulence. In DNS the complete set of equations is solved to find all details, LES only captures the large eddies and with RANS the equations are smoothed by time-averaging the parameters.

High frequency, small amplitude fluctuations in the velocity are a hallmark of turbulence. Since the pressure and temperature depend on the velocity, those parameters will fluctuate too. In the Reynolds Averaging Navier Stokes (RANS) equations are written in terms of time-smoothed variables. This means the properties of the flow are time-averaged (e.g. mean velocity, mean pressure, etc). In this way an idea is generated of the turbulent flow, but no full details can be obtained.

In Large Eddie Simulations (LES) the larger scale of motion is simulated by solving a spatially filtered form of the NS equation, whereas the effect of the smaller scale is modelled. To the extent that the mesh can be refined, LES becomes more and more like DNS.

For a Direct Numerical simulation (DNS), all spatial scales -from the smallest dissipative scales up to the total box length L- must be solved with the Navier Stokes Equations in the computational mesh without any turbulence model. The smallest length scale is determined by the Kolmogorov scale [1]. On the Kolmogorov scale the smallest vortexes are seen. This is important since during vortex break up energy is transferred from large scale into small ones, and energy is dissipated in small vortices. Energy is generated in the larger vortexes and dissipated in the smaller ones. The idea in this theory is that the smallest length scales of turbulence are similar for every turbulent flow and that they only depend on μ and energy dissipation ϵ_u.

One can estimate that the number of required mesh points to perform a DNS simulation on is proportional to Re^3 [39]. Therefore, the computational cost is very high, even for low Re numbers. However, by using DNS it is possible to perform numerical simulations and extract information that is difficult or impossible to obtain from experiments. Moreover, DNS data are useful in the development of turbulence models like LES and RANS. For this project data is obtained from DNS simulations, since a one-to-one comparison can be made with the information obtained from natural convection experiments by Nima Rounaghi and Iman Ataei Dadavi. For the future, steps will be made towards a LES or RANS model so that higher Ra and Re number can be reached.

3

Numerical methods

This chapter explains the methods with which the governing equations are solved. Section 3.1 gives an introduction to the toolbox used to find solutions for the problem. The governing equations and the boundary conditions are discussed in section 3.2. The geometry and mesh are discussed in section 3.3 and lastly section 3.4 elaborates on the methods to numerically solve the equations.

3.1. Introduction

The side heated cavity filled with coarse-grained porous media is simulated by varying different parameters in the 'Open source Field Operation and Manipulation' toolbox (OpenFOAM version 2.4.0) with the boussinesqChtMultiRegionFoam solver (see subsection 3.4.1). This is a C++ solver developed for customized numerical solvers to find solutions to Computational Fluid Dynamic (CFD) problems. CFD is the analysis of systems involving fluid flow, heat transfer and associated phenomena (like chemical reactions) by means of computer based simulation. The fundamental basis of a CFD problem is the Navier-Stokes equation. A more complete derivation of the Navier-Stokes equations is presented in section 3.2. The post-processing programs ParaView and Tecplot360 are used to analyze and visualize the data.

The code from OpenFOAM is a free and open source software, making it interesting for Tata Steel to use. The results from this research validated with experiments will be used to model the blast furnace at Tata Steel. This part of the model focuses on the hearth of the reactor while other parts will focus more on the gasification part for example.

3.1.1. Studied cases

To address the research objectives three main cases are defined and developed that will give more insight and the results will form the basis of the answer to the research questions.

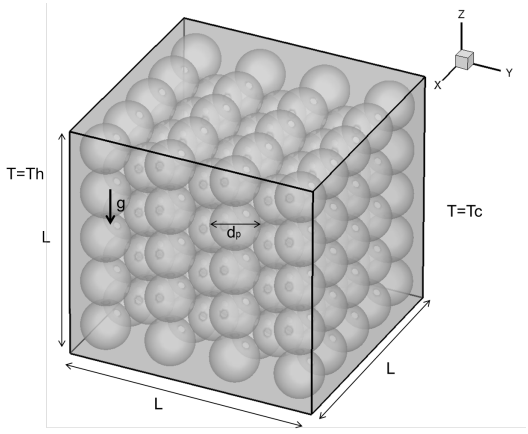

Figure 3.1: 3D sketch of the cavity of the intersection at an arbitrary point along the x-axis. The cubic cavity has a length L, and the spheres have a diameter d_p. The left wall has as a hotter temperature (T_h), and the right wall a colder temperature (T_c).

A 3D representation of the geometry of interest is depicted in figure 3.1. This sketch shows the intersection of the box at an arbitrary point along the X-axis. The cubic cavity of length L=0.1 m is filled with coarse-grained porous media with diameter d_p=0.02 m. The Z-coordinate is chosen to be in the vertical direction, i.e. along the direction of gravity. Furthermore, the spheres are arranged in a BCT packing. Due to this configuration of the spheres, slices in any direction will show a different section of the spheres resulting in more/less spaces for the fluid to flow.

The walls of the cavity are differentially heated; the left wall is hot (T_h) and the right wall is colder (T_c). This is implemented in the boundary conditions of the problem (see subsection 3.2.2)

The influence of the sphere on the heat transfer and flow characteristics in the cavity filled with coarse-grained porous media is investigated by comparing them with the phenomena in an empty box. The empty box has the same dimensions (figure 3.2).

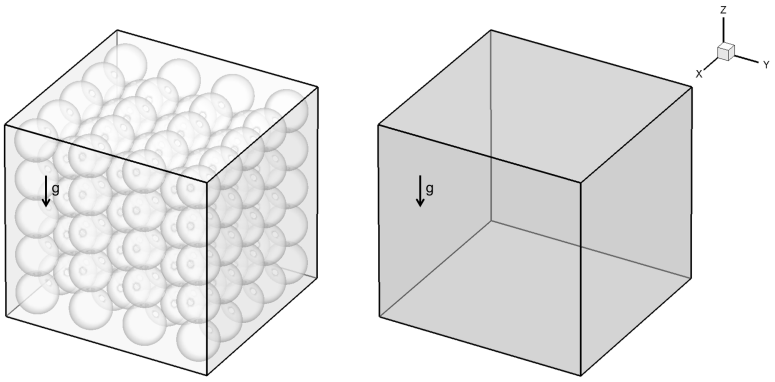

(a) Water filled cavity with hydrogel spheres in a BCT packing arrangement.

(b) Cavity filled with water.

Figure 3.2: The two geometries considered with a) the box with coarse-grained porous media and b) the empty box. Both configurations have the same dimensions.

3.2. Specification

Before the code can be further developed, the equations with their boundary and initial conditions have to be found that describe the temperature and motion of the fluid inside the cavities that are depicted in figure 3.2.

3.2.1. Governing equations

In the convection problem involving a non-isothermal fluid, the unknowns are: velocity, pressure, temperature and density. The governing equations are: continuity, conservation of momentum, conservation of energy and an equation for the state of the fluid. In case of an ideal gas, the equation of state is the ideal gas law. For this problem, the flow problem is dependent on the heat transfer problem through the equation of state: ρ=$\rho(P,T)$ [5].

The governing coupled equations for a problem with convection, Newtonian and non-isothermal fluid, with constant viscosity μ are: continuity, Navier Stokes, the incompressible form of the energy equation and the energy balance for the solid region (indicated with T_s).

The conservation of mass for the 3D system can be written as:

$$\frac{\partial u_i}{\partial x_i} = 0 \tag{3.1}$$

Where u_i is the velocity in the i direction. This incompressible form of the continuity equation states that the divergence of the velocity field is zero everywhere. Since the assumption is made that the density is constant there is no time-derivative term because there is no accumulation/loss in the system.

In parallel, the Navier-Stokes equation can be stated as:

$$\underbrace{\frac{\partial(u_i)}{\partial t}}_{\text{Time rate of change}} + \underbrace{u_j\frac{\partial(u_i)}{\partial x_j}}_{\text{Convective transport}} = \underbrace{-\frac{\partial}{\partial x_i}(\frac{p}{\rho_0}+g\cdot z)}_{\text{Pressure forces}} + \underbrace{\nu_0\frac{\partial^2 u_i}{\partial x_j^2}}_{\text{Viscous forces}} \underbrace{-\beta_0 g(T_0-T)\delta_{i3}}_{\text{Buoyant forces}} \tag{3.2}$$

Here, p, ρ_0, g and β_0 are the pressure, density at reference condition, acceleration due to gravity and volume expansion coefficient respectively. The first two terms on the left hand side of the equation are for the inertial forces, which describe the acceleration in a material reference frame. The term $u_j\frac{\partial(u_i)}{\partial x_j}$ is associated with the convective transport of momentum. At the right hand side there are three terms: the pressure forces, the viscous forces and external forces (buoyant forces in this case) respectively. The viscous forces are represented by the term $\nu_0\frac{\partial^2 u_i}{\partial x_j^2}$ and comes from the variations in viscous stresses. The net buoyancy force is the force on a control volume caused by the combined effects of static pressure variations and gravity. Since the local density differences are small, the Boussinesq approximation is applied. Even for the simplest situations, the solution of the set of equations is complex so that almost all published work assumes this approximation [40]. Here, all density differences are ignored except in the case where it is multiplied with g, the gravitational acceleration. A full derivation can be found in appendix C.

The energy equations for the fluid part in the domain reads:

$$\underbrace{\frac{\partial T_f}{\partial t}}_{\text{Time rate of change}} + \underbrace{u_j\frac{\partial T_f}{\partial x_j}}_{\text{Convection of heat}} = \underbrace{\alpha\frac{\partial^2 T_f}{\partial x_j^2}}_{\text{Diffusivity of heat}} \tag{3.3}$$

The next equation applies to the energy in the solid part of the cavity:

$$\underbrace{\frac{\partial T_s}{\partial t}}_{\text{Time rate of change}} = \underbrace{\alpha\frac{\partial^2 T_s}{\partial x_j^2}}_{\text{Diffusivity of heat}} \tag{3.4}$$

Where T, T_s α are the fluid temperature, solid temperature and thermal diffusivity respectively. The right hand side of both equations represents the conductive heat transfer. This is a measure of the rate of heat transfer of a material from the hot side to the cold side. If the thermal diffusivity α is high, heat will move rapidly through the system because the material conducts the heat quickly. This quantity is a material property and measured in m^2/s.

3.2.2. Boundary and initial conditions

The problem can be fully specified by determining the boundary and initial conditions of equations 3.1 to 3.4. The parameters that need specification are velocity, temperature and time. This will be discussed in the paragraphs below.

Velocities

To address the research questions, the direction and magnitude of the forced component is of great importance. The walls of interest get a positive or negative velocity component, this value is obtained from the results for pure natural convection. The no-slip velocity boundary condition is applied to the walls that do not move. For the second research objective the direction of the forced component is investigated. Therefore, a box with the sides of the cavity are imposed with a Dirichlet boundary condition of a constant velocity.

So the velocity boundary conditions for the different setups are:

NC	$u_x = u_y = u_z = 0$	at x=0, L; y=0, L; z=0, L.
MC by moving sides	$u_x = u_y = 0$	at x=0, L; z=0,L and $u_z = \pm\, u$ at y=0, L.

Left wall	$T = T_h$	at y=0
Right wall	$T = T_c$	at y=L
Front/back wall	$\frac{\partial T}{\partial x} = 0$	at x=0, L (adiabatic wall)
Top/bottom wall	$\frac{\partial T}{\partial z} = 0$	at z=0, L (adiabatic wall)

Temperature

A temperature gradient is imposed by maintaining the side walls of the cavity at different temperature. The temperature of the hot and cold wall will be varied to create a difference in Ra. The temperature conditions are given by:

There is a thermal equilibrium at the interface i between the fluid and solid spheres where there is only conductive heat transfer normal to the interface. Therefore the following Neumann boundary condition implies at the interface:

$$k_f \frac{\partial T_f}{\partial x_j}|_i = k_s \frac{\partial T_s}{\partial x_j}|_i$$

Time

The initial conditions for the solid and fluid phase are:

$$T_s(t=0) = T_f = T_0 = \frac{1}{2}(T_h + T_c)$$

3.2.3. One domain formulation

The one domain formulation requires a single set of governing equations for the entire domain that can give scaling laws. This is mainly important for the post-processing step of the data.

The temperature is scaled by:

$$T^* = \frac{T - T_H}{T_H - T_C} \tag{3.5}$$

In the mixed convection situations, the velocity magnitude can be scaled by the velocity of the forced component (moving wall velocity):

$$u_{Mag} = \sqrt{u_x^2 + u_y^2 + u_z^2} \tag{3.6}$$

$$u^*_{Mag} = \frac{u_{Mag}}{u_{FC}} \tag{3.7}$$

The velocity scale for natural convection is based on [3]. See section C.1 in appendix C for more information.

$$u_i = Ra^{\frac{3}{7}} \frac{\alpha}{H} \tag{3.8}$$

3.2.4. Numerical treatment

The governing equations are solved sequentially with a finite-volume discretisation process since this method provides good results with a minimum number of computation points [41]. The equations are discretized using the finite-volume method, employing an unstructured grid. The name 'Finite Volume' refers to the small volume that surrounds every node on a mesh. This method converts partial differential equations into a set of coupled equations and values are calculated at discrete places on the meshed geometry.

The `fvSchemes` dictionary in the `system` directory sets choice of finite volume discretisation scheme for the terms in equations. The models and settings used are listed in table 3.1.

Setting	Value
Time scheme	First order implicit Euler scheme
Gradient scheme	Linear
Divergence scheme	VanLeer scheme
Laplacian scheme	Linear limited 0.5
Interpolation scheme	Linear
Pressure and velocity coupling	PISO (see section 3.4.1)

Table 3.1: Solver settings used in OpenFOAM.

3.3. Domain and mesh

In CFD, the flow and temperature equations presented in section 3.2 are solved on a grid that is confirming the geometry depicted in figure 3.1. The equations are approximated over the elements of the geometry. Therefore, a mesh is made from the cubic cavity, which is made out of cells. The number of cells has an influence on for example the computational time and solution precision. Besides, different cell shapes have an influence on the accuracy of the solution [41].

For an empty cavity, the hexahedron cell shape is used. For the same cell amount, the accuracy of the solutions in hexahedral meshes is the highest [42]. The reference empty 3D cavity consists of 128^3 elements, so 2,097,152 hexahedron shaped cells in total. Section 4.1 elaborates more about the grid independence study.

The filled cavity is built up from tetrahedron cells. The spheres inside the cavity makes the connectivity of the grid structure inside the box highly irregular. The mesh size is based on the diameter of the spheres, for this configuration d/16 is used making the total number of cells 4,701,863.

All cells together form the mesh of the geometry. Figure 3.3 shows the structured mesh of the empty water filled cavity and the irregular configuration of cells for the beads filled cavity. The mesh closer to the boundary should be fine enough to capture the physics in the boundary layer. Figure 3.3a clearly shows a mesh refinement near the walls, and more coarse cells in the center of the cavity. In the case of a domain with coarse-grained porous media, the number of grid cells increases to fulfill the requirement of a fine mesh close to a solid boundary.

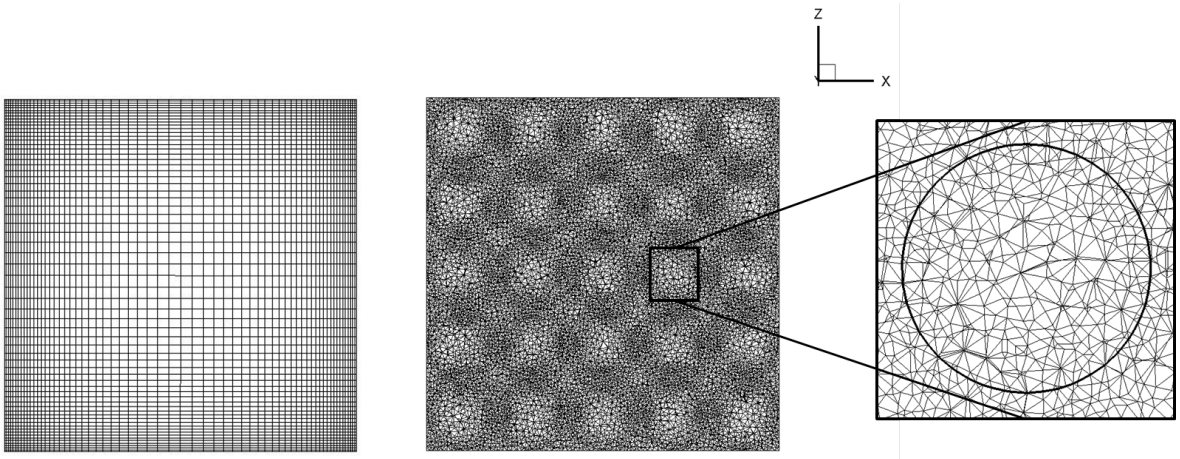

(a) The resulting mesh for the water filled cavity.

(b) Mesh for the cavity filled with coarse grained porous media.

Figure 3.3: Mesh for the two different cavities.

The size of the mesh on which the equations are solved are based on the required detailedness of the solution. In section 2.5 already touched upon this requirement. Here it is stated that for a DNS all spatial scales must be solved, and the smallest length scale is determined by the Kolmogorov scale [41].

A detailed literature review on the spatial resolution requirements in a convective turbulent flow is reported in [1]. An overview of the requirements in the boundary layer and global mesh size can be found in appendix D. Table 3.2 gives an overview of a rough estimation of thermal and velocity boundary layer

thickness and the number of cells for different Ra numbers. This numbers are calculated for the situation of an empty cavity. In case of a domain filled with coarse grained porous media, the number of grid cells required increases. This results form the thermal and velocity boundary layer that will be generated around the spheres.

Ra	h^{global} (m)	δ_{Th}(m)	δ_u (m)	$N_{Th.BL}$	$N_{v.BL}$	No. of cells
1.17×10^5	0.00395	0.00357	0.00637	2	3	1.63×10^4
1.17×10^6	0.00180	0.00175	0.00178	3	4	1.72×10^5
1.17×10^7	0.000833	0.00086	0.000833	3	6	1.74×10^6

Table 3.2: Overview of the rough estimation of the mesh size of a cavity filled with water for different Ra numbers. The calculations are done based on [1] and appendix D gives the equations.

3.4. Numerically solving the Navier-Stokes equations

The governing equations introduced in section 3.2 are solved using the CFD software from OpenFOAM. The convection of heat in the system depends on the magnitude and the direction of the local velocity field. The two equations (3.1 and 3.2) are intricately coupled because every velocity component appears in each momentum and the continuity equation. The most complex issue to resolve is the role of the pressure; since the flow is incompressible the density is constant and hence by definition not linked to the pressure. The coupling between pressure and velocity gives a constraint on the solution of the flow field: if the correct pressure field is applied in the momentum equations the resulting velocity field should satisfy continuity. So, at this point there are two issues to deal with: finding a way to deal with the non-linearity in the set of equations and the linkage of the pressure and velocity. These problems can be resolved by adapting an iterative solution strategy with the help of an algorithm.

3.4.1. The algorithm

Solving the Navier-Stokes equations requires numerical techniques for coupling the pressure and momentum quantities, this is done by for example SIMPLE, PISO or PIMPLE algorithms. All these algorithms are iterative solvers. In this project, a solver is developed in-house that combines the boussinesqPimpleFoam and the chtMultiRegionFoam solver. The chtMultiRegionFoam is meant to be used for heat transfer between a solid and a fluid. The developed solver is validated by checking if the obtained results are in agreement with literature. This is done based on the article from Kaminski [43].

PISO

The boussinesqChtMultiRegionFoam solver uses the iterative PISO algorithm, which is an abbreviation for "Pressure Implicit with Splitting of Operator". Figure 3.4 gives a schematic overview of the steps taken in the algorithm. The loop consists of a time step loop and this inner loop there is one predictor step and two corrector steps. In the first step, the predictor step, the momentum equation is solved with a guessed pressure p^* to give velocity components u_i^*. These obtained velocities will not satisfy continuity unless the pressure p^* is correct. So the first corrector step is introduced to give a velocity field u_i^{**} which satisfies the discretized continuity equation. A second correction step is made to by solving the momentum equations once more. This gives a second pressure corrector from where the twice-corrected velocity field u_i^{***} is obtained. These velocities are considered to be the correct twice-corrected velocity u_i and p. If the solution is converged, the loop starts over again for a new time step.

For this procedure under-relaxation is required to stabilize, i.e. decrease the possibility of divergence or oscillations in the solution, the calculation process.

The time steps in the algorithm are done explicitly, meaning that the computation of the variables at the new time step are done based on the previous time level.

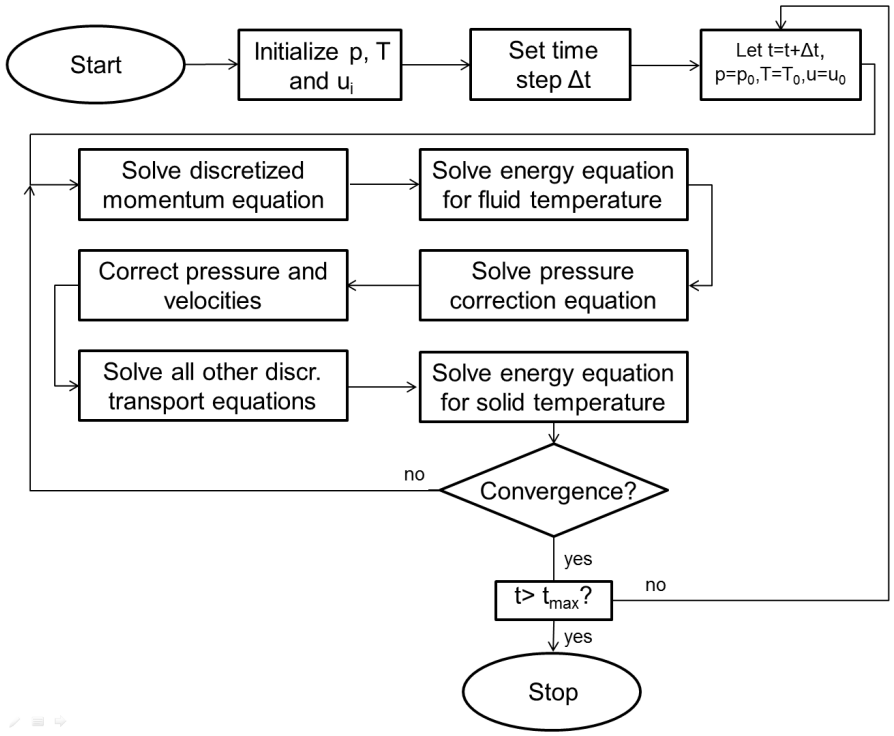

Figure 3.4: Flow chart of PISO scheme.

MultiRegions

The coupling of heat transfer between the fluid and solid phase is done with the chtMultiRegionFoam solver. The different phases in the system are seen by OpenFOAM like a set of multiple simple cases running simultaneously and linked by their boundary conditions. Variables are taken from one region boundary to the corresponding neighbouring region boundary. Each region (fluid and solid) have their own directories within each of the main directories. In these directories the parameters are defined.

The regions are defined in the mesh and, before starting the simulation, splitted into segments according to the pre-defined zones. For the post-processing of the data, the regions need to be reconstructed into one file.

3.4.2. Material properties

The two materials in the domain are hydrogel spheres and water as fluid phase. Table 3.3 lists all the used material properties [44].

Parameter	value	unit
Pr	5.4	-
ρ_{f}	998	kg/m^3
ρ_{s}	998	kg/m^3
C$_p$	4182	m^2/s^2 K
k$_f$	0.6	W/ (m K)
k$_s$	0.6	W/(m K)
α	0.143 $\times 10^{-6}$	m^2/s

Table 3.3: This table lists all the material properties of the problem. The fluid phase is water and the solid phase hydrogel.

3.5. Convergence

The steady state situation is the moment when the flow and heat transfer are unchanging in time. There are multiple ways to check the state of the system. One possibility is finding the Nusselt number in the 'hot' and

'cold' region (i.e. the region near the wall with the higher/lower temperature). Nusselt is calculated by the temperature gradient near the wall divided by the temperature difference.

This equation is derived from the local heat transfer coefficient [5]:

$$\phi''_q = hA_{\text{box}}(T - T_\infty) \tag{3.9}$$

$$\phi''_q = -kA_{\text{box}}\frac{\partial T}{\partial x} \tag{3.10}$$

Where k is the thermal conductivity and A_{box} the surface where heat transfer takes place.

Equation 3.9 and 3.10 are equated to obtain the Nu number at the wall:

$$Nu_y = \frac{-L\frac{\partial T}{\partial y}|_{x=0}}{\Delta T} \tag{3.11}$$

$$\tag{3.12}$$

The convergence of the simulation is checked by using probes at difference locations in the geometry. Appendix F gives the computational code that can be found in `controlDict` dictionary in the `system` directory and that calculates the flux at the probes in the cavity.

The flow was found to be steady based on the graphs depicted in figure 3.5. Here it can be seen that the average Nusselt number (figure 3.5a) reached a constant number at one point, this also counts for the temperature values (figure 3.5b). For this graph, multiple points are taken in the domain and their temperature values are depicted as function of time divided by the large circulation time (LSC). A derivation of τ_{LSC} can be found in appendix D. The convergence plotted in figure 3.5 came from a mixed convection situation where the wall velocity was u_{FC}=0.00141 m/s. With the help of both graphs, it can be concluded that this simulation has reached a steady flow.

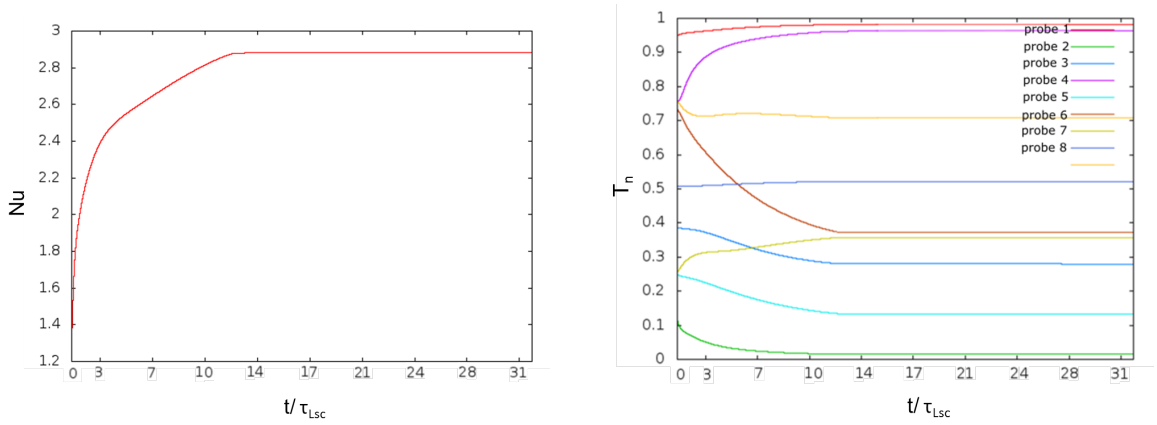

(a) Average Nu number

(b) Normalized temperature at various probes in the domain

Figure 3.5: Convergence of two quantities in time for a) the average Nu and b) temperature at different probes in the system.

4

Natural convection

This chapter elaborates natural convection in a side heated cavity. Figure 4.1 depicts a schematic 2D representation of natural convection in a water filled and water filled cavity with packed beads. The temperature difference between the hot and cold wall creates a flow: the natural convection flow. The obtained numerical results for an empty cavity are compared with experiments performed by master student Nima Rounaghi. The following sections will present the information on fluid flow, temperature and resulting heat transfer fields for an empty cavity figure 4.1a and a cavity filled with coarse grained porous media 4.1b.

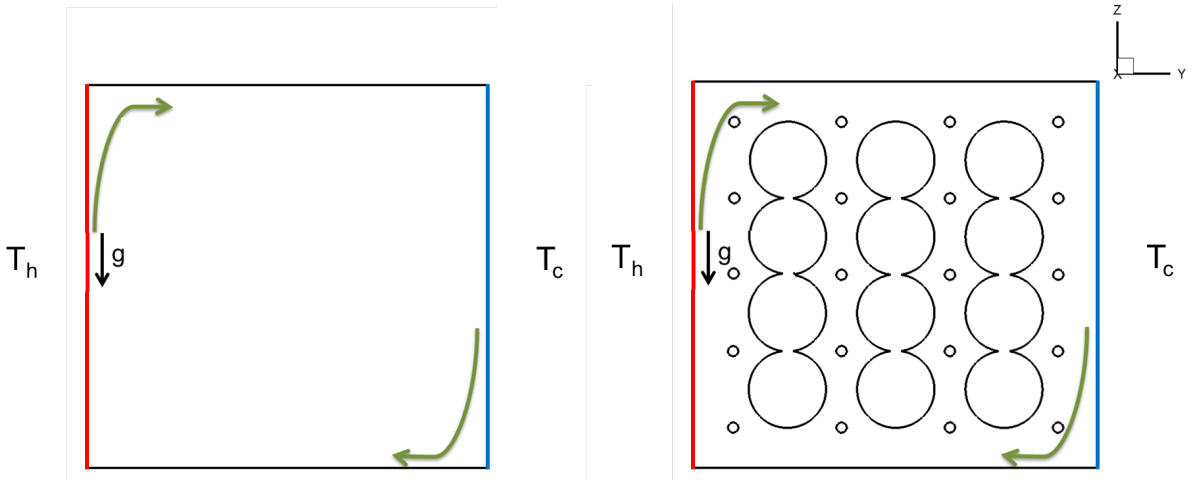

(a) Schematic 2D representation of natural convection in a water filled cavity.

(b) Schematic 2D representation of natural convection in a cavity filled with coarse grained porous media.

Figure 4.1: Schematic 2D representation of natural convection in a) an empty cavity and b) a cavity filled with coarse grained porous media. The heat transfer for the two situation are compared with each other.

4.1. Mesh dependency for an empty cavity

In the case of natural convection in an empty cavity (see figure 3.3a) the mesh quality is verified. One of the factors that determines the quality of the mesh is the independence of the grid on the obtained solution. This implies that the desired property of the fluid does not vary with respect to increasing mesh elements. This is an essential tool to know how good your mesh is.

In this study, the simulation is ran various times with increasing finer mesh size. For this purpose, a cavity filled with water with different number of elements is used. The simulations were performed for the case of natural convection in a empty cavity with water as fluid and Ra=10^8. Table 4.1 gives an overview of the number of elements, the corresponding cell size and the average Nu number in the domain.

The mesh is validated with literature and summarized in table 4.2. The values founded for a cavity filled

Mesh	1	2	3
Grid	32^3	64^3	128^3
Cell size (m)	3.13×10^{-3}	1.56×10^{-3}	7.81×10^{-4}
Nu	36.8	34.1	33.6
Difference relative to fine mesh	8.70%	1.47%	-

Table 4.1: The Nu number over the domain of an empty cavity at Ra=10^8 for various grid sizes.

with water show agreement with the data obtained in the present study. It can be concluded that a mesh with 128^3 is fine enough to capture the physics.

Study	Grid	Pr number	Nu number
This study	128^3	5.4	33.6
Lage and Bejan et al [45]	52^2	10	35.2
Snoussi *et al* [46]	129^3	7.6	34.2
Experimental solution by Nima	-	7.6	34.4
Janssen and Henkes [47]	120^3	0.71	30.0
Markatos and Pericleous [48]	40^2	0.71	32.0
Peng Wand *et al* [49]	200^3	0.71	29.9

Table 4.2: Nusselt numbers from literature for a differentially heated empty cavity for Ra=10^8.

The mesh independence study for the porous media filled cavity was carried out by Manu Chakkingal (figure 3.3b). A mesh size based on the sphere diameter was determined. It was found that a mesh of d/16 fulfilled the mesh independence criteria [1]. This resulted into 4.7 million cells for this case.

4.2. Comparison with experiments

The results obtained for natural convection in a side heated cavity are compared with the experiments performed by master student Nima Rounaghi. This step is an extra verfication for the mesh and the solver. The experimental data in the Nu-Ra curve depicted in figure 4.2 obeys a power-law relationship: Nu=0.239 $Ra^{0.2677}$. The results are in good agreement with literature [45, 46].

The results obtained from simulations are represented with red dots in figure 4.2. The difference between the experimental and simulated data shows a deviation of about ±1.1-2.3%.

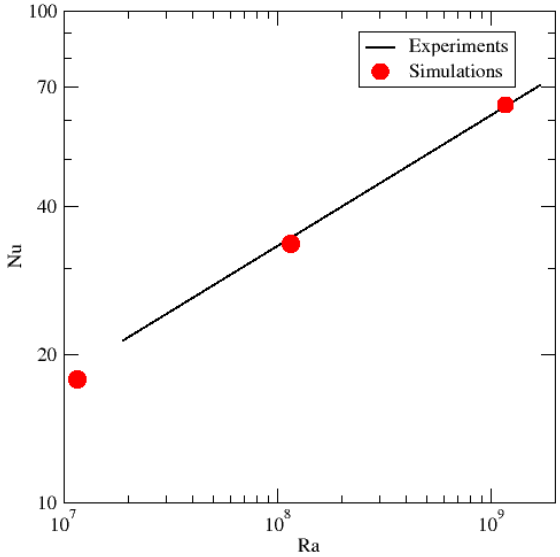

Figure 4.2: Nu-Ra relationship for natural convection in a side heated empty cavity. The solid curve present the experimental obtained power law; symbols, simulations at different Ra numbers.

4.3. Natural convection flow field

The natural convection flow in the domain is visualized by plotting isocontours of the velocity magnitude. The u_{mag} is normalized with the scaling factor for natural convection of $u_{scale}=Ra^{\frac{3}{7}}\ \frac{\alpha}{L}$ [3].

Very small magnitudes of velocity are observed for at Ra (Ra=10^5, figure 4.3a). The buoyant force is small so the fluid in the domain is barely affected. With an increase in Ra the u^*_{mag} at the walls and inside the domain is higher. Higher magnitudes are observed at higher Ra (Ra=10^6, figure 4.3b). For even higher Ra (Ra=10^7, figure 4.3c) the buoyant forces is getting stronger and creates a wall driven flow. The highest natural convection velocities are observed in proximity walls of the cavity. This is characteristic for a side heated cavity.

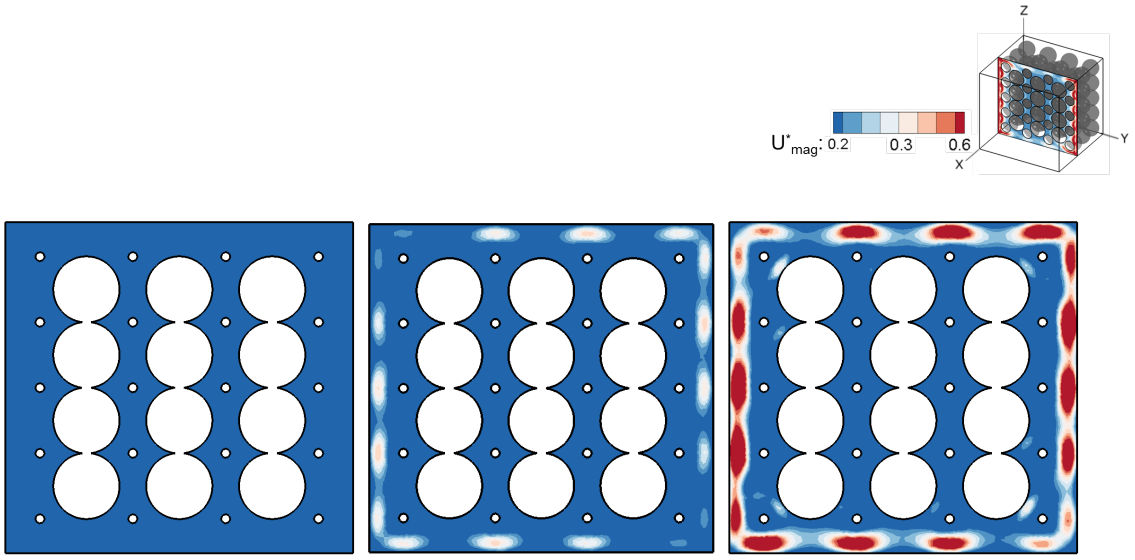

(a) Ra=10^5 (b) Ra=10^6 (c) Ra=10^7

Figure 4.3: Normalized velocity magnitude u^*_{mag} for different Ra numbers. The velocities are scaled with the scaling factor [u]=$Ra^{\frac{3}{7}}\ \frac{\alpha}{L}$ [3]. The isocontours are taken at slice $\frac{y}{L}$=0.57.

4.4. Temperature

The temperature isocontours are plotted for three different Ra numbers. With an increase in Ra the buoyant force increases and the u^*_{mag} increases. This has also an effect on the temperature distribution.

For small Ra (Ra=10^5) the isocontours show a linearly behaviour indicating that conduction is the dominant mechanism of heat transfer. With an increase in Ra, the normalized temperature isocontours is getting less linear and the isocontours are more curved. Besides, due to the increase in flow the thermal boundary layer is more spread out in the Y-direction. An increase in Ra gives an increase in buoyant forces. As observed in figure 4.3, an increase in Ra results in a higher momentum in the cavity. This makes convective heat transfer the main mode of heat transfer at higher Ra.

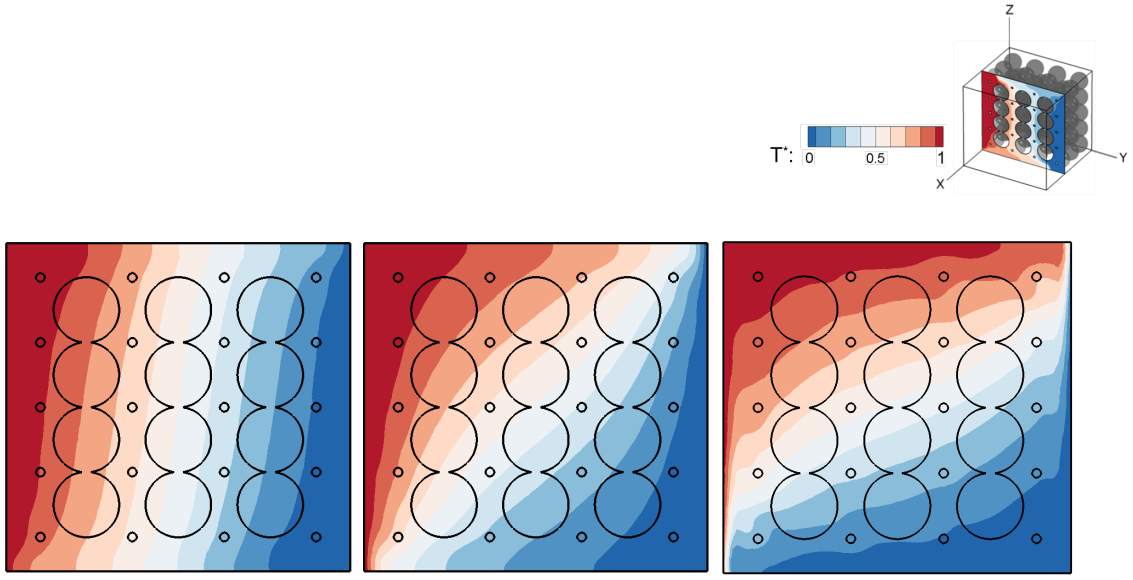

(a) Ra=10^5 (b) Ra=10^6 (c) Ra=10^7

Figure 4.4: Instantaneous temperature isocontours for different Ra numbers. The isocontour slices are taken at $\frac{y}{L}$=0.57.

4.5. Heat transfer

The flow and temperature field presented above have an effect on the total heat transferred. This is depicted with isocontours of the Nu number at $\frac{y}{L}$=0 (the hot wall) in figure 4.5.

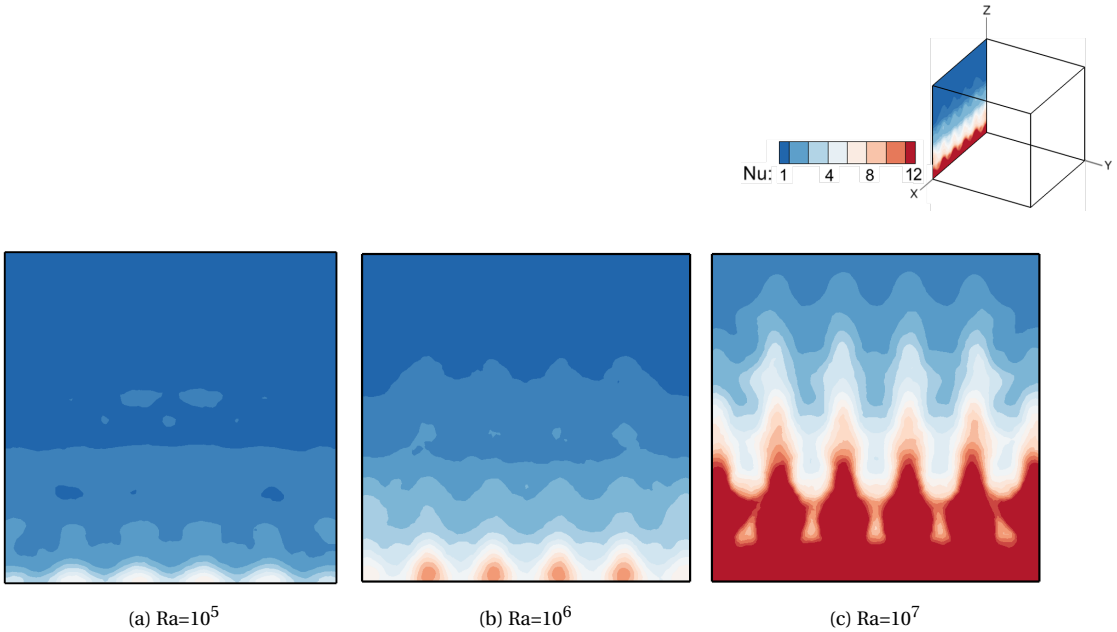

(a) Ra=10^5 (b) Ra=10^6 (c) Ra=10^7

Figure 4.5: Instantaneous Nu number isocontours at $\frac{y}{L}$=0 (the hot wall) for different Ra numbers.

For low Ra (Ra=10^5, figure 4.5), the Nu isocontour plot indicates a conduction dominant plane. It is due to the low flow velocity as observed in figure 4.3. With a small magnitude, the heat is transferred by diffusion and Nu is approximately 1 in this case. For Ra=10^6 a small thermal gradient is visible at the bottom of the plane depicted in figure 4.5b. Furthermore, the gradient is exists further along the plane compared to figure 4.5a. For larger Ra, Ra=10^7, the buoyant force is stronger. The thermal gradient is able to penetrate further over the plane as seen in figure 4.5. The temperature isocontour depicted in figure 4.4 shows a thermal boundary layer that is more spread-out in the lateral direction.

Figure 4.6 shows Nu versus Ra for the empty cavity and the cavity filled with coarse grained porous media. For lower Ra (Ra=10^5) the empty cavity the heat transfer rate is about five times higher compared to the filled cavity. The spheres create friction for the fluid flow and therefore the heat transfer mainly goes through conduction. With an increase in Ra, Nu increases for both cavities.

The discrepancy in Nu between the empty and filled cavity decreases with increasing Ra. For Ra=10^6 the heat transfer rate is about four times higher and when Ra=10^7 Nu for the empty water filled cavity is twice as high than for the filled cavity. The buoyancy force generates more momentum by which the fluid can move more easily between the spheres. For high Ra (Ra=10^8) the heat transfer for both situations are in the same order of magnitude. The fluid flow has more momentum by which it can overcome the viscous forces from the spheres. Convection is the dominant heat transfer mechanism here.

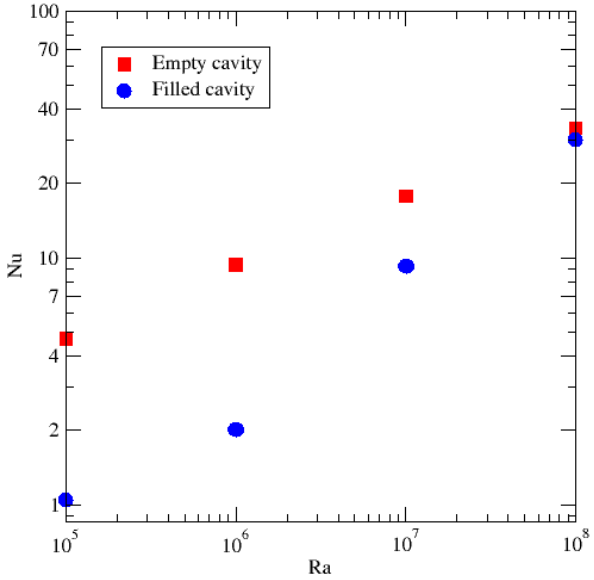

Figure 4.6: Nu versus Ra plot for an empty cavity and a cavity filled with coarse grained porous media.

4.6. Summarized

The following things can be concluded about natural convection in a side heated cavity.

- The data obtained by the simulations for an empty cavity showed close agreements with experiments.
- For low Ra (Ra=10^5) conduction is the dominant heat transfer mechanism. With an increase in Ra the buoyant force increases and the total heat transfer in the domain increases too.
- The difference in Nu between an empty and filled cavity is decreasing with an increase in Ra. Nu for the water filled cavity at low Ra (Ra=10^5) is about five times higher, and for Ra=10^7 the water filled cavity transports about 10% more heat than the water filled cavity. The higher buoyancy forces gives the fluid more momentum to meander through the coarse grained porous media.

5

Forced convection

This chapter elaborates forced convection in a side heated lid-driven cavity. Forced convection will be obtained by making the gravitational constant g=0 and this results in Ra=0. The forced convection part in a mixed convection situation can be created by a wide range of variables a topic that was briefly touched upon in section 2.3. The scope of this project is on lid-driven cavities, where the side walls are moving as schematically depicted in figure 5.1. In this chapter the forced component is discussed and the resulting flow and temperature field for an empty cavity (figure 5.1a) are compared with a cavity filled with hydrogel spheres (figure 5.1b). The wall velocity is varied while all other parameters are fixed.

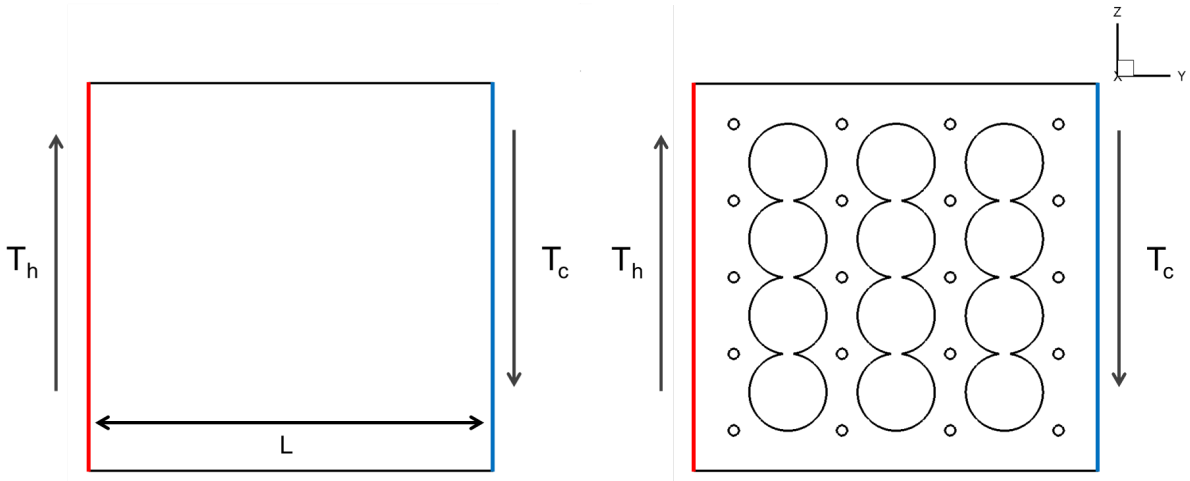

(a) Schematic 2D representation of forced convection by moving side walls in an empty cavity.

(b) Schematic 2D representation of forced convection by moving side walls in a cavity filled with coarse grained porous media.

Figure 5.1: Schematic 2D configurations of forced convection created by moving side walls. The flow, temperature and heat transfer are compared for a cavity filled with hydrogel spheres with an empty cavity. In this research, the wall velocity is varied while all other parameters are fixed.

5.1. Flow in empty and filled cavity

The magnitude for the flow in both empty and filled cavity is expressed in terms of the Re number. The number is determined based on the wall velocity.

Figure 5.2 shows the normalized velocity magnitude for three different Re numbers. The definition for Reynolds is based on:

$$Re = \frac{\rho v L}{\mu} \tag{5.1}$$

Where ρ and μ are the density and viscosity of the fluid. The length L is based on the length of the cavity and the velocity u is determined by the wall velocity (see figure 5.1). See appendix A for more information.

The magnitude is normalized with the wall velocity corresponding with Re=319 (figure 5.2b). Figure 5.2a shows u^*_{mag} for low Re. The wall velocity is low and therefore the magnitude inside the center of the domain is not affected. With an increase in Re higher magnitudes are observed inside the domain and around the walls. The flow is mostly wall dominated.

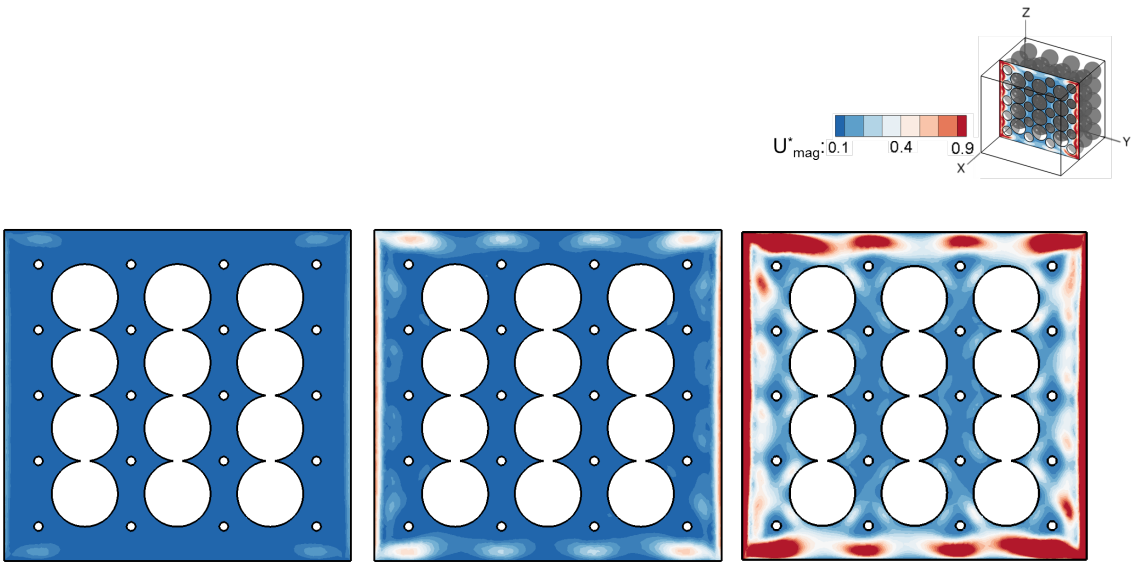

(a) Re=91 (b) Re=319 (c) Re=1150

Figure 5.2: Normalized velocity magnitude isocontours at x-plane $\frac{x}{L}$=0.57 for Ra=0 varying Re.

5.2. Temperature distribution

The temperature distribution is plotted as isocontour at slice $\frac{x}{L}$=0.57 varying Re. With an increase in Re, the wall velocity is a higher by which the fluid flows with a higher magnitude in the clockwise direction as depicted in figure 5.1. The temperature isocontours in figure 5.3c show more oscillation compared to figure 5.3a. The higher Re creates a higher domain velocity, as seen in figure 5.3, which reflects the temperature distribution. Moreover, with an increase in Re the thermal boundary layer increases. Besides, the layer shows more lateral spread in the Y-direction. The width of the isocontours close to the wall decreases due to the higher wall velocity. The thermal boundary layer for high Re (Re=1150, figure 5.3c) is not a continuous isocontour line. The higher wall velocity gives the fluid near the wall a higher momentum. A re-circulation flow arises due to the change in momentum of the fluid that is hitting the top wall. Fluid with a higher temperature gradient goes along with this recirculation loop.

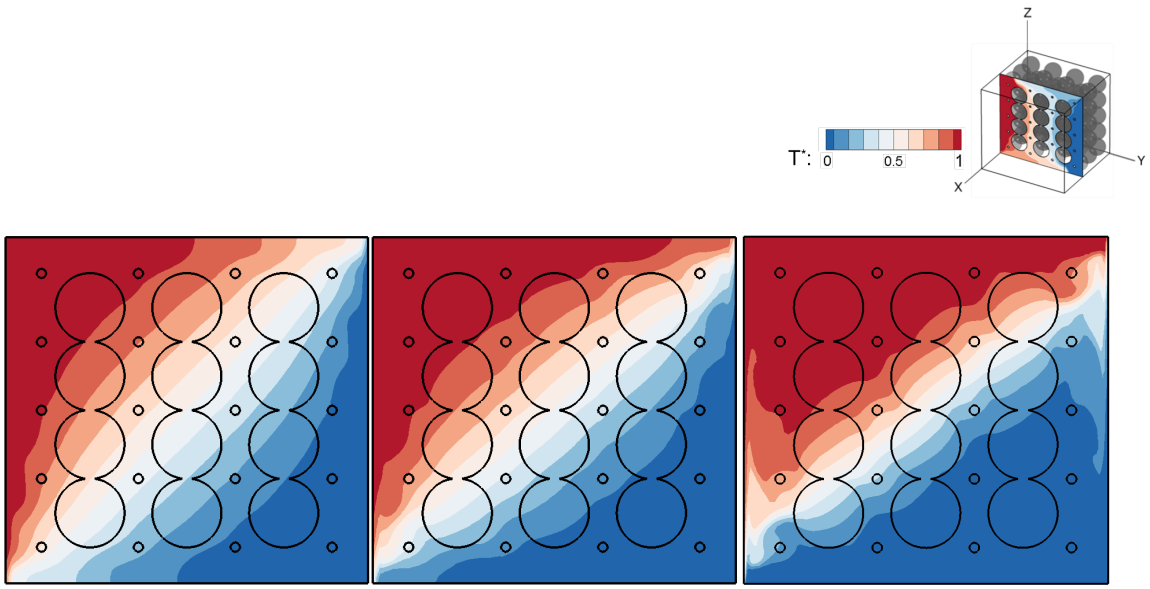

(a) Re=91 (b) Re=319 (c) Re=1150

Figure 5.3: Instantaneous normalized temperature isocontours at x-plane $\frac{x}{L}$=0.57 for Ra=0 varying Re.

5.3. Heat transfer

The flow field and temperature distribution affect the total heat transfer in the domain. This is depicted in figure 5.4 with isocontours of the Nu number varying Re at $\frac{y}{L}$=0 (the hot wall). With an increase in Re a higher temperature gradients is observed. The higher wall velocity results in the hot fluid to be carried further upstream across the heated wall.

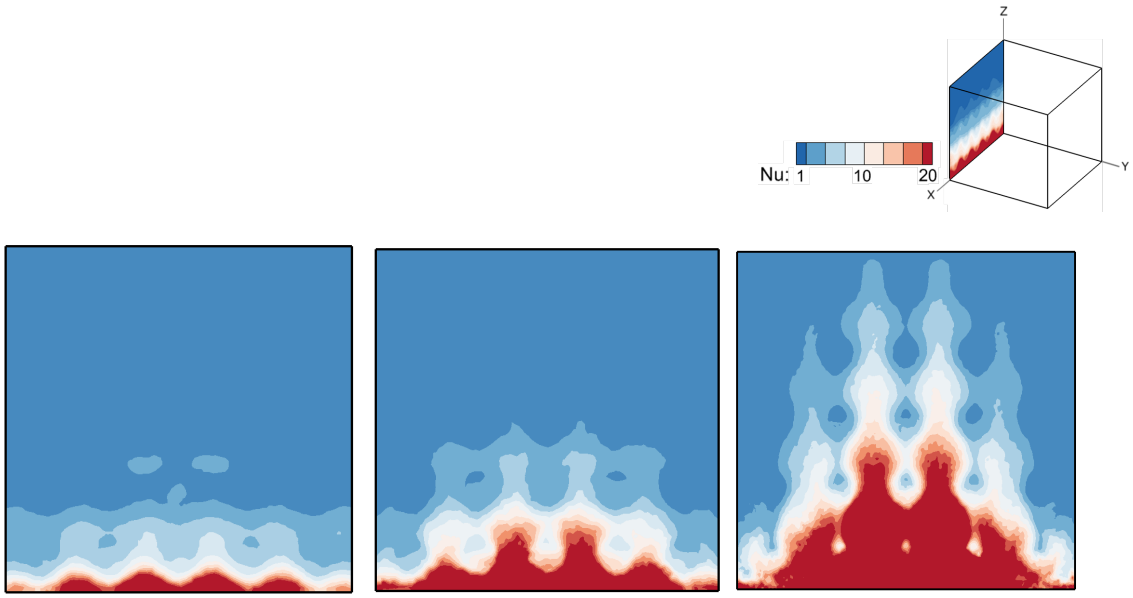

(a) Re=91 (b) Re=319 (c) Re=1150

Figure 5.4: Instantaneous Nu isocontours for forced convection situation at $\frac{y}{L}$=0 (the hot wall) with Ra=0 varying Re.

For higher Re, the dominant heat transfer mechanism is convection. In the situation of low Re (Re=91, figure 5.4a) conduction is the main mechanism of heat transfer. Nu values close to 1 are observed in the plane depicted in figure 5.4a.

Besides, the highest temperature gradients are observed in the center of the planes depicted in figure 5.4. Here the wall velocity affects the fluid more compared to the locations close to the other walls. In the locations

close to the walls, lower Nu values are observed.

Figure 5.5 shows the Nu-Re plot for both situations. For low Re in the cavity filled with coarse grained porous media, the main mode of heat transfer is by conduction since Nu is close to 1. The wall velocity is too low to create a circulating flow in the domain. With an increase in Re the total heat transfer increases too. This results from a higher domain velocity by which the heated fluid can travel along with.

The heat transfer in the empty cavity is higher than in the cavity filled with coarse grained porous media. In the case that Re~100, the water filled cavity transports about 5 times more heat than in the case of the cavity filled with coarse grained porous media. The fluid in the cavity filled with coarse grained porous media the flow has to meander through the spheres. This is hindering the convective heat transfer and results in a lower Nu. With an increase in Re, the difference between the two cavities decreases. For the situation where Re~1000, the Nu number for water filled cavity is almost twice as high compared to the water filled cavity. The higher wall velocity gives the fluid more momentum by which it can overcome the viscous forced generated by the spheres in the domain. Plotted on a log-log scale, both situations obey a power law relation above a certain Re.

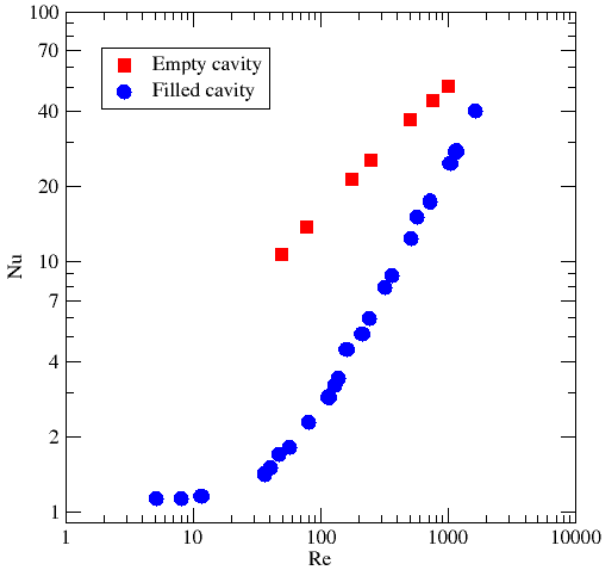

Figure 5.5: Nu versus Re plot where Ra=0. The cavity filled with water is indicated with red squares and the cavity filled with coarse grained porous media is represented by blue dots.

5.4. Summarized

The following things can be concluded about the situation with a side heated cavity and moving side walls were Ra=0.

1. The movement of the walls create a wall-dominant flow.
2. A higher wall velocity creates a higher domain velocity.
3. A higher Re creates a thicker thermal boundary layer.
4. With an increase in Re, the total heat transfer increases. For moderate Re values (Re=10-1000) the heat transfer in an empty cavity is higher then in a cavity filled with coarse grained porous media. For Re=100, Nu is about five times higher for the water filled cavity. With an increase in Re, the discrepancy in heat transfer rate between the water filled and cavity filled with beads decreases: for Re=1000 Nu is about two times higher for the empty cavity. The spheres are blocking the flow due to which with the convective heat transfer is hindered.

6

Assisting mixed convection

In this chapter, the situation of assisting mixed convection is discussed. Here, the forced convection created by the movement of the wall is in the same direction as the natural flow. This is schematically depicted in figure 6.1. Section 6.1 gives information about porosity in the cavity filled with coarse grained porous media. Section 6.2 will elaborate more about the flow profiles for an assisting mixed convection case. The focus of section 6.3 is on the resulting temperature isocontours. Section 6.4 discusses the effect of the flow and temperature fields on the total heat transfer in the domain. Lastly, section 6.5 states the most important points found based on the figures and graphs in this chapter.

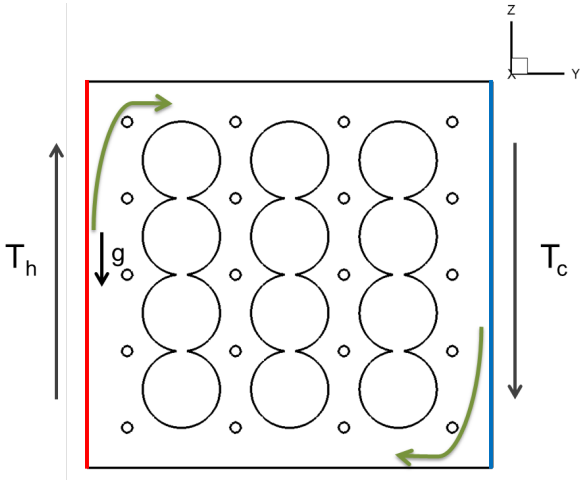

Figure 6.1: 2D representation of assisting mixed convection in a side heated cavity filled with coarse grained porous media.

6.1. Porosity

In this section the spatial variation of available space for the fluid is discussed. This is expressed in terms of porosity.

The porosity is a measure of the void (empty) spaces in a cavity. This is the ratio of the volume fraction of the void-space divided by the total volume. The average porosity of the total cavity is ε=0.38. A closer look is taken to the local porosity inside the cavity, since this is an important parameter in the context of flow channeling near the wall.

This porosity is calculated by the surface area of the solid part of the y-slice divided by the total area. In figure 6.2 the variation of ε inside the box is plotted versus the normalized wall distance in the y-direction (between the hot and cold wall). The particles are packed in an ordered way, therefore a repeating structure of oscillations is visible in figure 6.2. Close to the walls $\varepsilon \approx 1$, indicating a layer of fluid between the walls and spheres. Towards and in the center of the cavity the porosity varies between ε=0.2-0.6, that points out the presence of solid in this part of the domain.

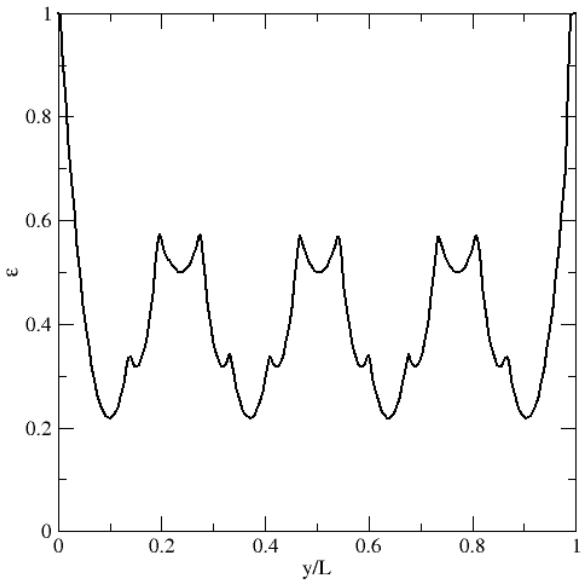

Figure 6.2: Porosity as function of the position at the y-axis. A high porosity means that there is a lot of fluid while a lower velocity is an indication of more solid in the domain.

These findings are to be kept in mind when looking at the flow and temperature profiles in the following sections. Since a momentum and thermal boundary layer will be created around the spheres, the velocity field, temperature distribution and the heat transfer will be influenced. This behaviour was for example described in an article by Vafai et al [28].

6.2. Assisting flow

The title of this section, assisting flow, refers to the situation where the forced component is in the same direction as natural convection and therefore can assist the natural flow as depicted in figure 6.1. U_z is normalized with the maximum velocity obtained for Ri_m=0.13. In figure 6.3 u_z^* isocontours are depicted at x-slice $\frac{x}{L}$=0.57 for three different Ri_m numbers at Ra=10^7.

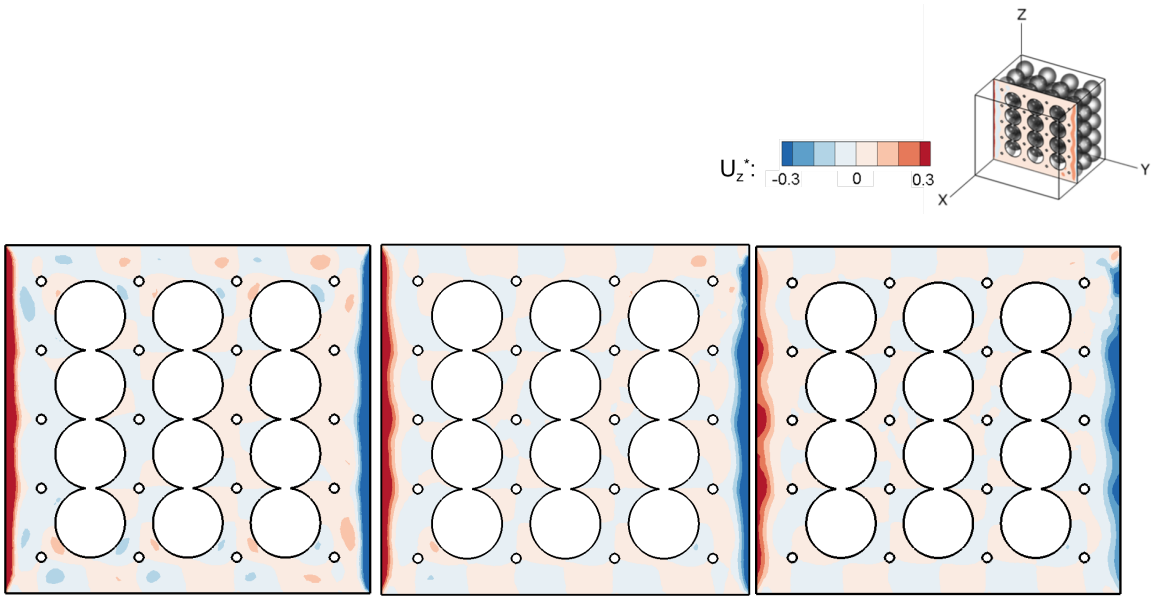

(a) Ri_m=0.04 (b) Ri_m=0.1 (c) Ri_m=0.52

Figure 6.3: Normalized u_z velocity for x-planes at $\frac{x}{L}$=0.57 for Ra=10^7 varying Ri_m.

At the first glance, all three figure in figure 6.3 show the same behavior: a positive (upward) velocity at the left boundary and a negative (downward) movement at the right wall, the cooled wall. This is caused by the moving walls: the left wall is going up and the right wall down. The circulation of fluid in the domain is in clockwise direction. Some perturbations are seen in the isocontour lines in the corners, which is characteristic for lid-driven problems according to [50]. The wall movement and buoyancy force gives the fluid an upward/downward movement, and a change in momentum is created when the flow hits the top/bottom wall. Moreover, an aligned velocity is observed for the forced dominated regime (figure 6.3a, Ri_m=0.04). The u_z^* is getting less aligned to the walls when natural convection is becoming more dominant. In the center of the cavity, low values of u_z^* are observed due to the scarcity of available space.

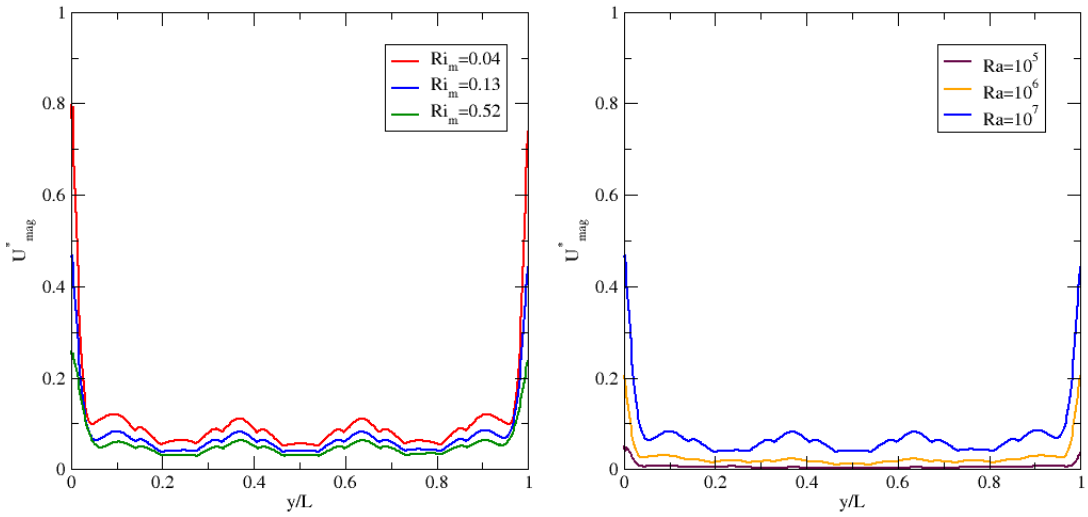

(a) Normalized average velocity magnitude for Ra=10^7 for different Ri_m.

(b) Normalized average velocity magnitude for Ri_m=0.1 while varying Ra.

Figure 6.4: Normalized average velocity magnitude over y-slices in the domain.

To see the influence of the assisting force on the velocity in the total domain, the average normalized velocity magnitude is determined for various planes in the y-direction. This is plotted against the normalized wall distance in the y-direction (between the hot and cold wall) in figure 6.4.

Here, the influence of the solid spheres in the domain is clearly visible. The wiggling and repeating nature of the different lines shows the presence of an ordered structure that can block the flow. This blocking of space is better visible in figure 6.3; here the spheres are in contact with each other at certain locations making it not possible for the flow to penetrate through. At other places, the availability of less space is making it impossible for the fluid to flow. There is relatively a lot of empty space in the regions near the wall, which makes the flow mostly wall dominated. This is also visible in figure 6.4a and 6.4b: the maximum velocity magnitude is observed at $\frac{y}{L}$=0 or 1. Next to the walls, a strong decrease/increase is visible in the normalized average velocity magnitude. This indicates that the highest velocities are obtained near the walls.

Figure 6.4a shows the average normalized velocity magnitude in the cavity for three different Ri_m at Ra=10^7. It can be seen that as Ri_m increases the average normalized magnitude decreases. The forced convection dominant case (Ri_m=0.04), the red line, shows the highest magnitudes throughout the total domain. The higher wall velocity gives the fluid more momentum to move to the center of the domain that is more densely packed with the spheres.

In figure 6.4b the average normalized velocity magnitude is shown for different Ra while keeping a constant of Ri_m=0.1 (mixed convection regime). A higher Ra gives a higher normalized average velocity magnitude in the domain.

6.3. Temperature

The direction of the motion of wall as depicted in figure 6.1 with respect to the natural convection stream also has an influence on the temperature field. This is first shown based on instantaneous temperature isocontours as depicted in figure 6.5 and 6.6.

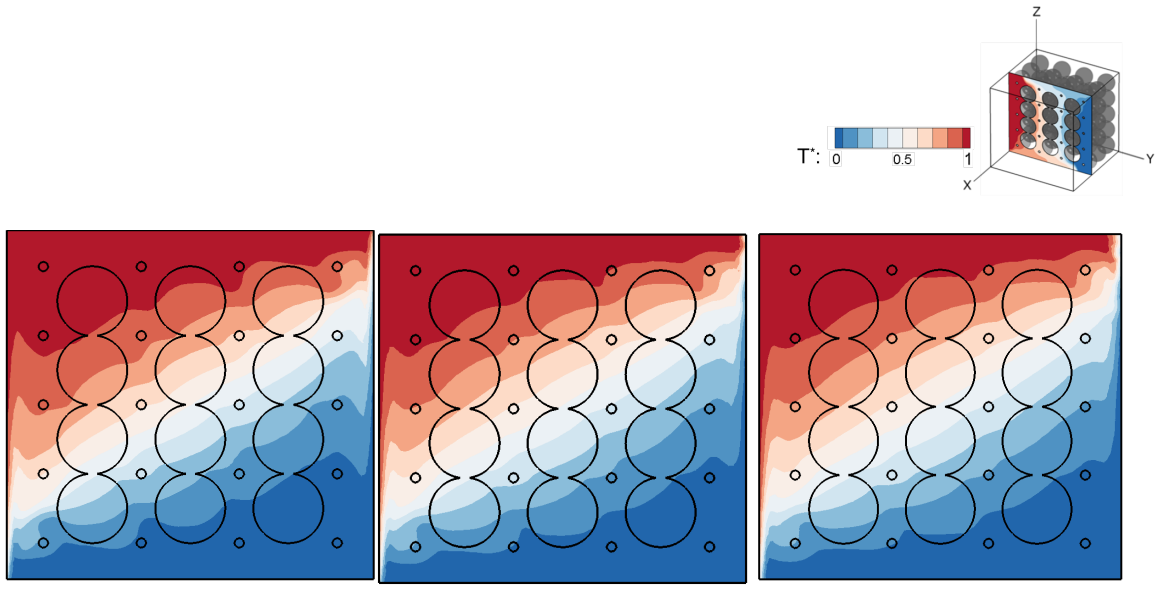

(a) Ri_m=0.04 (b) Ri_m=0.13 (c) Ri_m=0.52

Figure 6.5: Normalized instantaneous temperature isotherms at x-slice $\frac{x}{L}$=0.57 for Ra=10^7 for different Ri_m numbers.

Temperature isocontours at Ra=10^7 varying Ri_m are shown in figure 6.5. The isocontour lines in figure 6.5a show more oscillation compared to figure 6.5c. The forced convection creates a higher velocity in the domain as seen in figure 6.4a which reflects the temperature distribution. Furthermore, the width of the isocounts close to the wall is getting less wide with an increase in Ri_m. For Ri_m=0.52 (figure 6.5c) natural convection is more dominant so the buoyancy force is making the curve more smooth.

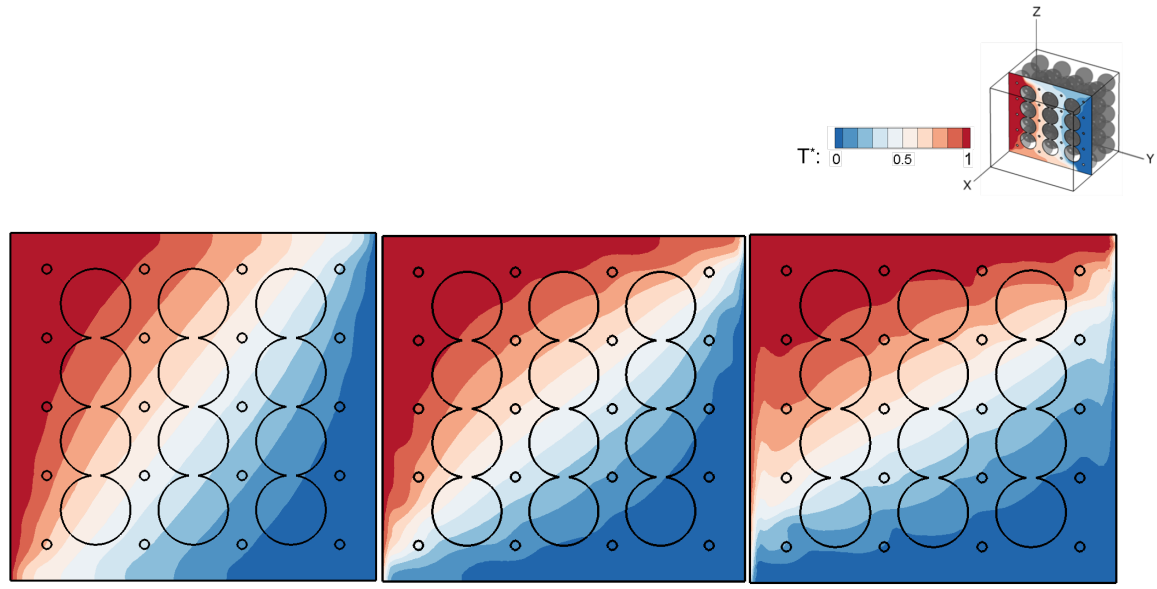

(a) Ra=10^5 (b) Ra=10^6 (c) Ra=10^7

Figure 6.6: Normalized instantaneous temperature isotherms at x-slice $\frac{x}{L}$=0.57 for Ri_m=0.1 at different Ra.

In figure 6.6 the temperature isocontours are shown for Ri_m=0.1 (mixed convection regime) varying Ra. Ra

is changed by adjusting the gravitational constant while keeping all other parameters fixed. Two main things are noticeable for the three situations depicted: the difference in the thermal boundary layer and the shape of the lines of the isocontours.

Firstly, the thermal boundary layer refers to the layer where the effects from viscous forces are significant. With increasing Ra, the buoyancy force increases, and the layer is moving away from the side walls and shifted more to the top/bottom wall.

With increase in Ra the lines of the isocontours are getting less straight. The isocontour lines are giving information on the mechanism of heat transfer. At small Ra (Ra=10^5 figure 6.6a) the isocontours indicate that conduction will be the dominant mechanism of heat transfer. With an increase in Ra, the isocontours are getting more curved and showing more wiggles. This is an indication of more convective heat transfer.

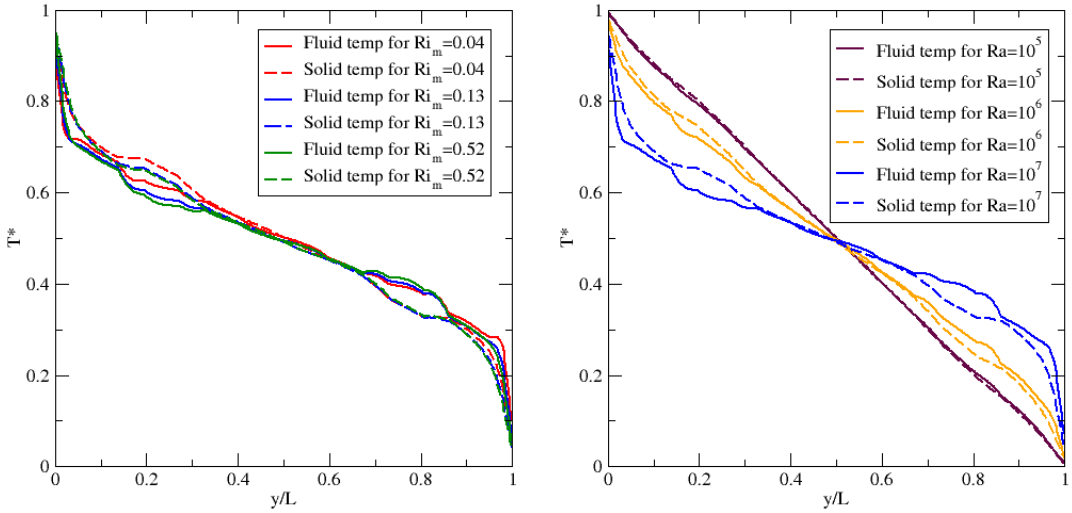

(a) Solid and fluid temperature for Ra=10^7 at different Ri_m numbers.

(b) Solid and fluid temperature for different Ra numbers at Ri_m=0.1.

Figure 6.7: Solid and fluid average temperature over y-slices in the domain. The dotted lines represent the solid parts and the straight lines visualize the fluid part.

The main mode of heat transfer can also be observed from the averaged normalized domain temperature depicted in figure 6.7. Here, the average solid and fluid temperature over y-slices are plotted versus the normalized wall distance.

At figure 6.7a the solid and fluid temperature are plotted for different Ri_m at Ra=10^7. The solid (dashed lines) and fluid temperature (solid lines) do not show much variation from each other since the thermal conductivity of both regions is the same. Furthermore, a small shift in average temperature distribution in the solid and fluid region is visible for different Ri_m.

In the center region ($\frac{y}{L}$=0.3-0.7) the average normalized solid and fluid temperature coincide for all Ri_m. Outside the center the fluid and solid temperature have more deviation. For the regions between the wall and the center ($\frac{y}{L}$=0.1-0.3 and $\frac{y}{L}$=0.7-0.9), a higher wall movement gives a slower decrease in average solid and fluid temperature. This is caused by the thicker thermal boundary layer compared to higher Ri_m, as can be seen in figure 6.5.

The average temperature distribution in figure 6.7b show more variation compared to figure 6.7a. Here, the solid and fluid temperature are depicted for Ri_m=0.1 varying Ra. For small Ra (Ra=10^5), the light blue dotted and solid line, a linear temperature decrease is observed for the solid and fluid region. With an increase in Ra, the temperature distribution is less linear. This indicates that convection becomes more dominant. This transition from conduction dominated to more convection dominated was also seen in the 2D slices depicted in figure 6.6.

6.4. Heat transfer

The flow and temperature fields have an influence on the total amount of heat transferred in the domain. This is expressed in terms of the Nu number, which is the ratio of total heat transfer by the conductive heat transfer. In this case, the total heat transfer is the sum of convective and conductive heat transfer.

The instantaneous Nu isocontours for the heated side wall at $\frac{y}{L}$=0 are depicted in figure 6.8.

The fluid flows in a clockwise direction (see figure 6.1) in the cavity. It brings a plume of relatively colder fluid perpendicular to bottom of the heated wall. This results in a higher temperature gradient and a higher Nu as can be seen in figure 6.8. The higher wall velocity (Ri_m=0.04, figure 6.8a) gives the fluid more magnitude by which the temperature gradient can penetrate deeper across the wall. The presence of spheres are also visible in the instantaneous isocontour. The lower regime of the slice in figure 6.8 has areas with lower Nu. This spots visualize the conducting nature of the spheres. Along the objects, a convective stream is penetrating and is represented by the higher Nu numbers.

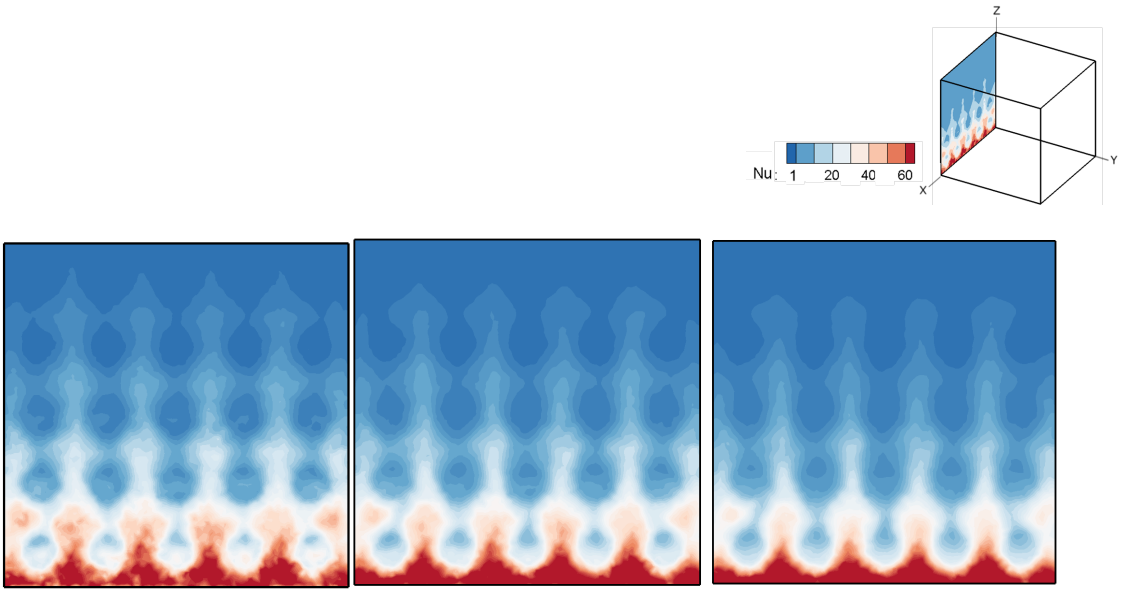

(a) Ri_m=0.04 (b) Ri_m=0.13 (c) Ri_m=0.52

Figure 6.8: Instanteneous Nu isocontours at y-slice $\frac{y}{L}$=0 (the heated wall) for Ra=10^7 for different Ri_m numbers.

The overall heat transfer is depicted by plotting Nu_{eff}, the effective Nu, and Nu number versus Ri_m for different Ra in figures 6.9a and 6.9b.

First figure 6.9a. An increase in Ra number results in an increase in Nu number. In the mixed convection zone (Ri_m) the Nu number for higher Ra (Ra=10^7) is about 12 times higher compared to lower Ra (Ra=10^5). As Ra is a measure for the strength of the buoyancy force, a higher Ra will lead to more convective heat transfer since the heat can travel along with the created velocity.

Furthermore, for both Ra the highest Nu are observed at lower Ri_m. This is the forced convection dominated regime. With increasing wall velocity, Ri_m decreases, Nu increases.

Besides, with an increase in Ri_m Nu is approaching the Nu value for pure natural convection. This asymptote will coalesce with the value for pure natural convection that is represented by the solid coloured line.

From figure 6.9 it is possible to determine the two extremes regimes can, but the mixed convection zone is hard to determine.

Therefore, the Nu number is refined into an effective Nu number for a situation with natural and forced convection. This reads:

$$Nu_{eff} = \frac{Nu_{MC}}{Nu_{FC} + Nu_{NC} - 1} \tag{6.1}$$

Where Nu_{MC} is the Nu number obtained in the mixed convection situation, Nu_{FC} the value for Nu for only forced convection and Nu_{NC} when there is only natural convection.

The definition stated in equation 6.1 is used as parameter on the y-axis in figure 6.9b. With Nu_{eff} on the vertical axis and the Ri_m on the horizontal one, Nu shows an optimum.

This peak is visible in the region where Ri_m=0.1-1: the mixed convection zone. The regions indicates the situation in which natural and forced convection are in the same order of magnitude. Left and right from the top Nu_{eff} approaches 1. Here, one of the two convection streams is more dominant resulting in a Nu_{eff} closer to 1.

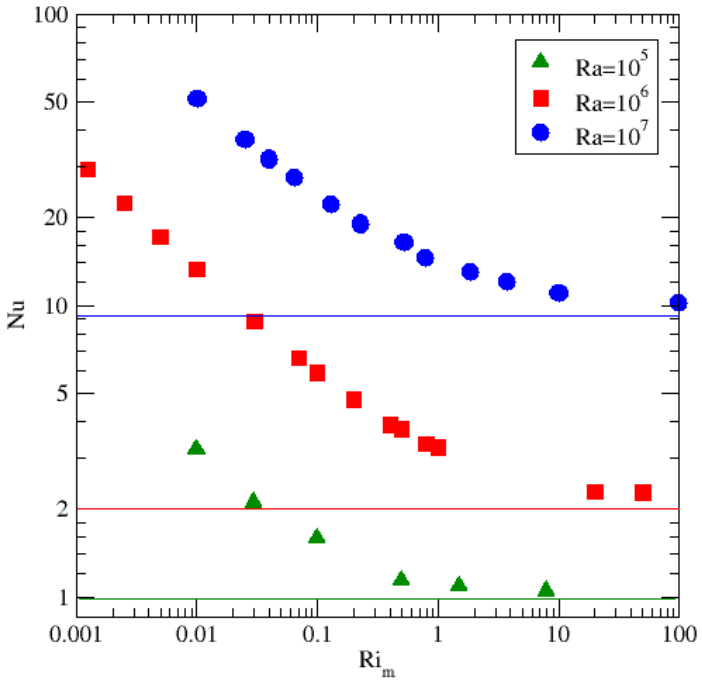

(a) Nu number versus Ri_m.

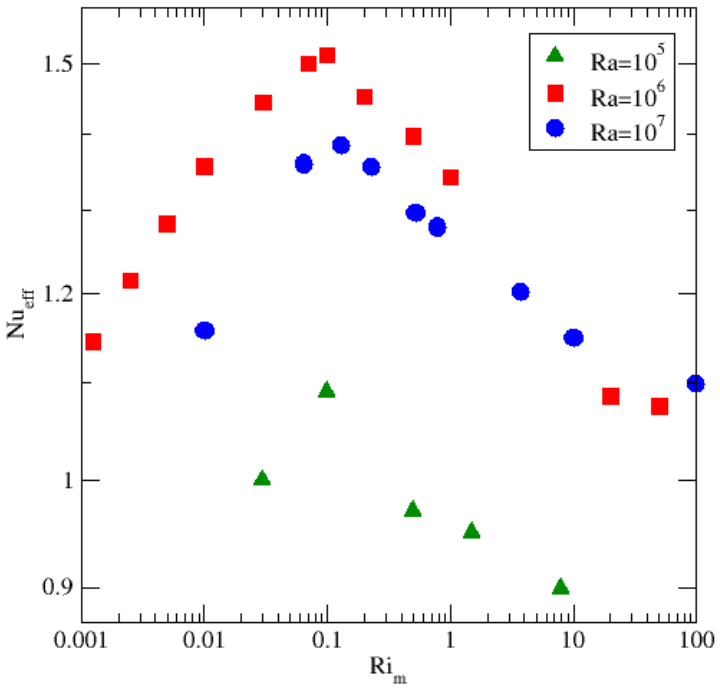

(b) Effective Nu number versus Ri_m. The solid lines represent the values for pure natural convection.

Figure 6.9: Heat transfer for different Ra numbers in an assisting mixed convection situation.The solid lines indicate the values for pure natural convection.

6.5. Summarized

The following things can be concluded about the situation with assisting mixed convection:

1. The magnitude of the wall velocity has little influence on the u_z^* isocontour plot.
2. The magnitude of the wall velocity has also little influence on the temperature distribution in the domain.
3. An increase in Ra number results in an increase in Nu number. In the mixed convection zone (Ri_m) the Nu number for higher Ra (Ra=10^7) is about 12 times higher compared to lower Ra (Ra=10^5).
4. With Nu defined as Nu_{eff}, the Nu_{eff} vs Ri_m plot shows a maximum in the area where Ri_m=0.1-1. This is an indication for the mixed convection zone.

Reflecting the assisting mixed convection situation, the lowest Nu numbers will be achieved when the forced convection is very small compared to the natural convection stream. The points in figure 6.9a show that with increasing Ri_m the Nu numbers are approaching the value for pure natural convection.

7

Opposing mixed convection

In this chapter, the results are described in the case where the forced convection is in the opposing direction of the natural flow in the cavity. This is schematically depicted in figure 7.1. Section 7.1 will elaborate more about the flow profiles while varying parameters. Next, section 7.2 gives more information about the temperature profiles. Section 7.3 tells more about the effect of the flow and temperature field on the heat transfer in the domain. Lastly, section 7.4 gives a summary of the findings.

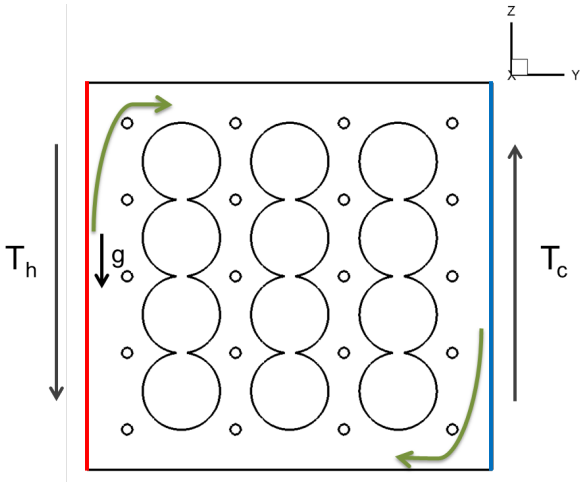

Figure 7.1: 2D representation of opposing mixed convection inside the cavity.

7.1. Opposing flow

There are two flow streams in the mixed convection system; one caused by natural convection and the other one caused by the wall movement as depicted in figure 7.1. The influence of the strength of this wall movement on the flow in the domain is visualized by plotting the isocontours of the velocity in the Z-direction. The velocity is normalized with the maximum magnitude obtained in the situation where Ri_m=0.13. This is depicted in figure 7.2: x-slices are taken at $\frac{x}{L}$=0.57 from the domain for Ra=10^7 varying for three different Ri_m numbers.

In figure 7.2, a second plume is visible next to the thin layer at the wall that has an opposite direction to that of the first layer. This flow is caused by the buoyancy force.

With increasing Ri_m number, i.e. natural convection becomes more dominant, the isocontours located at the wall are decreasing. Since the wall velocity decreases, the fluid has near the walls and inside the domain has a lower magnitude.

The same trend is observed in the overall domain. Figure 7.3 represents the normalized average velocity magnitude over various y-planes in the domain where at figure 7.3a Ra=10^7 and Ri_m is varied and at figure 7.3b Ri_m=0.1 and Ra is changing. The highest velocities are observed in the regions close to the wall. This

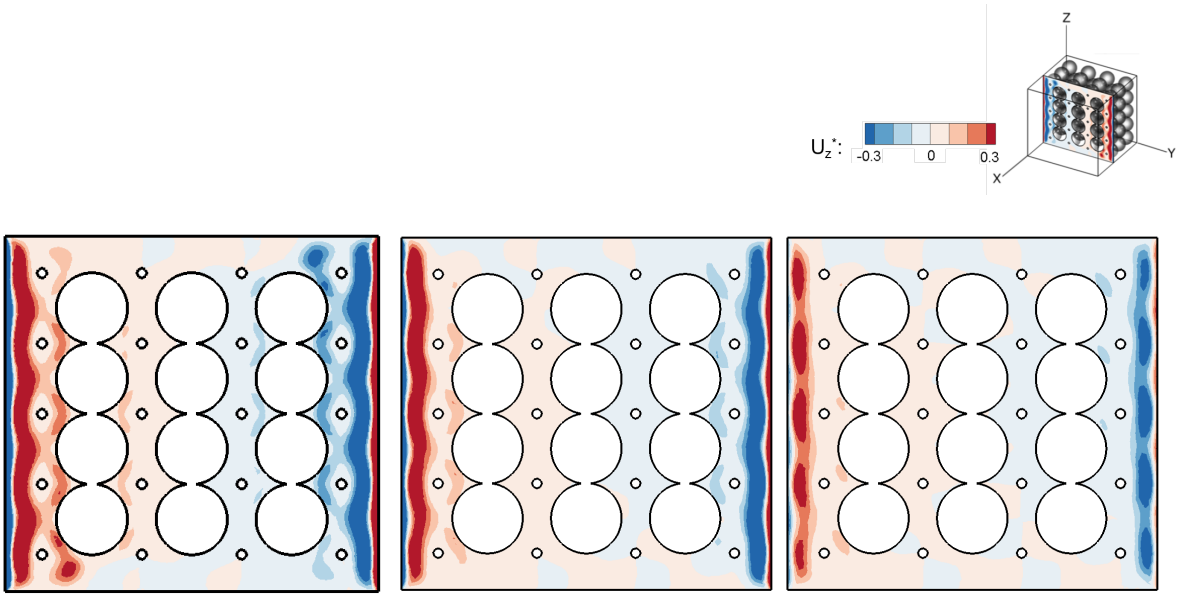

(a) Ri_m=0.04 (b) Ri_m=0.13 (c) Ri_m=0.52

Figure 7.2: Instanteneous normalized u_z velocity for x-planes at $\frac{x}{L}$=0.57 for Ra=10^7 varying Ri_m.

observation is in line with the findings based on the porosity profile depicted in figure 6.2. Logically, the amount of space of void for the fluid to flow through clearly influences the velocity field.

Figure 7.3a shows a higher magnitude around $\frac{y}{L}$=0.05 and 0.95: this is the influence of natural convection in the domain. The wall pulls the fluid close to the wall in the direction of gravity, while the next layer feels the buoyancy force and gets pulled in the upward direction as depicted in the 2D plane in figure 7.2 The Ri number is the ratio of these two forces, and in the case of mixed convection both are in equilibrium. This behaviour and the two layers created by the forces is visible in figures 7.2.

Figure 7.3b has a constant Ri_m of 0.1 (mixed convection) while varying the Ra number. Ra is varied by chnaging the gravitational constant while keeping all other parameters fixed. With increasing Ra number the velocity magnitude in the domain increases.

Comparing figure 7.3a with 7.3b, one can see that the forced component has a significant influence on the total velocity in the domain: the normalized velocity magnitude for Ri_m=0.04 in figure 7.3a shows a high peak around $\frac{y}{L}$=0.2 and $\frac{y}{L}$=0.8. The higher wall velocity gives the fluid a higher momentum by which it can penetrate deeper into the cavity. The velocity in the center of the cavity, $\frac{y}{L}$=0.4-0.6, are for all Ri_m and Ra in the same order of magnitude.

Furthermore, the nature of the behaviour of the normalized average momentum inside the cavity shows similarities with the porosity profile plotted in figure 6.2; the lack or surplus of empty space influences the velocity. As observed in figure 7.2, the u_z^* velocity is the highest at the walls and decreasing towards the centre of the cavity.

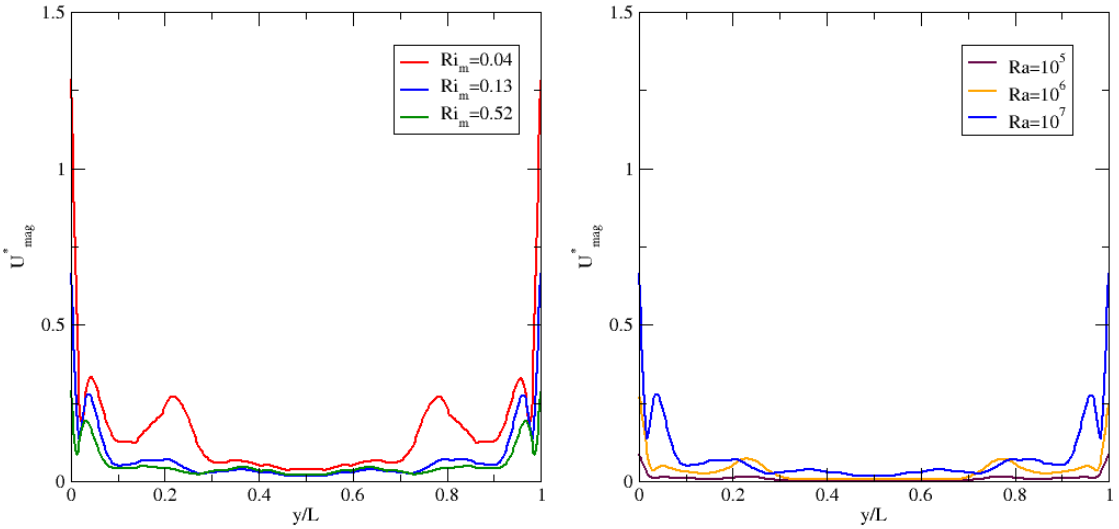

(a) Normalized averaged velocity magnitude for Ra=10^7 for different Ri_m.

(b) Normalized averaged velocity magnitude for Ri_m=0.1 while varying Ra.

Figure 7.3: Normalized average velocity magnitude over y-slices in the domain.

7.2. Temperature

Instantaneous temperature isocontours are plotted to visualize the influence of the strength of the opposing wall (see figure 7.1) direction on the temperature distribution.

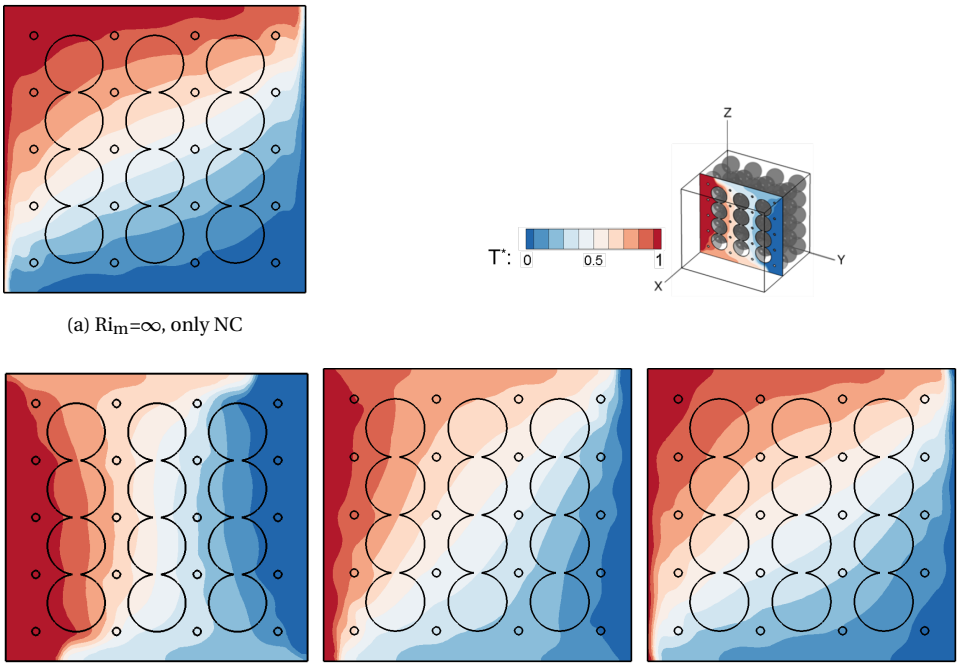

(a) Ri_m=∞, only NC

(b) Ri_m=0.04

(c) Ri_m=0.13

(d) Ri_m=0.52

Figure 7.4: Normalized instantaneous temperature isocountors at x-slice $\frac{x}{L}$=0.57 at Ra=10^7 with varying Ri_m number. Subfigure a shows the case for pure natural convection.

Figure 7.4 shows the temperature isocontour at a slice at $\frac{x}{L}$=0.57 for Ra=10^7 varying Ri_m number. The three cases are compared for the situation with pure natural convection (figure 7.4d).

With increasing Ri_m the thermal boundary layer decreases. Besides, as Ri_m increases the nature of the iscontours are getting closer to the case for NC. This same behaviour is observed in the packed bed columns

in the article by Das et al [33].

For small values of Ri_m (Ri_m=0.04, forced convection-dominated regime), figure 7.4a indicates that the buoyancy effect is overwhelmed by the mechanical or shear effect due to the movement of the wall. The isocontours of the temperature for the opposing case are characterized by the fact that the bottom left corner has a higher temperature than the top left corner. This makes clear that the velocity and temperature field are coupled.

For moderate values of Ri_m (Ri_m=0.1, mixed convection regime), figure 7.4b shows that the buoyancy effect is of relatively comparable magnitude to the shear effect due to the sliding wall. The temperature in the two left corners are more identical by size and intensity.

For large values of Ri_m (Ri_m=0.5, natural convection dominated regime), the buoyancy effect is dominant and this results in increased temperature gradients along the top wall of the enclosure as seen in figure 7.4c. The isocontours depicted here show close agreement with figure 7.4d where only natural convection is presented. The main difference is that the thermal boundary layer is thicker and stretched more in the horizontal direction, this will influence the heat transfer and lead to a higher Nu number (see section 7.3).

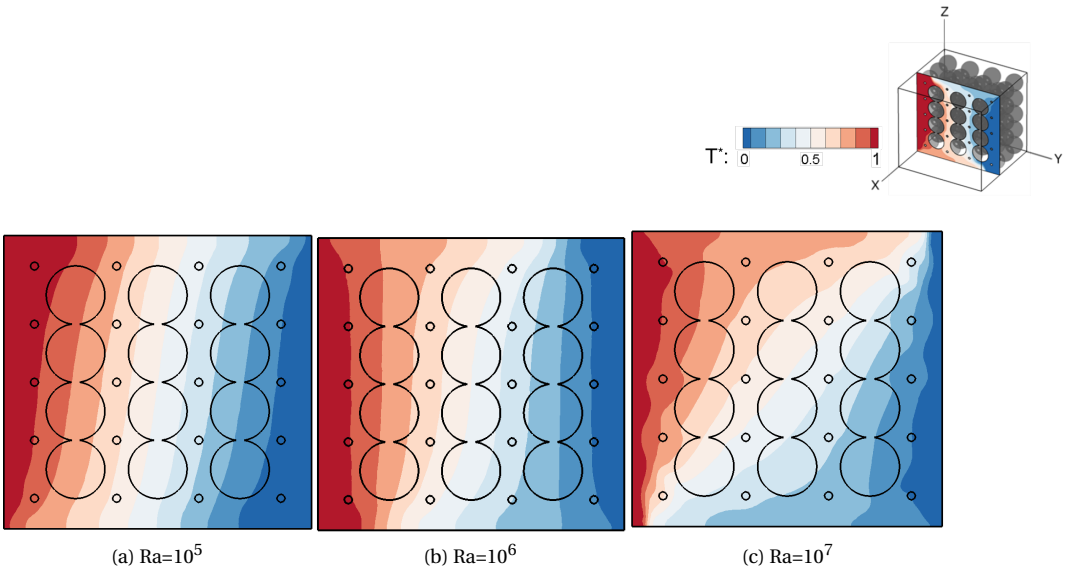

(a) Ra=10^5 (b) Ra=10^6 (c) Ra=10^7

Figure 7.5: Normalized instantaneous temperature at x-slice $\frac{x}{L}$=0.57 at Ri_m ≈0.1 varying Ra number.

Figure 7.5 shows the temperature contours at Ri_m=0.1, the mixed convection regime, for different Ra numbers. Increasing Ra means increasing buoyancy forces and overcome viscous forces, in this way convection becomes more dominant compared to conduction as heat transfer mechanism.

At lower Ra (Ra=10^5) the isocontour lines are linear indicating that conduction is the main mechanism of heat transfer. As Ra increases convection becomes more dominant, resulting in less straight isocontours and a decrease of thermal boundary layer thickness. This is seen for higher Ra (Ra=10^7), at figure 7.5c, where the contours are more curved and the thermal boundary layer is thinner.

Figure 7.6 shows the average solid and fluid temperature versus the non-dimensional wall distance at y-cross sections for different Ri_m and Ra numbers.

Figure 7.6a, where Ra=10^7 and Ri_m is varied, shows that the difference between the solid and fluid temperature decreases with increasing Ri_m. The most deviation between the solid and fluid temperature can be found for Ri_m=0.04 indicating that the heated/cooled fluid flow that is created by the forced wall-movement is flowing faster then the heat is conducted though the spheres.

The decrease for the solid temperature is close to a linear decrease which is an indication of conduction as main heat transfer mechanism. This is also visible in figure 7.4a.

Figure 7.4b shows the solid-fluid temperature for Ri_m=0.1 at different Ra numbers. At higher Ra number (Ra=10^7) convection becomes more dominant resulting in more difference between the solid/fluid temperature and a more S-shaped curve. For low Ra (Ra=10^5) the temperature decrease is showing close agreement to a linear decline indicating that most heat is transferred through conduction.

The last noteworthy point is that the differences between the solid and fluid temperatures are relatively small irrespective of the Ra number as the conductivity ratios are small.

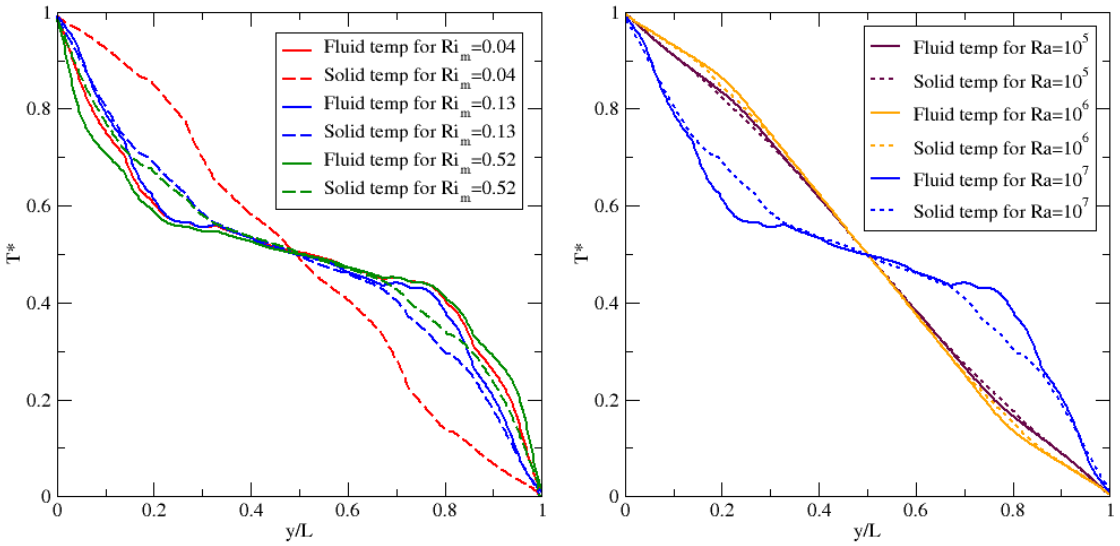

(a) Solid and fluid temperature for Ra=10^7 at different Ri_m numbers.

(b) Solid and fluid temperature for different Ra numbers at Ri_m=0.1.

Figure 7.6: Solid and fluid average temperature over y-slices in the domain. The dotted lines represent the solid parts in the domain and the straight lines visualized the fluid part. Subfigure a) shows the difference at Ra=10^7 for different Ri_m and at b) Ri_m=0.1 while Ra is varied.

7.3. Heat transfer

The wall-to-wall heat transfer rates for different Ri_m and Ra numbers are calculated based on the Nu number and plotted in figure 7.8. The value for pure natural convection is represented by the solid line. Nu is the ratio of convective heat transfer to the total heat transfer across the boundary. A higher Nu is a measure for more convective transfer of heat, while a Nu closer to 1 indicates that conduction is the main mode of transport.

The instantaneous Nu isocontours for the heated side wall at $\frac{y}{L}$=0 are depicted in figure 7.7. There are four figures: three figures represent different Ri_m numbers and one is for the situation with just natural convection and no wall movement. All four depicted figures show a different Nu isocontour.

For Ri_m=0.04, figure 7.7a, the wall movement is dominant with respect to the natural convection stream. A small layer of high temperature gradient is observed at the bottom of the heated wall. This is the location where the forced stream is perpendicular to the natural convection stream. A lot of movement results in a higher convection and thus a higher Nu.

The plane depicted in figure 7.7b shows the mixed convection situation. Nu at this heated wall is in the lower regime, so the heat is mainly transferred through conduction. The two forces are of the same order of magnitude and cancel each other out. Therefore, the main mode of heat transfer is by conduction.

In the situation where natural convection becomes more dominant (figure 7.7c) higher temperature gradients are observed. The relative small wall velocity creates a small layer at the bottom of the heated cavity of conduction dominant heat transfer. Higher temperature gradients will be achieved with increasing Ri_m. Figure 6.8d is depicted the situation for pure natural convection. The bottom of this plane is showing high Nu compared to the other figures.

The overall heat transfer is depicted by plotting Nu and Nu_{eff} versus Ri_m varying Ra in figure 7.8.

A quick first observation of figure 7.8a shows that as Ra increases Nu increases. For Ri_m=0.1 the Nu number is two times higher for high Ra (Ra=10^7) compared to low Ra (Ra=10^5). Moreover, the lowest values for Nu are observed in the region Ri_m=0.1-1. This indicates the mixed convection region.

At the right side of the mixed convection zone (Ri_m>1), natural convection is the dominant mechanism of heat transfer. Expected is that for higher Ri_m, Nu will get closer to the heat transfer value for pure natural convection.

At the left side (Ri_m<0.1) in figure 7.8a, here the force created by the moving wall increases, the Nu number will keep on increasing since more flow will move and convection will become more dominant. With a decrease in Ri_m Nu increases irrespective of Ra. All heat is transferred by convection that is generated by the wall movement.

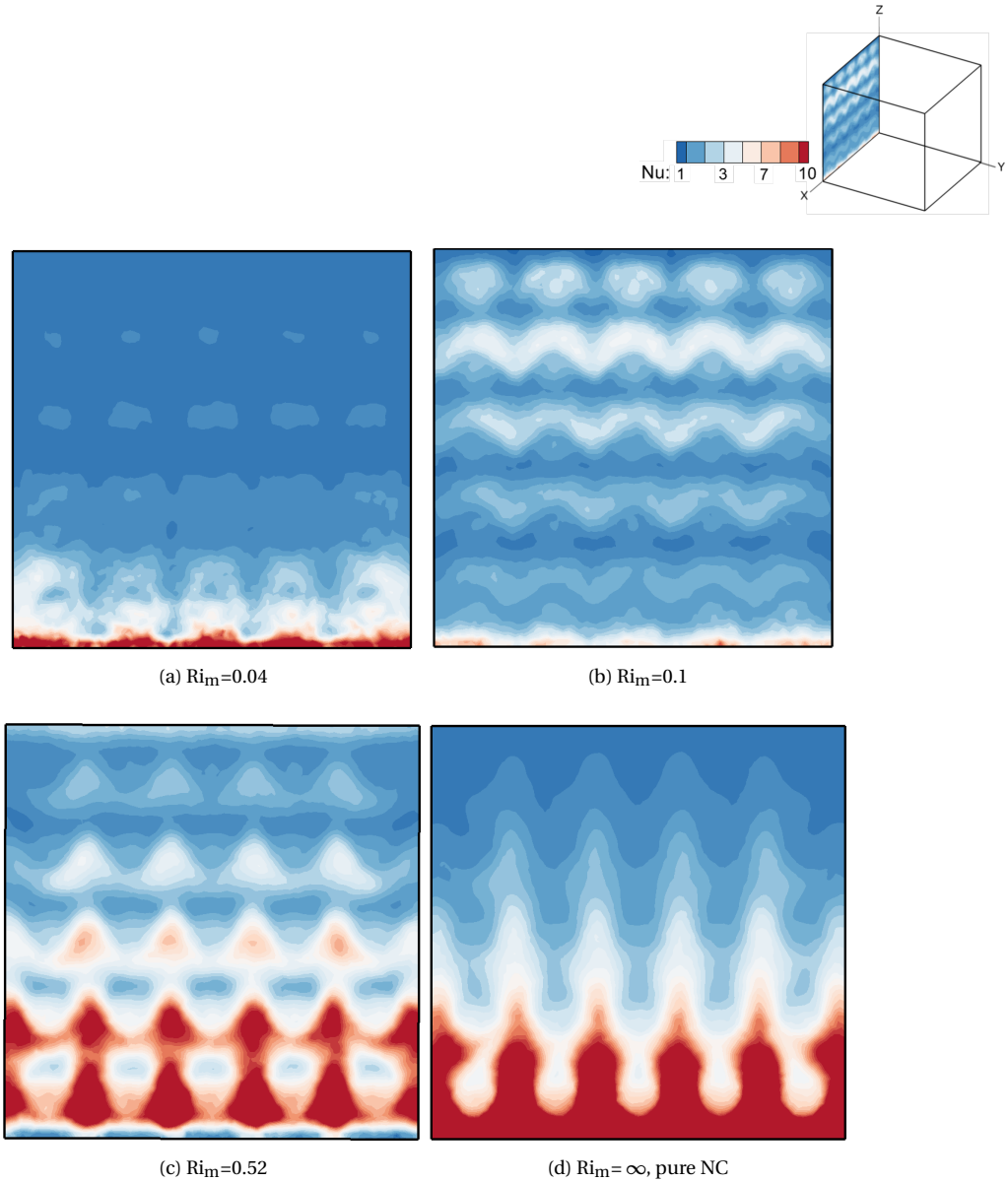

(a) Ri_m=0.04 (b) Ri_m=0.1

(c) Ri_m=0.52 (d) Ri_m= ∞, pure NC

Figure 7.7: Instanteneous Nu isocontours at y-slice $\frac{y}{L}$=0 (the heated wall) for Ra=10^7.

The expression for the Ri_m number in case of coarse-grained porous media derived in section 2.4 left out the Forcheimer Coefficient C_f in the expression (see equation E.7 in appendix E). Kathare et al [31] reported values in the order of magnitude of 0.1 for this coefficient based on his experiments. With an expected similar value for this situation, the x-axis of the graph will shift to the right and the mixed convection zone will lie in between Ri_m=1-10, just like the regular definition for Ri.

Figure 7.8a shows also the coupling of flow and temperature field on the total heat transfer. The minimum of the three lines is representing the case where the opposing forced and natural streamlines are of equal strength and therefore they cancel each other out. For Ra=10^5 and Ra=10^6, the lowest point is close to Nu=1 indicating that all convection is killed and all the transfer of heat will go through conduction.

At the left and right side of this minimum, the flow (natural or forced) becomes more dominant and therefore heat will go along with this flow. In this way, more heat will be transferred through convection and Nu increases.

Figure 7.8b depicts the Nu_{eff} (see equation 6.1) versus Ri_m for $10^5 \leq Ra \leq 10^7$. The graph shows a minimum in Nu_{eff} for $Ri_m \approx 0.1$. In this situation the Nu number for Nu_{MC} (the numerator in equation 6.1) has the lowest value and is therefore creating a minimum for Nu_{eff}. With an increase or decrease in Ri_m, the forced

or natural component is becoming more dominant respectively. The value for Nu_{MC} is dominated by one of the two components and, this leads to an increase in Nu_{eff}. Moreover, values for Nu_{eff} depicted in figure 7.8b are below one. This indicates that the heat transfer is reduced, especially when comparing this situation with the assisting mixed convection (figure 6.9b).

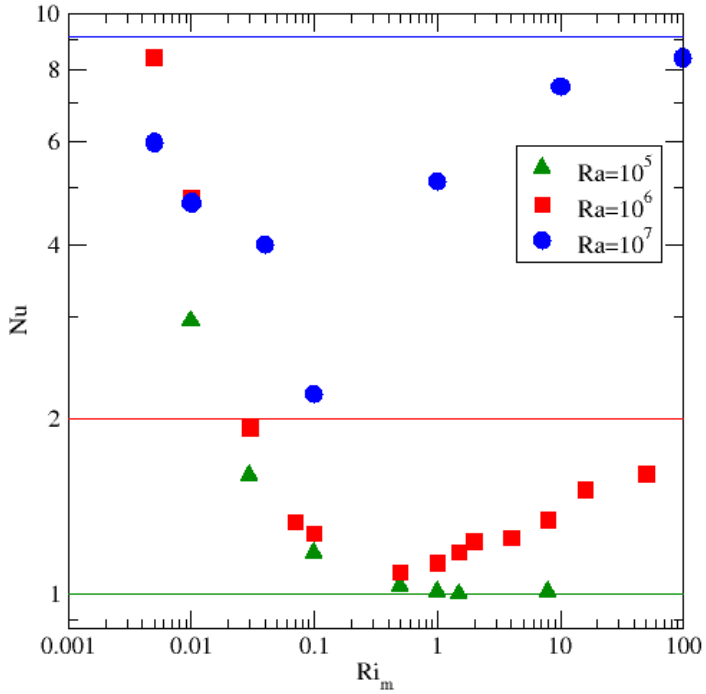

(a) Nu versus Ri_m for different Ra numbers. The solid lines represent the values for pure natural convection.

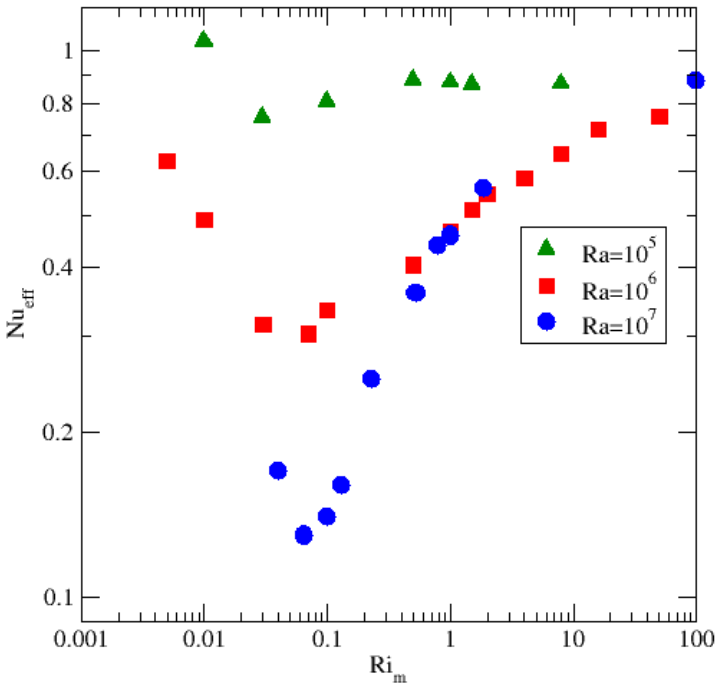

(b) Nu_{eff} versus Ri_m for different Ra numbers.

Figure 7.8: Heat transfer for different Ra numbers in an opposing mixed convection situation.

7.4. Summarized

In this chapter the flow and heat characteristics are described for the case that the forced convection works in opposing direction on the natural stream. Based on the graphs and figures published above, the following things can be concluded:

1. In general, the velocity is the highest close to the walls and smaller towards the center of the cavity.
2. Velocity and temperature field are coupled: convection as heat transfer mechanism will be more dominant if the velocity in the field is higher.
3. If the two forces are opposing and in the same order of magnitude, Nu will have a minimum value around Ri_m=0.1. For Ra=10^5 and Ra=10^6 all convection is killed and Nu=1. The minimum value for Ra=10^7 is about two times higher than for Ra=10^5, convection still is present here.

Reflecting an opposing mixed convection on the problem stated in chapter 1 about the arising hot spots in the blast furnace, this chapter has shown that the forced component has a lot of influence on the velocity in the total domain. Furthermore, if the forced stream is of opposing nature and in the same order of magnitude with natural convection stream Nu will reach a minimum. These insights can help to reduce the hot spots and create a longer lifetime for the reactor.

Assisting versus opposing

The assisting mixed convection chapter 6 and this chapter, chapter 7, had different observations. Summarizing the most important points:

1. Higher velocities are observed in the case for assisting mixed convection. The scaling velocity used in the assisting case (figure 6.3) is about 75% higher compared to the opposing situation (figure 7.2).
2. The temperature isocontours for assisting mixed convection showed a more curved thermal boundary layer for the presented Ri_m and Ra numbers.
3. Opposing mixed convection showed a minimum Nu number around Ri_m=0.1 for Ra=10^7 where convection is largely killed.
4. For the range where $0.1 \leq Ri_m \leq 1$, significantly higher values for Nu are found for the assisting case compared to the opposing mixed convection situation. In the situation where Ra=10^7 the heat transfer rate is about nine times higher in the assisting situation than the opposing situation. With a decrease in Ra, the difference between the two configurations decreases. For Ra=10^6 the transfer is about three times higher, and for Ra=10^5 the Nu for the assisting case is about one and a half times higher than the opposing case.

Aydm et al [22] found a wider mixed convection range for opposing-buoyancy then for aiding-buoyancy. This conclusion can not be made from the graphs depicted in figure 6.9 and figure 7.8. More data is needed to see if this statement also holds for the cavity filled with coarse-grained porous media.

If an opposing mixed convection situation at the blast furnace can be created, it is expected based on the results presented above that the operating conditions will be better manageable. With lower flow rates and Nu numbers it will be easier to control the situation.

8

Concluding remarks

In this research, CFD simulations on a side heated water filled cavity with coarse grained porous media have been done to investigate the influence of the spheres on flow and temperature field. From the studies on the resulting heat transfer mechanism, concluding remarks can be made.

The following research questions were formulated and their answers are given:

1. **How does natural convective heat transfer in a side heated water filled cavity with coarse grained porous media differ from heat transfer in a water filled cavity?**

Side heated natural convection is characterized by a wall dominated flow. This behaviour is also observed in the side heated water filled cavity with coarse grained porous media. For low Ra (Ra=10^5) the total heat transfer is about five times lower in the cavity filled with coarse grained porous media compared to the cavity filled with water. The buoyant force can not overcome the viscous forces created by the spheres, making conduction the dominant mode of heat transfer. This is also visible in the temperature isocontour at low Ra. The isocontour lines are close to a linear behaviour, indicating that heat is transferred through conduction. With an increase in Ra, the temperature isocontour lines are getting more curved. This indicates that convection is getting more dominant as mode of heat transfer.

With an increase in Ra the difference in heat transfer between the water filled cavity and the cavity with packed beads decreases. At high Ra (Ra=10^7), the Nu number for the water filled cavity is about 10% higher compared to the cavity filled with beads. The higher buoyancy force gives the fluid more momentum to meander through the coarse grained porous media.

To summarize, the difference in natural convective heat transfer between the water filled cavity and the cavity filled with coarse grained porous media is decreasing with increasing Ra.

2. **How is the mixed convective flow in a porous media filled side heated lid-driven cavity influenced by the direction of the forced component of the flow?**

In this project two configurations are elaborated. The heated/cooled side wall was moving in assisting direction or in the opposing direction with respect to the natural convection flow. Different observations were made for the two configurations.

Higher velocities were observed in the case of assisting mixed convection. Based on the scaling velocities, the velocities in the assisting case are about 75% higher compared to the opposing case. This results in a more curved thermal boundary layer in the case of assisting mixed convection. Comparing Nu at different Ra number for assisting mixed conveciton, the heat transfer rate at high Ra (Ra=10^7) is about 13 times higher compared to low Ra (Ra=10^5). Furthermore, Nu increases with increasing wall velocity. This characteristic is independent of Ra. With a low wall velocity, Nu will approach the same value for pure natural convection.

In the case of opposing mixed convection, the velocity from the wall and the buoyancy forces are in opposite direction. The two forces damped each other. If the forces are in the same order of magnitude, heat transfer by convection decreases and a minimum Nu number is observed. The minimum Nu number for high Ra (Ra=10^7) is about two times higher than for lower Ra (Ra=10^5). If one of the two forces is more dominant, the total amount of heat transfer increases with respect to the minimum value.

Significant difference were found in the comparison of the Nu number for the assisting and opposing mixed convection range. In the range where $0.1 \leq Ri_m \leq 1$ and $Ra=10^7$, the heat transfer rate is about nine times higher in the assisting situation than the opposing situation. With a decrease in Ra, the difference in Nu between the two situation decreases. For $Ra=10^6$ the transfer is about three times higher, and for $Ra=10^5$ the Nu for the assisting case is about one and a half times higher than the opposing case.

To summarize, lower Nu values are found for opposing mixed convection compared to assisting mixed convection. The lowest value is created when the two forces (buoyancy force and shear stress from the wall) are in opposing direction.

3. **How can mixed convection in a coarse grained porous medium be expressed in a non-dimensional number?**

Mixed convection in a cavity filled with water can be described with the dimensionless Ri number. A modification was proposed to include the influence of the coarse grained porous media on the heat transfer:

$$Ri_m = Ri \times \sqrt{Da}$$

This equation was elaborated for the side heated lid-driven cavity filled with coarse grained porous media for assisting and opposing mixed convection for $Ra=10^5 \leq Ra \leq 10^7$. A mixed convection region was found for Ri_m=0.1-1. The unmodified definition for Ri defines mixed convection for 1<Ri<10. The Ri_m expression left out the Forcheimer Coefficient. In literature values of about C_f=0.1 are reported, with this value the mixed convection zone of Ri_m will shift. Besides, it was found that this expression is not valid in case ε=0 or ε=1.

To summarize, it was found that the expression for Ri_m showed a mixed convection regime for Ri_m=0.1-1 for this specific and very bounded situation. More cavities with a difference in sphere material, difference in working fluid, geometries, configuration of the spheres and situations have to be elaborated to see if this expression is still valid.

Concluding

Reflecting back on the situation outlined in chapter 1, some more conclusions can be made. The question and problem stated for this project came from the blast furnace at Tata Steel. Their aim is to have more insight in the local hot spots at the wall of their reactor. This research showed that the coarse grained porous media has an influence on the flow profile and temperature distribution.

Another point of interest is that the lowest heat transfer values are found in case of opposing mixed convection. Besides, it was found that Nu increases with an increase in wall velocity. These two points can help during the design and operation of the furnace.

With the expression for Ri_m, the mixed convection regime can be found. But first, this expression needs to be validated for other situation. These insight can help Tata Steel in the use and design of their equipment, even though the simulated situation is very simplified from reality. Further research is needed to find more information about the characteristics of the hot spots and the physics inside the blast furnace.

9

Recommendations

In this chapter, several recommendations will be made for further research.:

- Further develop the model to investigate the influence of coarse grained porous media for higher Ra. This can be done by modelling the turbulence behaviour of the flow with a LES or RANS model. The idea behind these mathematical models is to reduce computational cost by ignoring the smallest length scales. The motion of flow is modelled by a time and spatial averaged form of the Navier Stokes equation. In this way, higher Ra numbers can be achieved. Higher Ra shows closer agreement with industrial applications.
- Further analyze the influence of coarse grained porous media on the flow and temperature field.
  - By making different packing types with the solid spheres.
  - By looking more into materials with different thermal conductivities This will have an influence on the dominant mode of heat transfer.
- Creating mixed convection by another geometry. It would be interesting to see the influence of an in and outlet on the flow and temperature profiles. At the blast furnace, the liquid metal is tapped off at the reactor wall. Simulating a cavity with an in- and outlet will show closer agreements with the situation at the reactor of Tata Steel.
- Comparison of the mixed convection results obtained from the simulations with experimental results.
- Further analyze the modified Ri number for coarse grained porous media, Ri_m :
  - By verifying the mixed convection zone for higher Ra numbers.
  - By elaborating this definition for different geometries for the coarse grained porous media.
  - By investigating the influence of the material of solid spheres.
- Expanding the model for liquid metal flows. Liquid metals are characterized by low Pr numbers. The Pr number controls the relative thickness of the momentum and thermal boundary layers. This has an influence on the total amount of heat transferred.

A

Non-dimensional numbers

A.1. Dimensionless numbers

An overview of the important non-dimensional numbers commonly observed in natural, forced and mixed convection situations are discussed in this section.

Rayleigh number

The Rayleigh number is associated with buoyancy-driven flow. Since the scope of the project is a side heated cavity, there is no critical value for the flow to start. A high Ra number indicates that the predominant mechanism of heat transfer within the fluid itself is convection. The definition of Rayleigh based on the fluid properties is :

$$Ra_f = \frac{g\beta\Delta T L^3}{\nu\alpha}$$

Where g is the acceleration due to gravtiy, β the volume expansion coefficient of the fluid, ΔT the temperature difference and L the characteristic length.

Nusselt number

The Nusselt number describes the dominant mechanism of heat transfer across a boundary at a certain point. It is defined as the total heat transfer to the conductive heat transfer of the specified fluid. The Nusselt number based on the fluid properties is:

$$Nu_f = \frac{hL}{k_f}$$

Where h is the convective heat transfer coefficient of the flow and k_f the thermal conductivity of the fluid.

A large Nu indicates a stronger flow and that convection plays a bigger role in the heat transfer compared to the conduction component.

Prandlt number

The Prandlt number reflects the ratio of momentum diffusivity to thermal diffusivity. Diffusivity is a rate of diffusion, a measure of the rate at which particles or heat or fluids can spread. It can also be interpreted as an indicator of the relative importance of the thermal and viscous boundary layers. Unlike the other numbers mentioned above, Pr is only based on fluid properties and not influenced by geometry or temperature.

$$Pr = \frac{\nu}{\alpha}$$

For the scope of this project, water, Pr=5.43, is taken to be the fluid of the cavity.

Reynolds number

Reynolds is defined as the ratio of inertial forces to viscous forces. This number gives an indication whether the flow is turbulent or laminar. An increase in Re results in the transition from the laminar regime to the turbulent.

$$Re = \frac{\rho v L}{\mu}$$

With v the characteristic velocity and L the length of the cavity.

Richardson number

The Richardson number represents the importance of natural convection relative to the forced convection.

$$Ri = \frac{Ra}{PrRe^2} = \frac{Gr}{Re^2}$$

When Ri«1, the situation is dominated by a forced convection stream while Ri»1 natural convection is the main phenomena. For 1<Ri<10, there is mixed convection.

Ri for porous media

The porosity dependency of the box into dimensionless number is introduced by the Darcy number, based on the article of Keene [35].

The Darcy number is based on the length of the box and the permeability of the porous media:

$$Da = \frac{K}{L^2}, \qquad K = \frac{\varepsilon^3 D^2}{150(1-\varepsilon)^2}$$

Where K is the permeability, with ε the fluid volume fraction and D the sphere diameter. The box used during this project has a BCT packing and fluid volume fraction of ε=0.38, which makes K=4.4·10^{-6} m^2.

The derivation for Ri_m, the Richardson number based on the medium, is based on the derivation from the article of Kathare et al [31] and is stated in Appendix E.

The final equation is:

$$Ri_m = \frac{Gr\sqrt{Da}}{Re^2} \tag{A.1}$$

B

Flow through porous media

B.1. Volume averaging

With irregular shapes of the pores, quantities like velocity or temperature distribution will be clearly irregular too. Since the pore scale is in the micrometer range, it costs a lot of computational power to carry out detailed studies in complex geometries and extreme conditions.

This is the reason that most numerical studies are using a volume averaging concept, to obtain the macroscopic equations by averaging them over volumes or areas containing many pores. This makes the situation simplified and more manageable.

According to Nield and Bejan [4], there are two ways to do the averaging: spatial and statistical.

A schematic view of the REV is depicted in figure B.1, the length scale of the REV is much larger then the pore scale, but considerably smaller than the length scale of the flow domain (box).

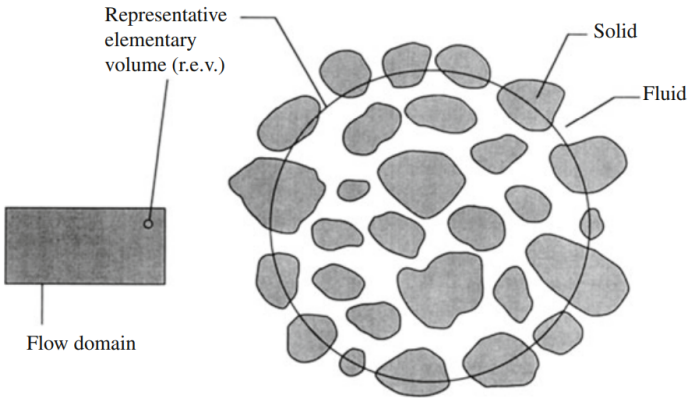

Figure B.1: The representative elementary volume (r.e.v.): the figure represents the intermediate size relative to the size of the flow domain and the pores [4].

This approach is very suitable when a porous medium consists of a large number of small particles, but it does not predict the velocity and temperature in the pore scale.

B.2. The Darcy model

The study of heat transfer in porous media has been mostly based on Darcy's model for porous media [26–28]. Here, the porosity is accounted for in a volume-averaged sense (for example with a REV) , assuming that the porous length scales are small compared to the thermal and flow length scales. Besides, this model is based on the assumption that inertia is negligible compared to viscous effects.

Darcy's law is expressed by [4]:

$$u = \frac{-K}{\mu}\frac{\partial P}{\partial x} \tag{B.1}$$

Here $\partial P/\partial x$ is the pressure gradient in the flow direction, μ the dynamic viscosity of the fluid, and K the Darcy permeability (in m^2). Values of K for natural materials vary widely, and can be found in literature. Besides, in case of a simple geometry, K can be determined based on geometrical parameters:

$$K = \frac{d_p^2 \varepsilon^3}{180(1-\varepsilon)^2} \tag{B.2}$$

With d_p the diameter of the particle and ε the porosity.

In case of an isotropic material (having identical values of a property in every direction), equation B.1 can be rewritten as:

$$\nabla P = \frac{-\mu}{K} \mathrm{u} \tag{B.3}$$

Brinkman form of Darcy's law

In Darcy's law, effects of the solid boundary or the inertial forces on the fluid flow are neglected. These effects are expected to become more significant near the boundary and in high-porosity media, causing Darcy's law to be invalid. Brinkman accounted for the presence of a solid boundary by adding a viscous term to Darcy's law [51]:

$$\nabla P = \frac{-\mu}{K} \mathrm{u} + \tilde{\mu} \nabla^2 \mathrm{u} \tag{B.4}$$

There are two viscous terms in this equation, the first term is the Darcy term similar to equation B.1. The second term is analogous to the Laplacian term in the Navier-Stokes equation. In the NS for a Newtonian incompressible flow, $\mu(\nabla^2 v)$ represents the viscous stresses of the fluid with the vector Laplacian of the velocity field. The coefficient $\tilde{\mu}$ is an effective viscosity, and is in general not equal to μ. This correction term accounts for the flow through media where the grains of the medium are porous themselves. The term that has been added is the force per unit volume volume resulting from all fixed objects which might be particles, fibers, pore walls, depending on the type of material being modelled [5].

The equation reduces to a form of the Navier-Stokes equation as $K/L^2 \rightarrow \infty$ and to the Darcy equation (B.1) as $K/L^2 \rightarrow 0$.

Because Brinkman's equation has second order derivatives, it can satisfy boundary conditions that Darcy's law cannot. For the case where the dimensions of a reactor are much greater than the packing size, and it is desired to impose a no-slip condition at the wall Brinkman's equation permits this. Therefore, this solution is more exact than Darcy's law. However, even without the ability to satisfy the no-slip boundary condition satisfactory results can be obtained with Darcy's law on the condition that the system dimensions greatly exceed the microstructural length scales [5].

Forchheimer law

When Re_k<1 (Reynolds based on the permeability), the Darcy flow assumption is sufficient to describe the relation with between the Darcy velocity and the pressure drop, but when Re_k>10 the pressure drop is dominated by the form drag. This is called the Forchheimer effect. With the Forchheimer law the fluid flow through porous media in the high velocity regime can be described. As the flow velocity increases, there is a smooth transition in Re number. This is due to the fact that form drag (drag because of the shape of the objects) is now comparable with the surface drag due to friction. According to Joseph et al [52], the appropriate adjustment to take inertial effects into account, is modify Darcy's equation (B.1) by:

$$\nabla P = \frac{-\mu}{K} \mathrm{u} - C_F K^{-1/2} \rho_f |\mathrm{u}| \mathrm{v} \tag{B.5}$$

Where C_F is the dimensionless form-drag constant and can be determined by a general formula: C_F=0.55(1-5.5$\frac{d}{D_e}$).

The Forchheimer model describes the effect of inertia as well as viscous forces in porous media and was used by Lauriat and Prasad [11], Beckermann et al [53] to examine the natural convection in a vertial

Validity of Darcy's law

Darcy's law neglects the effects of a solid boundary or the inertial forces on the fluid flow and heat transfer through a porous media. These effects are expected to become more important

The focus of the present study is on coarse-grained porous media, i.e. porous media in which length scales (here: diameter of the spheres) are not small compared to the flow and thermal length scales in the fluid. This makes that the Darcy model is no longer valid.

The Brinkman equation is only valid when the porosity is sufficient large, ε>0.6 [54]. Besides, there is concluded by Nield and Bejan [4] that for many practical purposes the addition of the Laplacian term is not needed. The usage of the Brinkman equation is not without difficulty, so typically the term is neglected. Furthermore, Basak et al [55] indicates that the Brinkman model accounts not adequately for the transition from porous medium flow to pure fluid flow as the permeability of the porous medium increases.

C

Boussinesq approximation

The governing coupled equations for a problem with free-convection, Newtonian and non-isothermal fluid, with constant μ are: continuity, Navier Stokes and the incompressible form of the energy equation .

$$\underbrace{\frac{\partial \rho}{\partial t}}_{\text{Time rate of change}} + \underbrace{\frac{\partial}{\partial x_j}(\rho u_j)}_{\text{Divergence of the velocity}} = 0 \tag{C.1}$$

$$\rho\left(\underbrace{\frac{\partial u_i}{\partial t}}_{\text{Time rate of change}} + \underbrace{u_j\frac{\partial u_i}{\partial x_j}}_{\text{Convection}}\right) = \underbrace{-\frac{\partial p}{\partial x_i}}_{\text{Pressure forces}} + \underbrace{\mu\frac{\partial^2 u_i}{\partial x_j^2}}_{\text{Viscous forces}} - \underbrace{\rho g_i}_{\text{Buoyant forces}} \tag{C.2}$$

$$\rho c_p\Big(\underbrace{\frac{\partial T}{\partial t}}_{\text{Time rate of change}} + \underbrace{u_j\frac{\partial T}{\partial x_j}}_{\text{Convective heat transfer}}\Big) = \underbrace{\frac{\partial}{\partial x_j}(\lambda\frac{\partial T}{\partial x_j})}_{\text{Diffusivity of heat}} \underbrace{+2\mu(\frac{\partial u_i}{\partial x_i})^2 + \mu(\frac{\partial u_i}{\partial x_j} + \frac{\partial u_j}{\partial x_i})^2}_{\text{Viscous dissipation}} \tag{C.3}$$

The Boussinesq approximation assumes that the density variations are small compared to the reference state: $\Delta\ \rho \ll \rho_0$. It is convenient to apply this approximation to make the math more manageable. So, $\rho \rightarrow \rho_0$ can be substituted, on the inertial terms and in the continuity equation. However, even the small density variations are important in the buoyancy term, the force acting on the flow due to temperature differences [56], so we retain variations in ρ in the buoyancy term in the vertical equation of motion.

The state of a substance in thermodynamic equilibrium can be described by two state variables: ρ and T. This gives:

$$d\rho = \frac{\partial \rho}{\partial p}\Big|_T dp + \frac{\partial \rho}{\partial T}\Big|_p dT \tag{C.4}$$

$$\frac{d\rho}{\rho} = \frac{1}{\rho}\frac{\partial \rho}{\partial p}\Big|_T dp + \frac{1}{\rho}\frac{\partial \rho}{\partial T}\Big|_p dT \tag{C.5}$$

$$\frac{d\rho}{\rho} = k_T dp - \beta dT \tag{C.6}$$

With k_T the coefficient of isothermal compressibility and β the thermal expansion coefficient. Coefficient k_T does not apply since the fluid can be assumed as incompressible , therefore the equation the differential equation for ρ reads:

$$\frac{d\rho}{\rho} = -\beta \cdot dT \tag{C.7}$$

With the condition that T is T_0 at ρ_0, the expression for the density fluctuation is:

$$ln\frac{\rho}{\rho_0} = -\beta \cdot (T - T_0) \tag{C.8}$$

It is convenient to take a Tailor expansion of C.8 and rewrite the density as:

$$\rho = \rho_0[1 - \beta(T - T_0)] \tag{C.9}$$

Using the Boussinesq approximation and after some rearrangement , the continuity reduces to the incompressible form because the small magnitude of $\frac{1}{\rho}\frac{D\rho}{Dt}$ in respect to the velocity gradient. The continuity and momentum equation for a Newtonian fluid becomes:

$$\frac{\partial u_j}{\partial x_j} = 0 \tag{C.10}$$

$$\frac{\partial(u_i)}{\partial t} + u_j\frac{\partial(u_i)}{\partial x_j} = -\frac{\partial}{\partial x_i}(\frac{p}{\rho_0} + g \cdot z) + \nu_0\frac{\partial^2 u_i}{\partial x_j^2} - \beta_0 g(T_0 - T)\delta_{i3} \tag{C.11}$$

With the last term in C.11 represents the buoyancy force in the Z-direction of gravity. Equation C.11 is coupled with the energy equation stated in C.3, since the temperature is still unknown. The viscous terms can be neglected since they are small compared to the conductive term in C.3. Thus, the final form of the energy equation is:

$$\frac{\partial T}{\partial t} + u_j\frac{\partial T}{\partial x_j} = \alpha\frac{\partial^2 T}{\partial x_j^2} \tag{C.12}$$

Where α=$\frac{k}{\rho c_p}$. Together, equations C.10, C.11 and C.12 are the Boussinesq equations and they describe the motion of fluid.

For the Boussinesq approximation to hold, two necessary conditions must be hold:

$$C_1 = \beta\Delta T << 1 \tag{C.13}$$

$$C_2 = \frac{\alpha^2}{L^2 C_p \Delta T} << 1 \tag{C.14}$$

For this project, β=2.18×10^{-4} K^{-1}, ΔT=1 (gravity was varied for difference in Ra), α=0.143×10^{-6} m^2/s, C_p=4182 m^2/s^{2}K making the two conditions:

$$C_1 = 2.18 \times 10^{-4}$$
$$C_2 = 4.89 \times 10^{-16}$$

This verifies that the two conditions are met since both values are much smaller than 1.

Boundary and initial conditions

The problem can be fully specified by determining the boundary and initial conditions of equations 3.1 to 3.4. The parameters that need specification are velocity, temperature and time. This will be discussed in the paragraphs below.

Velocities

To address the research questions, the direction and magnitude of the forced component is of great importance. The walls of interest get a positive or negative velocity component, this value is obtained from the results for pure natural convection. The no-slip velocity boundary condition is applied to the walls that do not move. For the second research objective the direction of the forced component is investigated. Therefore, a box with the sides of the cavity are imposed with a Dirichlet boundary condition of a constant velocity.

So the velocity boundary conditions for the different setups are:

NC	$u_x = u_y = u_z = 0$	at x=0, L; y=0, L; z=0, L.
MC by moving sides	$u_x = u_y = 0$	at x=0, L; z=0,L and $u_z = \pm\, u$ at y=0, L.

Left wall	$T = T_h$	at y=0
Right wall	$T = T_c$	at y=L
Front/back wall	$\frac{\partial T}{\partial x} = 0$	at x=0, L (adiabatic wall)
Top/bottom wall	$\frac{\partial T}{\partial z} = 0$	at z=0, L (adiabatic wall)

Temperature

A temperature gradient is imposed by maintaining the side walls of the cavity at different temperature. The temperature of the hot and cold wall will be varied to create a difference in Ra. The temperature conditions are given by:

There is a thermal equilibrium at the interface *i* between the fluid and solid spheres where there is only conductive heat transfer normal to the interface. Therefore the following Neumann boundary condition implies at the interface:

$$k_f \frac{\partial T_f}{\partial x_j}|_i = k_s \frac{\partial T_s}{\partial x_j}|_i$$

Time

The initial conditions for the solid and fluid phase are:

$$T_s(t=0) = T_f = T_0 = \frac{1}{2}(T_h + T_c)$$

C.1. Scaling factor velocity for natural convection

In the case of a mixed convection or forced convection dominated situation, it is quite trivial to scale the domain velocity with the forced component (wall velocity). For natural convection a scaling factor was proposed based on the article of [3]. The derivation will be done here.

The velocity scale comes from the speed that is needed for merning the hot fluid into the the central region flow of the cavity:

$$u_{cental} \sim \frac{g\beta\Delta T (Ra^{-2/7} L)^2}{\nu} \tag{C.15}$$

The exponent of Ra of -2/7 comes from scaling arguments.

D

Spatial Resolution

Flow around a submerged object creates a boundary layer next to the object. In the cavity filled with coarse grained porous media there may be boundary layers at the top, bottom, sides of the cavity but also around the solid spheres.

The thickness of the boundary layer depends on the Pr number. When Pr is very large or very small the thickness of the momentum boundary layer and thermal boundary layer are no longer in the same order of magnitude. The momentum boundary layer increases with the kinematic viscosity (for a Newtonian fluid): $\delta_{\mathrm{M}} \sim \nu^{1/2}$. Similarly, the thermal boundary layer should increase with α. This is schematically depicted in figure D.1. For very small Pr (for example a liquid metal) most of the thermal boundary layer is in the momentum outer region.

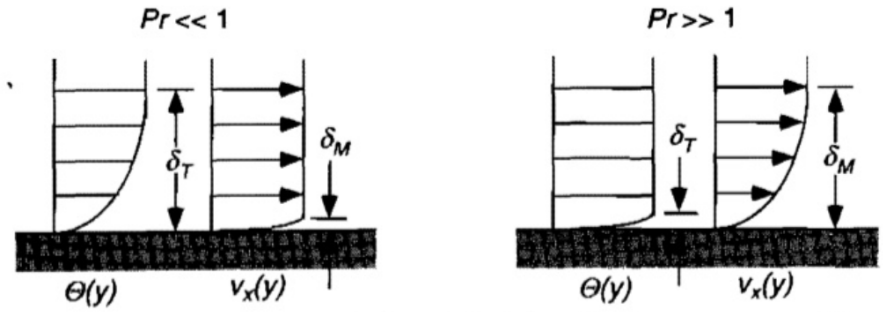

Figure D.1: Thermal and velocity boundary layer for two different Pr number [5].

It has been well established that the Nu number is very sensitive to the grid resolution used in the boundary layer. When DNS is underresolved the calculated Nu is too high [57].

There was found that there is an increase in required grid points in the boundary layer with increasing Ra number [58, 59]. However, the Nu obtained in the simulations not only depend on the grid solution in the boundary layer but also in the bulk. The thermal plumes have to pass along the centre of the cavity and the side walls, this influences Nu too.

A detailed literature review on the spatial resolution requirements in a convective turbulent flow is reported in [1]. For a perfect DNS simulation of the flow, the local mesh size should be smaller than the Kolmogorov scale η_{Kolm}:

$$\eta_K = (\frac{\nu^3}{\epsilon_u})^{1/4} \tag{D.1}$$

Where ϵ_u is the (local) energy dissipation rate of the velocity (or in other words: the amount of energy lost by the viscous forces) and μ the kinematic viscosity.

The kinetic energy dissipation rate is:

$$\epsilon_u = \frac{\nu^3}{H^4}(\mathrm{Nu}-1)\mathrm{RaPr}^{-2} \tag{D.2}$$

So equation D.1 represents the ratio of the viscosity over the kinetic energy dissipation.

The smallest length scale for the heat transport phenomena is coupled with the velocity length scale. It is given by:

$$\eta_T = \eta_K Pr^{-3/4} \tag{D.3}$$

For large Pr the flow field is smooth at those scales at which the temperature field is still fluctuating. For large Pr, the viscous diffusion rate is much larger than the thermal diffusion rate.

For small Pr (Pr<1) $\eta_T > \eta_{Kolm}$, so the grid resolution should be based on the smallest length scale, η_{Kolm} the Kolmogorov scale.

For large Pr (Pr>1) $\eta_T < \eta_{Kolm}$ and one can argue that η_T is the length scale where the grid resolution should be based on. But for larger Pr the velocity field becomes smooth and then the grid resolution should be compared to the Bachelor scale η_B. It is an intermediate scale between η_{Kolm} and η_T. This scale describes the size of a droplet scalar that will diffusive in the same time it takes the energy in an eddy with size η to dissipate. The Bachelor scale is defined as:

$$\eta_B = \eta_{Kolm} Pr^{-1/2} \tag{D.4}$$

Global mesh size

For a cavity with length L the global Kolmogorov length η_K^{global} is determined as:

$$\eta_{Kolm}^{global} = \frac{\nu^{3/4}}{\epsilon^{1/4}} = \frac{Pr^{1/2}L}{Ra^{1/4}(Nu-1)^{1/4}} \tag{D.5}$$

In the case for Pr>1 the global mesh size h^{global} is with relation between Batchelor and Kolmogorov:

$$h^{global} < \frac{L}{Ra^{1/4}(Nu-1)^{1/4}} \tag{D.6}$$

The mesh size reported in equation D.6 is the safe limit for all the relevant sales to be captured.

Nu is estimated based on the hard turbulence assumption:

$$Nu = 0.124 \times Ra^{0.309} \tag{D.7}$$

Boundary layer mesh size

The mesh close to the boundary layer should be fine enough to capture the physics. In the cavity with length L, the thickness of the kinetic boundary layer, δ_u for large Pr (Pr>3) is given by:

$$\delta_u = 0.5 Nu^{-1/2} Pr^{-1/3} E^{-1} L \tag{D.8}$$

Where constant E is defined as $E \approx B\frac{\sqrt{2}}{0.478}$, where B is a constant that has to do with the thickness of the kinetic boundary layer. It can be determined by the tangent to the longitudinal velocity. For present case (large Pr), $E \approx 0.982$.

The thermal boundary layer is related to the velocity boundary layer thickness by:

$$\frac{\delta_{Th}}{\delta_u} = EPr^{-1/3} \tag{D.9}$$

The mesh size in the boundary layer is given by:

$$h^{BL} = 2^{-2/3} a^{-1} E^{-3/2} Nu^{-3/2} L \tag{D.10}$$

From which the estimation can be made for the minimum number of nodes of the computation mesh which must be placed in each thermal $N_{Th.BL}$ and kinetic boundary layer $N_{v.BL}$:

$$N_{Th.BL} = \sqrt{2} a Nu^{1/2} E^{3/2} \tag{D.11}$$

$$N_{v.BL} = \sqrt{2} a Nu^{1/2} Pr^{1/3} E^{1/2} \tag{D.12}$$

The minimum number of cells is calculated by:

$$N_{\text{total cells}} = \frac{L}{h^{global}} \tag{D.13}$$

Spatial resolution

Based on the above equations a rough estimation of the global mesh size h^{global}, thermal boundary layer thickness δ_{Th}, velocity boundary layer thickness δ_u, minimum number of grid points in the thermal ($N_{Th.BL}$) and velocity ($N_{v.BL}$) boundary layers at different Ra for water as fluid (Pr=5.4) and a cavity with L=0.1 m is tabulated below.

Ra	h^{global} (m)	δ_{Th}(m)	δ_u (m)	$N_{Th.BL}$	$N_{v.BL}$	No. of cells
1.17×10^5	0.00395	0.00357	0.00637	2	3	1.63×10^4
1.17×10^6	0.00180	0.00175	0.00178	3	4	1.72×10^5
1.17×10^7	0.000833	0.00086	0.000833	3	6	1.74×10^6

Table D.1: Overview of the rough estimation of the mesh size of a cavity filled with water for different Ra numbers. The calculations are done based on [1].

The number of cells reported above is a rough estimation based on a article for pure Rayleigh-Bénard convection (bottom heated cavity) [1]. In case of a domain filled with coarse grained porous media, the number of grid cells required increases. This results from the thermal and velocity boundary layer that will be generated around the spheres. The contact area of the sphere with the fluid increases. The numbers reported in this section are used as a starting point.

Temporal resolution

There are different temporal scales that exists in this situation.

The Kolmogorov time scale is associated with the smallest eddies:

$$\tau_{Kolm} = (\frac{\nu}{\epsilon})^{1/2} = \frac{(\eta_K^{global})^2}{\nu} \tag{D.14}$$

This equation can be used to estimate the $\tau_{Kolmogorov}$ in case of natural convection. In case of mixed convection the forced flow U_{FC} would influence the dissipation rate ε (in that case: ε=$\frac{U_{FC}^3}{L}$). This would also effect the time scale associated with the Kolmogorov scales. The smallest time scale can be obtained from the smallest velocity.

The other time scale that can be determined in is the time scales based on eddy turn-over time. This is the time scale for an eddy to undergo significant distortion. It can also been seen as the typical time scale for the transfer of energy to smaller scales, since this distortion is the mechanism for energy transfer. The eddy turn over time is given by:

$$\tau_{LSC} = \frac{4L}{u_i} \tag{D.15}$$

Where U is the circulation velocity. In the case of mixed convection, the velocity is based the magnitude of the forced component. That is the wall velocity. Usually the simulations are run for about 8-10 τ_{LSC} to ensure that averaging is done after the flow has reached a statistically steady state.

E

Richardson number determination

The Richardson number for the empty box is determined by:

$$Ri = \frac{Gr}{Re^2}$$

In the case for a box filled with spheres, the porosity of the spheres has an influence on the heat and flow characteristics. This also affects the Richardson number.

To find the mixed convection regime in a box with porous media, the Darcy number (Da) have to be taken into account in the expression for Ri number. Da represents the relative effect of permeability of the medium versus its cross-sectional area. The proposed equation was founded by Keene [35]:

$$Da = \frac{K}{L^2}, \qquad K = \frac{\varepsilon^3 d_p^2}{150(1-\varepsilon)^2} \tag{E.1}$$

Where K is the permeability of the medium (m^2), ε is the porosity or void fraction of the material and d_p the diameter of the particle. The following dimensionless numbers are proposed based on the medium m based on the article from Katare et al [31].

The Re number based on the permeability:

$$Re_K = Re_f\sqrt{Da} = \frac{\rho_f u\sqrt{K}}{\mu_f}, \tag{E.2}$$

where subscript f refers to the fluid phase and K to the permeability of the medium.

The Ra number based on the fluid properties:

$$Ra_m = Ra_f Da\lambda, \tag{E.3}$$

where λ=$\frac{k_f}{k_s}$, the conductivity ratio of fluid to solid. Furthermore, Pr is based on two articles. First, the effective Pr number was based on [38]:

$$Pr_{eff} = Pr_{por} Da, \tag{E.4}$$

where the subscript *por* stands for porosity.

Kathare et al [31] gives a definition for Pr_p:

$$Pr_{por} = Pr_m \frac{Da^{-1/2}}{C_f} \tag{E.5}$$

Where C_f is the dimensionless Forcheimer coefficient, this parameter can be found empirical.

Together, this forms the expression for Pr_m (Pr based on k_m):

$$Pr_m = \frac{\mu C_p}{k_m} = Pr_{eff} Da^{-1/2} C_f \tag{E.6}$$

The relationship for Ri based on the medium, Ri_m, is formed on the dimensionless numbers based on the medium and permeability:

$$Ri_m = \frac{Ra_m}{Pr_m Re_K^2} = \frac{Ra_f \sqrt{Da}\lambda}{Pr_{eff} Re_f^2 C_f} \tag{E.7}$$

This equation is valid for values between ε=0-1, but not the values ε=0 or ε=1 itself. In this work the conductivities of the solid region (hydrogel) and the fluid part (water) are in the same order of magnitude, making λ=1. Furthermore, C_f is taken to be 1 since it is hard to determine this constant. Literature reported values for C_f of about $C_f \sim O(0.1)$ [31].

The notation that will be used in this thesis is the Richardson number for the medium Ri_m [31]:

$$Ri_m = \frac{Gr\sqrt{Da}}{Re^2}$$

Where Gr and Re are based on the fluid properties and the length of the box. Da is calculated by the following steps. This begins with the determination of the porosity of the system, this can be calculated by the fraction that is free for the fluid to move through.

$$\varepsilon = \frac{V_{\text{voids}}}{V_{\text{total}}} = 1 - \frac{V_{\text{spheres}}}{V_{\text{total}}}$$

The total volume of the box and the volume of the spheres are determined by:

$$V_{\text{total}} = 0.1 \cdot 0.1 \cdot 0.1 = 0.00010 \text{m}^3$$

$$\begin{aligned} V_{\text{spheres}} &= V_{\text{single sphere}} \cdot \text{number of spheres} \\ &= \frac{4}{3}\pi r^3 \cdot 148 = 4.18 \cdot 10^{-6} \cdot 148 = 0.0062 \text{m}^3 \end{aligned}$$

The porosity is defined as the fraction of the total volume of the medium that is occupied by void space [4]. This makes the porosity ε to be:

$$\varepsilon = 1 - \frac{0.0006186}{0.0001} = 1 - 0.62 = 0.38$$

With this porosity the permeability, K, can be calculated according to Keene et al [35]:

$$K = \frac{\varepsilon^3 D^2}{150(1-\varepsilon)^2} = \frac{0.38^3 \cdot 0.02^3}{150(1-0.38)^2} = 3.8 \cdot 10^{-7} \text{m}^2$$

The constant 150 in the equation was obtained by seeking a best fit with experimental results [4]. This equation is often not valid in the case when particles deviate strongly from the spherical shape.

The Darcy number is just the permeability over the length of the box:

$$Da = \frac{K}{L^2} = \frac{3.8 * 10^{-7}}{0.1^2} = 3.81 \cdot 10^{-5}$$

F

Convergence

```
/*--------------------------------*- C++ -*----------------------------------*\
| =========                 |                                                 |
| \\      /  F ield         | OpenFOAM: The Open Source CFD Toolbox           |
|  \\    /   O peration     | Version:  2.4.0                                 |
|   \\  /    A nd           | Web:      www.OpenFOAM.org                      |
|    \\/     M anipulation  |                                                 |
\*---------------------------------------------------------------------------*/
FoamFile
{
    version     2.0;
    format      ascii;
    class       dictionary;
    location    "system";
    object      controlDict;
}
// * * * * * * * * * * * * * * * * * * * * * * * * * * * * * * * * * * * * //

libs
(
    "libcompressibleTurbulenceModel.so"
    "libcompressibleRASModels.so"
     "libOpenFOAM.so"
      "libsimpleSwakFunctionObjects.so"
      "libswakFunctionObjects.so"
      "libgroovyBC.so"
     );


application     boussinesqChtMultiRegionFoam;

startFrom       latestTime;

startTime       1300;

stopAt          endTime;

endTime         52133;
deltaT          10.00;
```

```
writeControl    adjustableRunTime;

writeInterval   100;


purgeWrite      3;

writeFormat     ascii;

writePrecision  8;

writeCompression off;

timeFormat      general;

timePrecision   6;

runTimeModifiable yes;

maxCo           0.33;

// Maximum diffusion number
maxDi           10.0;

adjustTimeStep yes;



functions
(

NusseltNumber_hot
    {
        type           patchExpression;
      outputControl  timeStep;
      outputInterval 1;
      region          air;

                patches (
                                w_b
                            );
        verbose true;
                variables (
                                "Tsat=300.1;"
                "ln2D=0.1;"       /*length(.08)/k(.0261) */
                            );
        expression "ln2D*sum(snGrad(T)*area())/(sum(area())*(301-300))";
                accumulations (
                                        average
                        );
    }

NusseltNumber_cold
    {
        type           patchExpression;
      outputControl  timeStep;
```

```
    outputInterval 1;
    region          air;

            patches (
                            w_t
                        );
       verbose true;
            variables (
                            "Tsat=300.1;"
            "ln2D=0.1;"      /*length(.08)/k(.0261) */
                        );
       expression "ln2D*sum(snGrad(T)*area())/(sum(area())*(301-300))";
            accumulations (
                                    average
                    );
  }



probesair
   {
       // Type of functionObject
       type probes;

       outputControl   timeStep;
       outputInterval  1;
       region          air;

       // Where to load it from (if not already in solver)
       functionObjectLibs ("libsampling.so");

       // Locations to be probed. runTime modifiable!
       probeLocations
       (
          (.01                 .0499    -0.00549)
          (.01                 .011            .085)
          (.01                 .0314    .055929)
          (.04          .0810  .0128)
          (.04                 .02268   .071226)
          (.04          -.00343  .01502)
           (.08         .08298  .070)
           (.08         .04             .041337)
           (.08         -.00115         .01335)
       );

       // Fields to be probed. runTime modifiable!
       fields
       (
           p
           U
           T
       );
   }
```

```
probesplate
    {
        // Type of functionObject
        type probes;

        outputControl   timeStep;
        outputInterval  1;
        region          plate;

        // Where to load it from (if not already in solver)
        functionObjectLibs ("libsampling.so");

        // Locations to be probed. runTime modifiable!
        probeLocations
        (
            (-0.04322323 0.9205518  0.0)
                  (-0.1905864 0.9092162  0.0)
                  (-0.1701823 0.0613111  0.0)
                  (-0.01601768 0.258551  0.0)
        );

        // Fields to be probed. runTime modifiable!
        fields
        (
          T
        );
    }


);


// ************************************************************************* //
```

G

Overview Nusselt Numbers

Influence of BCT hydrogel spheres and Rayleigh number on heat transfer

Table G.1: Influence of spheres and Rayleigh numbers on Nusselt numbers

Hydrogel balls cavity, Ra=10^6	NC	Nu= 2	Empty cavity, Ra=10^6	NC	Nu=9.38
$v_{max,NC}$=	FC	Nu=2.8	$v_{max,NC}$=0.000489 m/s	FC	Nu=10.7
$v_{max,FC}$=0.00115	MC ass	Nu= 6.9	$v_{max,FC}$= m/s	MC ass	Nu=13.71
	MC opp	Nu=1.27		MC opp	Nu=6.19
Hydrogel balls cavity, Ra=10^7	NC	Nu= 9.2	Empty cavity, Ra=10^7	NC	Nu=17.8
$v_{max,NC}$=0.004820	FC	Nu=5.9	$v_{max,NC}$=0.00153863 m/s	FC	Nu=13.8
$v_{max,FC}$=0.00241	MC ass	Nu= 19.12	$v_{max,FC}$=0.000769315 m/s	MC ass	Nu= 21.9
	MC opp	Nu=3.5		MC opp	Nu= 14.3
Hydrogel balls cavity, Ra=10^8	NC	Nu= 30.1	Empty cavity, Ra=10^8	NC	Nu=33.6
$v_{max,NC}$=0.00700948	FC	Nu=33.2	$v_{max,NC}$=0.00490658 m/s	FC	Nu= 25.6
$v_{max,FC}$=0.01401896	MC ass	Nu= 65	$v_{max,FC}$=0.00245329 m/s	MC ass	Nu= 40.9
	MC opp	Nu=30		MC opp	Nu= 26.7

Influence on top/bottom or side walls moving on heat transfer

Table G.2: Influence on top or bottom (abbreviated: t/b) wall moving compared to side walls moving on Nusselt number

Hydrogel, Ra=10^7	sides MC ass	Nu= 19.12	Empty cavity, Ra=10^7	sides MC ass	Nu=21.9
v_{wall}=0.00241	sides MC opp	Nu=3.5	$v_{side-wall}$=7.69×10^{-4} m/s	sides MC opp	Nu=14.3
Ri_m=0.23	t/b MC ass	Nu=12.9	$v_{t/b-wall}$=6.15×10^{-3}m/s	t/b MC ass	Nu= 21.35
	t/b MC opp	Nu=7.6	Ri_{sides}=363 and $Ri_{t/b}$=5.68	t/b MC opp	Nu= 21.8

Determination of the Richardson number

Table G.3: Data from the Richardson number (with $\sqrt{Da}$) determination for Ra=10^6 and Ra=10^7. The column Nu-FC represents the Nusselt number in that case for forced convection.

Ra=10^6, walls assisting				Ra=10^6, walls opposing				Ra=10^7, walls assisting			
Ri	Nu_{MC}	v (m/s)	Nu_{FC}	Ri	Nu_{MC}	v (m/s)	Nu_{FC}	Ri	Nu_{MC}	v (m/s)	Nu_{FC}
∞ (NC)	2	-	-				-	∞ (NC)	9.2	-	-
20	2.3	$8.13 \cdot 10^{-5}$	-	0.1	1.27	$1.15 \cdot 10^{-3}$	2.8	3.75	12	$6.45 \cdot 10^{-4}$	1.79
0.1	6.9	$1.15 \cdot 10^{-3}$	2.8	0.01	4.8	$3.64 \cdot 10^{-3}$	8.8	1.88	13.05	$9.13 \cdot 10^{-3}$	-
0.01	13.3	$3.64 \cdot 10^{-3}$	8.8	0.005	8.4	$5.14 \cdot 10^{-3}$	-	0.94	14.6	$1.29 \cdot 10^{-3}$	3.2
0.005	17.2	$5.14 \cdot 10^{-3}$	-	0.5	1.09	$5.14 \cdot 10^{-4}$	-	0.26	19.13	$2.41 \cdot 10^{-3}$	5.9
0.0025	22.4	$7.27 \cdot 10^{-3}$	-	1	1.13	$3.64 \cdot 10^{-4}$	1.42	0.01	51	$1.15 \cdot 10^{-2}$	35.9
0.00125	29.4	$1.03 \cdot 10^{-2}$	-	2	1.25	$2.97 \cdot 10^{-4}$	1.25	0.005	64.5	$1.625 \cdot 10^{-2}$	-
				4	1.34	$1.82 \cdot 10^{-4}$	1.14	0.0025	77.8	$2.3 \cdot 10^{-2}$	-
				8	1.44	$1.29 \cdot 10^{-4}$					-
				16	1.51	$9.09 \cdot 10^{-5}$					-

Bibliography

[1] Olga Shishkina, Richard J.A.M. Stevens, Siegfried Grossmann, and Detlef Lohse. Boundary layer structure in turbulent thermal convection and its consequences for the required numerical resolution. *New Journal of Physics*, 12(7):075022, 2010.

[2] ClimateBooster. Meer comfort met minder energie. http://www.climatebooster.nl/ftp/downloads/brochure-climatebooster-2018-web.pdf.

[3] Bernard Castaing, Gemunu Gunaratne, François Heslot, Leo Kadanoff, Albert Libchaber, Stefan Thomae, Xiao-Zhong Wu, Stéphane Zaleski, and Gianluigi Zanetti. Scaling of hard thermal turbulence in Rayleigh-Bénard convection. *Journal of Fluid Mechanics*, 204:1–30, 1989.

[4] Donald A. Nield and Adrian Bejan. *Convection in porous media*, volume 3. Springer, 2006.

[5] W.M. Deen. *Analysis of Transport Phenomena*. Topics in Chemical Engineering. OUP USA, 2012.

[6] Raed Abed Mahdi, H.A. Mohammed, and K.M. Munisamy. Improvement of convection heat transfer by using porous media and nanofluid. *International journal of science and research IJSR, ISSN*, pages 2319–2335, 2013.

[7] Hasan Celik. A study on mixed convection heat transfer through a channel partially filled with porous medium. Master thesis, Izmir Institute of Technology, 2012.

[8] Peter de Waard. Nieuwe staalreus is een feit: Thyssenkrupp tata steel. https://www.volkskrant.nl/economie/nieuwe-staalreus-is-een-feit-thyssenkrupp-tata-steel b932c9b3/.

[9] UK Health and Safety Executive. The explosion of no. 5 blast furnace, corus uk ltd, port talbot, 2001.

[10] Tata Steel. Provide bf - advanced process controls for blast furnace, 2011. http://automationtatasteel.com/html/blast-furnace-level-2-system.html.

[11] G. Lauriat and Vish Prasad. Non-darcian effect on natural convection in a vertical porous layer. *International Journal of Heat and Mass Transfer*, 32:2135–2148, 11 1989.

[12] Nobuhiro Seki, Shoichiro Fukusako, and Hideo Inaba. Heat transfer in a confined rectangular cavity packed with porous media. *International Journal of Heat and Mass Transfer*, 21(7):985 – 989, 1978.

[13] Irfan Kurtbas and Nevin Celik. Experimental investigation of forced and mixed convection heat transfer in a foam-filled horizontal rectangular channel. *International Journal of Heat and Mass Transfer*, 52(5):1313 – 1325, 2009.

[14] Navdeep Singh and Debjyoti Banerjee. *Nanofins: Science and applications*. Springer, 2014.

[15] P. Bergé and M. Dubois. Rayleigh-Bénard convection. *Contemporary Physics*, 25(6):535–582, 1984.

[16] Siegfried Grosmann and Detlef Lohse. Scaling in thermal convection: a unifying theory. *Journal of Fluid Mechanics*, 407:27–56, 2000.

[17] Chong Shen Ng, Andrew Ooi, Detlef Lohse, and Daniel Chung. Vertical natural convection: application of the unifying theory of thermal convection. *Journal of Fluid Mechanics*, 764:349–361, 2015.

[18] S. Singh and M. A. R. Sharif. Mixed convective cooling of a rectangular cavity with inlet and exit openings on differentially heated side walls. *Numerical Heat Transfer, Part A: Applications*, 44(3):233–253, 2003.

[19] Ali J. Chamkha, Salam Hadi Hussain, and Qusay Rashid Abd-Amer. Mixed convection heat transfer of air inside a square vented cavity with a heated horizontal square cylinder. *Numerical Heat Transfer, Part A: Applications*, 59(1):58–79, 2011.

[20] Nelson O. Moraga and Sergio E. López. Numerical simulation of three-dimensional mixed convection in an air-cooled cavity. *Numerical Heat Transfer, Part A: Applications*, 45(8):811–824, 2004.

[21] R.B. Mansour and R. Viskanta. Shear-opposed mixed-convection flow and heat transfer in a narrow, vertical cavity. *International Journal of Heat and Fluid Flow*, 15(6):462 – 469, 1994.

[22] Orhan Aydm. Aiding and opposing mechanisms of mixed convection in a shear- and buoyancy-driven cavity. *International Communications in Heat and Mass Transfer*, 26(7):1019 – 1028, 1999.

[23] Hakan F. Oztop and Ihsan Dagtekin. Mixed convection in two-sided lid-driven differentially heated square cavity. *International Journal of Heat and Mass Transfer*, 47(8):1761 – 1769, 2004.

[24] M. Rajarathinam, N. Nithyadevi, and A.J. Chamkha. Heat transfer enhancement of mixed convection in an inclined porous cavity using cu-water nanofluid. *Advanced Powder Technology*, 29(3):590–605, 2018.

[25] V. Ambethkar and D. Kushawaha. Numerical simulations of fluid flow and heat transfer in a four-sided lid-driven rectangular domain. *International Journal of Heat and Technology*, 35(2):273–278, 2017.

[26] Duncan R. Hewitt, Jerome A. Neufeld, and John R. Lister. High Rayleigh number convection in a three-dimensional porous medium. *Journal of Fluid Mechanics*, 748:879–895, 2014.

[27] Jesse Otero, Lubomira A. Dontcheva, Hans Johnston, Rodney A. Worthing, Alexander Kurganov, Guergana Petrova, and Charles R. Doering. High-Rayleigh-number convection in a fluid-saturated porous layer. *Journal of Fluid Mechanics*, 500:263–281, 2004.

[28] Kambiz Vafai and C.L. Tien. Boundary and inertia effects on convective mass transfer in porous media. *International Journal of Heat and Mass Transfer*, 25(8):1183–1190, 1982.

[29] John M. House, Christoph Beckermann, and Theodore F. Smith. Effect of a Centered Conducting Body on Natural Convection Heat Transfer in an Enclosure. *Numerical Heat Transfer, Part A: Applications*, 18(2):213–225, 1990.

[30] N. Kladias and V. Prasad. Natural Convection in Horizontal Porous Layers: Effects of Darcy and Prandtl Numbers. *Journal of Heat Transfer*, 111(4):926–935, 1989.

[31] V. Kathare, J.H. Davidson, and F.A. Kulacki. Natural convection in water-saturated metal foam. *International Journal of Heat and Mass Transfer*, 51(15):3794 – 3802, 2008.

[32] Edimilson J. Braga and Marcelo J.S. de Lemos. Laminar natural convection in cavities filled with circular and square rods. *International Communications in Heat and Mass Transfer*, 32(10):1289 – 1297, 2005.

[33] Saurish Das, Niels G. Deen, and J.A.M. Kuipers. A dns study of flow and heat transfer through slender fixed-bed reactors randomly packed with spherical particles. *Chemical Engineering Science*, 160:1–19, 2017.

[34] Sakae Yagi and Noriaki Wakao. Heat and mass transfer from wall to fluid in packed beds. *AIChE Journal*, 5(1):79–85, 1959.

[35] Daniel J. Keene. Thermal Convection in Porous Media at High Rayleigh Numbers. *Journal of Heat Transfer*, 137:1–4, 2015.

[36] P. Ranganathan and R. Viskanta. Mixed convection boundary-layer flow along a vertical surface in a porous medium. *Numerical Heat Transfer*, 7(3):305–317, 1984.

[37] Shohel Mahmud and Ioan Pop. Mixed convection in a square vented enclosure filled with a porous medium. *International Journal of Heat and Mass Transfer*, 49(13):2190 – 2206, 2006.

[38] Mingyu Wang and Adrian Bejan. Heat transfer correlation for Bénard convection in a fluid saturated porous layer. *International communications in heat and mass transfer*, 14(6):617–626, 1987.

[39] Stephen B. Pope. *Turbulent flows*. IOP Publishing, 2001.

[40] David J. Tritton. *Physical fluid dynamics*. Springer Science & Business Media, 1988.

[41] H.K. Versteeg and W. Malalasekera. *An Introduction to Computational Fluid Dynamics: The Finite Volume Method*. Pearson Education Limited, 2007.

[42] The 8-node hexahedron. https://www.colorado.edu/engineering.

[43] D.A. Kaminski and C. Prakash. Conjugate natural convection in a square enclosure: effect of conduction in one of the vertical walls. *International Journal of Heat and Mass Transfer*, 29(12):1979–1988, 1986.

[44] L.P.B.M. Janssen and M.M.C.G. Warmoeskerken. *Transport Phenomena Data Companion*. Edward Arnold, 1987.

[45] J.L. Lage and A. Bejan. The Ra-Pr domain of laminar natural convection in an enclosure heated from the side. *Numerical Heat Transfer*, 19(1):21–41, 1991.

[46] L. Snoussi, R. Chouikh, N. Ouerfelli, and A. Guizani. Numerical simulation of heat transfer enhancement for natural convection in a cubical enclosure filled with Al_2O_3/water and Ag/water nanofluids. *Physics and Chemistry of Liquids*, 54(6):703–716, 2016.

[47] R.J.A. Janssen and R.A.W.M. Henkes. Instabilities in three-dimensional differentially-heated cavities with adiabatic horizontal walls. *Physics of Fluids*, 8(1):62–74, 1996.

[48] Nikos C. Markatos and K.A. Pericleous. Laminar and turbulent natural convection in an enclosed cavity. *International Journal of Heat and Mass Transfer*, 27(5):755–772, 1984.

[49] Zhaoli Guo Peng Wang, Yonghao Zhang. Numerical study of three-dimensional natural convection in a cubical cavity at high Rayleigh numbers. *International Journal of Heat and Mass Transfer*, 113:217 – 228, 2017.

[50] Raj Kamal Tiwari and Manab Kumar Das. Heat transfer augmentation in a two-sided lid-driven differentially heated square cavity utilizing nanofluids. *International Journal of Heat and Mass Transfer*, 50(9-10):2002–2018, 2007.

[51] H. C. Brinkman. A calculation of the viscous force exerted by a flowing fluid on a dense swarm of particles. *Flow, Turbulence and Combustion*, 1(1):27, Dec 1949.

[52] D. D. Joseph, D. A. Nield, and G. Papanicolaou. Nonlinear equation governing flow in a saturated porous medium. *Water Resources Research*, 18(4):1049–1052, 1982.

[53] C. Beckermann, R. Viskanta, and S. Ramadhyani. A numerical study of non-darcian natural convection in a vertical enclosure filled with a porous medium. *Numerical Heat Transfer*, 10(6):557–570, 1986.

[54] T. S. Lundgren. Slow flow through stationary random beds and suspensions of spheres. *Journal of Fluid Mechanics*, 51(2):273–299, 1972.

[55] Tanmay Basak, S. Roy, T. Paul, and I. Pop. Natural convection in a square cavity filled with a porous medium: Effects of various thermal boundary conditions. 49:1430–1441, 04 2006.

[56] K. Hanjalic, S. Kenjeres, M.J. Tummers, and H.J.J. Jonker. *Analysis and Modelling of Physical Transport Phenomena*. VSSD, 2008.

[57] Robert M. Kerr. Rayleigh number scaling in numerical convection. *Journal of Fluid Mechanics*, 310:139–179, 1996.

[58] Richard J.A.M. Stevens, Roberto Verzicco, and Detlef Lohse. Radial boundary layer structure and Nusselt number in Rayleigh–Bénard convection. *Journal of fluid mechanics*, 643:495–507, 2010.

[59] Roberto Verzicco and Roberto Camussi. Numerical experiments on strongly turbulent thermal convection in a slender cylindrical cell. *Journal of Fluid Mechanics*, 477:19–49, 2003.